

AGING IN CLOSED-CELL PHENOLIC FOAM

by

Timothy J. Fox

B.S., West Virginia University
May 1984

SUBMITTED IN PARTIAL FULFILLMENT
OF THE REQUIREMENTS OF THE
DEGREE OF
MASTER OF SCIENCE
IN MECHANICAL ENGINEERING

at the

MASSACHUSETTS INSTITUTE OF TECHNOLOGY

March 1986

© Massachusetts Institute of Technology

Signature of Author _____

Department of Mechanical Engineering
March 21, 1986

Certified by _____

Leon R. Glicksman
Thesis Supervisor

Accepted by _____

Ain A. Sonin
Chairman, Department Graduate Committee

MASSACHUSETTS INSTITUTE
OF TECHNOLOGY

JUL 28 1986

LIBRARIES

AGING IN CLOSED-CELL PHENOLIC FOAM

by

TIMOTHY J. FOX

Submitted to the Department of Mechanical Engineering
on March 21, 1986 in partial fulfillment of the
requirements for the Degree of Master of Science in
Mechanical Engineering

ABSTRACT

Closed-cell rigid board phenolic foam was recently introduced as a promising insulation alternative to polyurethane and isocyanurate foams. The apparent advantage of this new product is its relatively high resistance to the phenomenon known as aging, i.e., the degradation of the thermal properties over time. This is caused in the short term, by the diffusion of air components (mainly, oxygen and nitrogen) into the fluorocarbon gas occupied closed cells; and continues, over larger periods of time, as the fluorocarbon escapes to the atmosphere. This project is an initial investigation to determine the permeation properties of gases in closed-cell phenolic foam.

A geometric study of the phenolic foam cell structure was performed in order to determine the cell wall thickness, cell diameter, and polymer distribution between the struts and cell walls. The void fraction of the foam was also calculated. These parameters were useful in implementing an analytical model of the foam based on assumed cell shape. The study revealed that the phenolic foam doubled the percentage of polymer material in the cell walls when compared to the polyurethane foams.

A test cell was designed and built that measured the volumetric flowrates due to gas permeation through a film of phenolic polymer. These tests were needed to understand the diffusion properties of the material in the cell walls. The inability to obtain adequate representative films prevented the completion of these tests; therefore, by using experimental values for the foam permeability, a range of phenolic polymer permeabilities was calculated through the analytical models. This revealed that the permeability of the phenolic polymer was approximately 7 times less than that of polyurethane polymer (methane diisocyanate).

A foam permeability test apparatus was constructed which had improved sensitivity over those of previous design. Initial tests with three gases (carbon dioxide, oxygen and nitrogen) suggested that accelerated temperatures and gas pressure gradients across the sample would damage the delicate foam cells. This prohibited the successful testing of the various gases over a wide range of temperatures. A low temperature test with carbon dioxide determined the permeation rate in the phenolic foam to be 30-45 times less than that of various polyurethane foams under the same conditions. This was accounted for by the phenolic foam having

twice the density than the polyurethane foams, over two times the percentage of material present in the cell walls, and the cell wall polymer being 7 times less permeable to the test gas than the polyurethane polymer.

Thesis Supervisor: Leon R. Glicksman
Title: Senior Research Scientist

ACKNOWLEDGEMENTS

The author wishes to acknowledge Dr. Leon R. Glicksman of the Department of Mechanical Engineering at MIT for his role as Thesis Supervisor and Project Advisor. His continued support and advice throughout this research is greatly appreciated.

The funding for this project was provided by Koppers Company, Inc., Pittsburgh, PA. I would like to thank Hank Mader, Barbara Wojtechko, and Ed Kifer, all of Koppers Company for the technical aid they provided. Special thanks to John Bluhm for the excellent SEM photos.

The assistance offered by Mike Dvorchak during the initial stages of this project is gratefully acknowledged. Also appreciated is the testing done by Dr. Andre Desjarlais of the Dynatech Corporation.

I would like to thank the following members of the MIT Heat Transfer Laboratory for their friendship and the helpful insight they provided concerning this project and the course work at MIT: Dauddy Bahar, Santo Chiapetta, Albert Dyrness, Keith Gawlik, Robert Giglio, Richard "Corrosion" Keck, Hamid Saedi, Andy Shapiro, Mark Torpey and Anthony Varone, Jr. Special thanks to Alex Ostrogorsky, who provided an infinite amount of help and guidance. Also, thanks to John Krutko and John Jabour for their personal encouragement during my studies at MIT.

I find it difficult to adequately express my gratitude to Paul and Leslie Regan. Their friendship and generosity they offered to me while at MIT is greatly appreciated. In addition, I would like to thank Leslie for the excellent typing of this thesis.

And finally, thanks be to God. Without His help and my faith in Him, the completion of this graduate program would not have been possible.

DEDICATION

I am fortunate to have the family and friends that so vastly enrich my life. Therefore, I dedicate this work:

To my Mother and Father, the greatest blessing I have ever received.

To my Grandmothers, whom I cherish.

To my brothers; Ron, Dave, and Mark

And lastly, I devote this writing to Mary, whose love, support, and patience towards me enabled the completion of this project.

NOMENCLATURE

A	area
C	concentration
C^*	fractional gas concentration
d	diameter
D	diffusion coefficient
E_p	activation energy
J	mass flux
L	length
$\langle \lambda \rangle$	distance between cell walls
M	mass
N_L	number of polymer/test line intersections per length
p	partial pressure
Pe	permeability coefficient
R	universal gas constant
S	solubility
S_v	surface area to volume ratio
T	temperature
t	thickness
V	volume
x	diffusion distance

Subscripts

act	actual
eff	effective
f	foam
g	gas
s	solid polymer

Greek

ρ	density
δ	void fraction
ϵ	enhancement parameter

TABLE OF CONTENTS

	<u>PAGE</u>
ABSTRACT.....	2
ACKNOWLEDGEMENTS.....	4
DEDICATION.....	6
NOMENCLATURE.....	7
TABLE OF CONTENTS.....	8
LIST OF FIGURES.....	10
LIST OF TABLES.....	12
CHAPTER 1 - INTRODUCTION.....	13
1.1 Introduction.....	13
1.2 Development of Closed-Cell Phenolic Foam.....	15
1.3 Previous Work.....	16
1.4 Fundamentals of Permeation.....	19
1.5 Project Approach.....	26
CHAPTER 2 - EXPERIMENTAL APPARATUS AND PROCEDURES.....	30
2.1 Introduction.....	30
2.2 Foam Tests.....	32
2.2.1 Introduction.....	32
2.2.2 Apparatus.....	37
2.2.2.1 Introduction.....	37
2.2.2.2 Foam Cell.....	37
2.2.2.3 The Constant Temperature Bath.....	44
2.2.2.4 Data Acquisition.....	46
2.2.3 Foam Samples.....	47
2.2.4 The Outgassing Phenomenon.....	50
2.2.4.1 Cleaning Procedures.....	50
2.2.4.2 Seals and Greases.....	51
2.2.5 Cell Assembly.....	51
2.2.6 Testing Procedures.....	52
2.2.7 Calibration.....	53
2.3 Film Tests.....	55
2.3.1 Introduction.....	55
2.3.2 Apparatus.....	58

	<u>PAGE</u>
2.3.2.2 The Film Cell.....	58
2.3.2.3 Data Acquisition.....	63
2.3.3 Film Samples.....	63
2.3.4 Cell Assembly.....	66
2.3.5 Testing Procedures.....	69
2.3.6 Calibration of the Film Test Cell.....	70
2.4 Foam Geometry Studies.....	70
2.4.1 Introduction.....	70
2.4.2 SEM Techniques.....	71
2.4.2.1 Previous Techniques.....	71
2.4.2.2 Current Project Technique.....	72
2.4.3 Polymer Distribution Within Foams.....	75
2.4.4 Determination of Cell Size and Shape.....	82
CHAPTER 3 - THE FOAM MODELS.....	88
3.1 Introduction and Background Work.....	88
3.2 Project Modeling Approach.....	88
3.3 Foam Modeled as Various Polyhedra.....	91
3.4 Foam Modeled as Closed-Packed Spheres.....	96
3.5 Polymer Distribution Effects on Foam Permeability.....	101
CHAPTER 4 - RESULTS AND OBSERVATIONS.....	104
4.1 The Foam Geometry Study.....	104
4.2 The Polymer Film Tests.....	109
4.3 The Phenolic Foam Tests.....	112
4.4 Determination of the Polymer Permeability From the Foam Models..	118
CHAPTER 5 - CONCLUSIONS AND RECOMMENDATIONS.....	123
5.1 Introduction.....	123
5.2 Accomplishments and Conclusions.....	123
REFERENCES.....	126
APPENDIX A - PHYSICAL PROPERTIES OF PHENOLIC FOAM.....	128
APPENDIX B - SAMPLE CALIBRATION CURVE FOR FOAM TEST CELL.....	130
APPENDIX C - STRUT AREA ANALYSIS.....	132
APPENDIX D - USE OF TRANSIENT CHARTS TO DETERMINE THE FOAM PERMEABILITY COEFFICIENT.....	134

LIST OF FIGURES

<u>FIGURE NUMBER</u>	<u>TITLE</u>	<u>PAGE</u>
1.1	SEM Photo of Cell Wall and Strut Area (1000x).....	17
1.2	Permeation Process of a Gas Through a Polymer Film....	20
1.3	Permeation in Foam Modeled as Successive Cell Walls...	24
1.4	Electrical Analogy of Foam Structure.....	25
1.5	Knudsen and Fickian Diffusion of a Gas Through A Solid.....	27
1.6	Schematic of Project Approach.....	28
2.1	Foam Test Cell with Capillary Tube.....	33
2.2	Foam Test Cell with Pressure Transducer.....	35
2.3	Foam Test Apparatus.....	38
2.4	Foam Test Components.....	39
2.5	Volume of Upper Chamber.....	41
2.6	Mean Free Path Analysis at Foam/Support Interface.....	43
2.7	Constant Temperature Bath Assembly.....	45
2.8	Data Acquisition Schematic.....	48
2.9	Calibration Set-Up of Foam Cell.....	54
2.10	Permeation in the Film Test Cell.....	57
2.11	Film Test Apparatus.....	59
2.12	Film Test Cell.....	60
2.13	Film Sample Ring.....	62
2.14	Optical Microscope Photos of Micro-Bubbles and Micro- Cracks in Phenolic Polymer Films (50x).....	65
2.15	Optical Microscope Photo of Polymer Film Thickness (100x).....	67

<u>FIGURE NUMBER</u>	<u>TITLE</u>	<u>PAGE</u>
2.16	3-D SEM Photo of Phenolic Foam (100x).....	73
2.17	SEM Photo of Embedded Polyurethane Foam (100x)..	74
2.18	SEM Photo Assortment of Closed-Cell Phenolic Foam.....	76
2.19	SEM Photo Montage with Grid (200x).....	78
2.20	Phenolic Foam Cell Elongation and Orientation...	79
2.21	Cell Elongation in Polyurethane Foam (100x).....	80
2.22	SEM Photo Showing Cell Wall - Strut Distinction for Strut Area Survey (1000x).....	85
3.1	Simple Cubic Foam Structure.....	89
3.2	Staggered Cubic and Elongated Cell Structures...	90
3.3	Cubic Cell Foam Modeled as a Sum of Resistances.	94
3.4	Closed Packed Sphere Model of Foam.....	98
4.1	SEM Photo Montage to Determine S_v (200x).....	105
4.2	SEM Photos of Phenolic Cell Wall Thickness.....	107
4.3	Optical Microscope Photos to Determine Polymer Film Thickness (200x).....	110
4.4	Optical Microscope Photos of Defects in Phenolic Polymer without Formaldehyde Additive.....	113
4.5	Optical Microscope Photos Showing Defects and Excessive Thickness in Phenolic Polymer with Formaldehyde Additive.....	114
4.6	Strip Chart Data of Initial Foam Tests Sug- gesting Knudsen Diffusion (CO_2 at $25^\circ C$).....	115
4.7	Initial Results of Foam Test Suggesting the Presence of Knudsen Diffusion.....	117
4.8	Typical Strip Chart Data from CO_2 Foam Test at $30^\circ C$	119

LIST OF TABLES

<u>TABLE NUMBER</u>	<u>TITLE</u>	<u>PAGE</u>
2.1	Geometric Parameters of Various Polyhedra When Combined in Aggregate Form.....	84
4.1	Results of Foam Density Predictions Using Various Polyhedron Aggregates.....	108
4.2	Initial Results of Phenolic Polymer Film Tests Using Defected Film Samples.....	111
4.3	Predicted Permeabilities of Phenolic Polymer with CO ₂ at 30°C Using Various Polyhedron Shapes.....	122
A.1	Physical Properties of Closed-Cell Phenolic Foam.....	129
D.1	Calculation of Foam Diffusion Coefficient with Transient Charts.....	136

CHAPTER 1
INTRODUCTION

1.1 Introduction

Rigid closed-cell foam has proven to be an invaluable product for industry and for the personal consumer. Its use for aircraft shell panels and refrigeration units, as well as for flat roof and wall insulation, typifies the demand for thermal insulating properties and structural strength combined in one product.

Two major types of rigid closed-cell foam, isocyanurates and polyurethanes, have dominated the marketplace over the past several years. However, a new form of closed-cell insulation was recently developed: phenolic foam. Phenolic has been used for rigid insulation for some time, but always in an open-cell form. Modern techniques have permitted one major manufacturer of building products to successfully blow phenolic resin into rigid board while maintaining a closed-cell composition. (Section 1.2)

Closed-cell foam obtains its superior insulating value, not from the polymer itself, but from the gas captured within each cell. Fluorocarbon (Freon) gas is generally utilized as the blowing agent due to its low thermal conductivity (approximately $\frac{1}{2}$ of that for stagnant air). This permits R-values to be higher than those for an open-cell foam or fiberglass batting and yet be rigid enough to provide structural strength. These qualities make closed-cell foam increasingly attractive to the construction industry.

The major drawback of closed-cell foam is the R-value degradation over time. This phenomenon is termed "aging" and occupies the scope of this project. The aging can be significant in some foams (as much as a 50% decrease in R-value for some urethanes and isocyanurates) and results in increasing energy usage to the consumer. Aging occurs when the gas components in air, mainly oxygen and nitrogen, diffuse through the cell walls of the foam and occupy the cells with the Freon gas. The gas mixture then has a higher thermal conductivity, thus lowering the overall R-value of the foam. This process usually takes place within one or two years. The aging continues over a much larger time scale as the Freon gas diffuses out of the cell and escapes to the atmosphere. These processes will be discussed further in Section 1.4. The most common attempt at preventing diffusion through the foam has been the application of a diffusion barrier to the face of the foam, usually some type of aluminum foil. This method has had very limited success due to the manufacturer's inability to obtain an adequate seal at the foam/foil interface. [1]

After perfecting the production method, the closed-cell phenolic foam was periodically tested by the manufacturer for R-value. These tests revealed that there was no change in R-value over time, thus suggesting that the aging phenomenon was not present. M.I.T.'s Energy Efficient Buildings Program was then asked to explain this behavior, and determine how long the foam will continue to hold its original R-value. This would be accomplished through the use of experimental techniques developed in previous work with polyurethane foams. Therefore, the goal of this project is to provide an initial investigation into the rigid closed-cell phenolic foam to determine the gas diffusion characteristics of the foam product

as well as the phenolic polymer.

1.2 Development of Closed-Cell Phenolic Foam

Although the first totally closed-cell phenolic foam was manufactured in 1982, phenolic foam in open-cell form was made as early as 1937, while the phenolic resin dates back to 1909. The phenol formaldehyde polymer was noted for its excellent fire resistance and the minimal toxic gases produced when heated. This thermoset plastic was also economically attractive since it was derived from synthetic petro-chemical products and the by-products from the coking of coal. [2] These qualities encouraged chemists to further develop phenolic foam insulation, but the unacceptable R-values of open-cell foam could not compete in the marketplace with the superior closed-cell polyurethanes and isocyanurates.

Closed-cell foam becomes open-celled when the cell walls begin to rupture during foaming. This is due to resin which has not yet had time to cure and strengthen, and is also due to the moisture present in the polymer. Early successes in manufacturing closed-cell phenolic were hampered by the formation of tiny pinholes in the cell walls; also, the thin cell walls would tend to dry out due to the hygroscopic (moisture absorbent) nature of the resin and crack under thermal and mechanical stresses. In order to perfect the manufacturing of these foams, a method was developed and patented whereby a series of chemical additives and formation techniques were used to foam the resin with a fluorocarbon gas (a 50/50 mixture of Freon 11 and Freon 113) and maintain a closed-cell structure, while the resin in the cell walls strengthens and cures [3]. By creating thicker cell walls, the mechanical strength and diffusion properties were also

improved. For a more detailed description of the manufacturing process, see [4] and [5].

1.3 Previous Work

Early studies with foam insulation at M.I.T. have dealt primarily with polyurethane foams. This research has dramatically increased the understanding and insight into gas permeation through foam products. The initial study by Schuetz and Glicksman determined that there are three modes of heat transfer through rigid foam insulation: conduction through the solid polymer lattice, conduction through the entrapped gas in each cell, and radiation through the foam [6]. Convective heat transfer within the cells was neglected due to the small cell size. Later, work by Reitz and Glicksman was concerned with the aging phenomenon, and a mathematical model to predict aging was developed [7]. This model takes the physical properties of the foam and the polymer (determined experimentally) and combines them into a simple lattice structure that can be analytically examined. The important physical parameters are: cell wall thickness, the cell wall permeability, cell size and the distribution of the polymer between the cell walls and the cell struts.* Reitz also developed many of the techniques necessary to determine the physical parameters.

One of the most significant discoveries was that for polyurethane and isocyanurate foams, only 15% to 20% of the polymer is contained in the cell walls, while the balance of the polymer is in the struts. Early

* Struts are defined as the build-up of polymer that occurs at the intersection of the cell walls. In accordance with surface tension theory and three-dimensional lattices, there are usually three cell walls intersecting to form a strut separated by angles of 120° . Therefore, cross-sections of the struts appear triangular in shape. (see Figure 1.1)

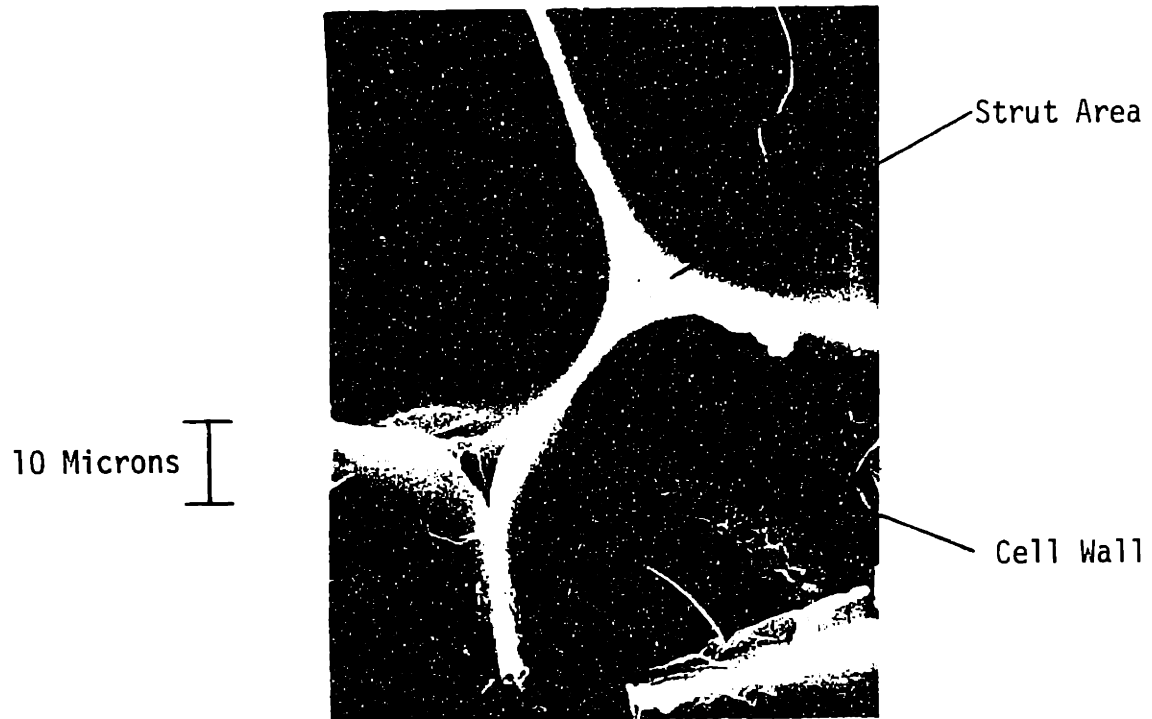


FIGURE 1.1: SEM Photo of Cell Wall and Strut Area (1000x)

reports cited an even distribution between the polymer in the walls and the polymer contained in the struts. Continuing efforts by Ostrogorsky at M.I.T. further developed the film and foam permeability tests (Chapter 2) and generated a computer code which would determine the R-value of the foam over long periods of time as a function of the foam's permeability to various gases [1]. He obtained correlations of the polymer permeability with the various gases and acquired excellent agreement between the analytical model and the foam permeability tests. Another significant achievement was the verification of the accelerated aging tests currently used in industry. These tests subject foam samples to elevated temperatures (60°C, 140°F) in order to expedite the aging process. A factor of 3 to 4 is generally used for the correlation between real-time and the simulated, "aged" time. Finally, he showed that diffusion of gases through closed-cell foams is driven solely by partial pressure gradients and is independent of temperature gradients other than the temperature affects on the polymer permeability.

Since closed-cell phenolic foam is relatively new to the marketplace, very little data are available concerning its permeation characteristics; however, the small data obtainable suggest that it possesses excellent diffusion properties, particularly for the molecularly larger fluoro-carbon gases. The addition of chemical additives by the manufacturer enhance the closed-cell formation and alter the resin to a unique chemical (and physical) composition. Therefore, the results obtained in this project will remain, for the most part, valid for the specific foam tested and not for phenolics in general.

1.4 Fundamentals of Permeation

Permeation is the process that governs the aging in closed-cell foams. It can be described as the movement of a gas from one side of a solid membrane, to the other side, and is divided into three parts:

- 1) absorption of the gas into the solid,
- 2) diffusion of the gas through the solid
- and 3) the release of the gas from the solid to the environment on the other side of the membrane. [8]

The driving potential for such a process is the gas concentration gradient (i.e., gas permeates from high gas concentrations to low gas concentrations) but, as it will be shown, is not solely dictated by a diffusion coefficient according to the molecular structure of the solid. The solubility of the gas within the polymer governs the initial stage of the permeation process and thus partially controls the overall procedure. A graphical explanation of this procedure is shown in Figure 1.2. Ostrogorsky describes a more detailed thermodynamic explanation based on chemical potential, but it is beyond the scope of this project [1].

From a mathematical perspective [9], the permeation can be calculated by first treating the solid material as a homogeneous medium and assuming Fick's Law of Diffusion applies:

$$J = -D \frac{\partial C}{\partial x} \quad (1-1)$$

- where
- J = gas flux through the solid (mass flow per unit time per unit area)
 - D = mass diffusion coefficient
 - C = gas concentration within the polymer

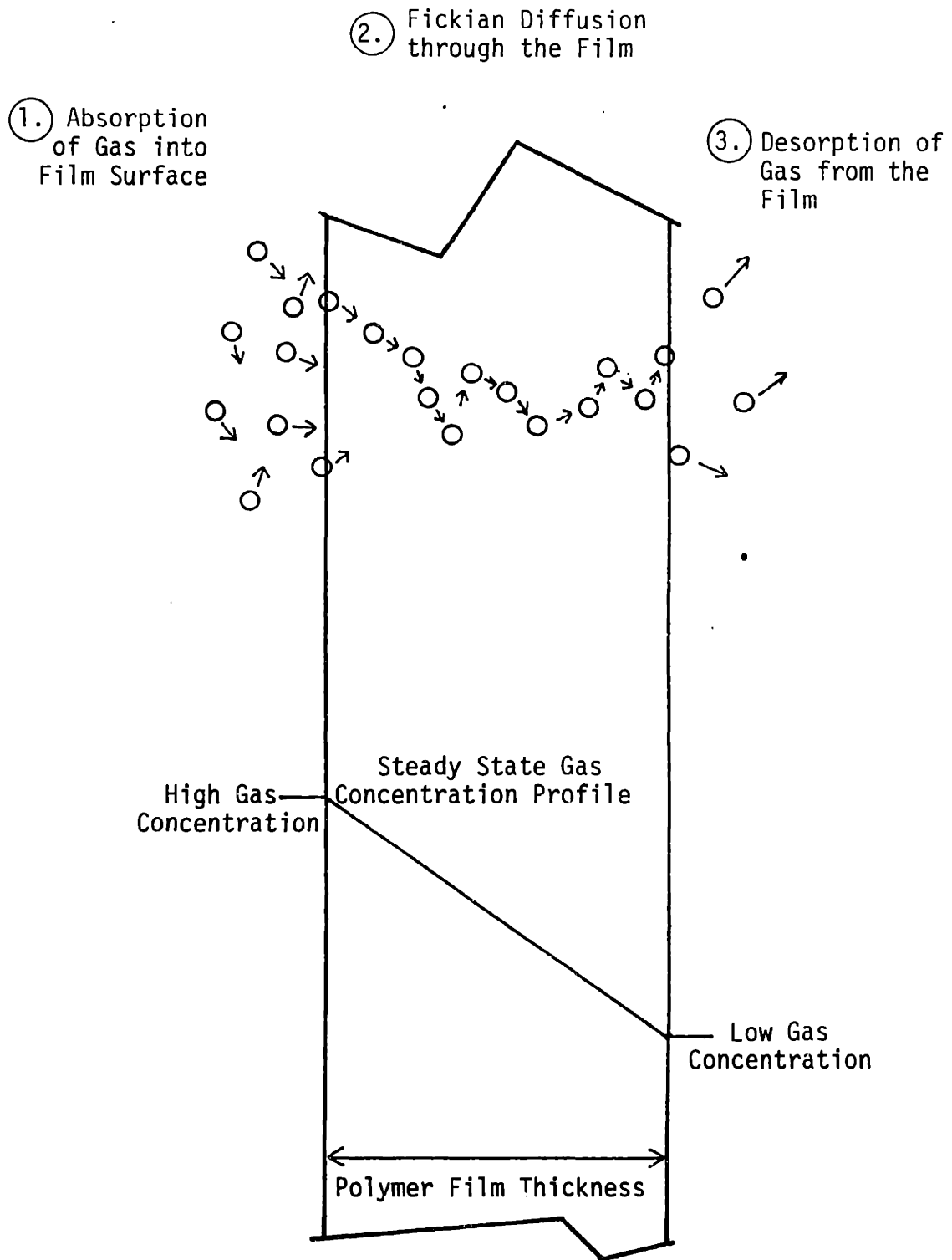


FIGURE 1.2: PERMEATION PROCESS OF A GAS THROUGH A POLYMER FILM

x = diffusion distance across the membrane wall

Now, define the fractional gas concentration as the gas concentration in the solid divided by the density of the gas:

$$C^* = \frac{C}{\rho_{\text{gas,mixture}}} \quad (1-2)$$

and let $x = t$ = the thickness of the solid,

then:

$$J = D \rho_{\text{gas,mixture}} \frac{(C_1^* - C_2^*)}{t} \quad (1-3)$$

where C_1^* = high fractional gas concentration

and C_2^* = low fractional gas concentration

The next assumption made is that the fractional gas concentration at the solid/gas interface is directly proportional to the partial pressure of gas above the interface [10]. This relationship is known as Henry's Law and the constant of proportionality is the solubility of gas within the solid, or:

$$C^* = Sp \quad (1-4)$$

where C^* = fractional gas concentration

S = solubility of the gas within the solid

p = gas partial pressure above the solid

The solubility has units of volume of gas dissolved per unit of solid per atmospheric pressure. If Equation (1-4) is substituted into Equation (1-3), then

$$J = \rho DS \frac{(p_1 - p_2)}{t} \quad (1-5)$$

or

$$\frac{\dot{V}}{A} = DS \frac{(p_1 - p_2)}{t} \quad (1-6)$$

where \dot{V} = volumetric flowrate
 A = diffusion area

Now define the permeability coefficient:

$$Pe \equiv (D)(S) \quad (1-7)$$

and Equation (1-6) becomes:

$$\frac{\dot{V}}{A} = Pe \frac{(p_1 - p_2)}{t} \quad (1-8)$$

and the permeability coefficient can be determined by:

$$Pe = \frac{(\dot{V})(t)}{(A)(p_1 - p_2)} \quad (1-9)$$

Equation (1-7) now clearly shows how the mass diffusion coefficient plus the solubility must be combined to describe the overall permeation process. It is interesting to note that the diffusion appears to be more of a physical parameter based on the size and structure of the molecular lattice of the solid. In other words, it is a question of whether the gas molecules can "fit" through the molecular voids of the polymer as they are driven by their own concentration gradients. Therefore, gas molecules of similar diameter should have similar diffusion coefficients through a given substance. Solubility, on the other hand, appears to be controlled by a chemical process. The molecular affinity between the gas and the solid, or the lack of it, seems to determine how readily soluble the gas

is within the polymer. Also, it should be remembered that the gas must first be absorbed into the surface layer of the polymer before the actual diffusion can take place. This is why the permeability of similar-size gas molecules can vary greatly for a particular solid.

The basis for permeation through a solid membrane can now be expanded to describe permeation through closed-cell foams. These foams can simply be thought of as a succession of cells and cell walls (Figure 1.3). Since the permeation of a gas through another gas is many orders of magnitude greater than that of a gas through a solid, the resistance to permeation of the cell voids can be considered negligible. Figure 1.4 shows an equivalent electrical analogy for the cell structure. The cell voids have negligible resistance, but they do provide the majority of the gas storage capacity for the entire foam. Also, the partial pressure gradient for each gas present in the cell is assumed to be zero across the diameter of the void. Therefore, a gas molecule, driven by its own partial pressure gradient, will be absorbed into a cell wall, diffuse through the membrane and be desorbed to the other side. The molecule will then be stored in the cell void until such time when it will again be absorbed into the next succeeding cell wall, and so on.

The effect of temperature on foam permeability is described by the Arrhenius expression:

$$P_e = P_{e_0} \exp(-E_p/RT) \quad (1-10)$$

where P_{e_0} = experimental constant
 E_p = activation energy of permeation
 R = universal gas constant
 T = absolute temperature

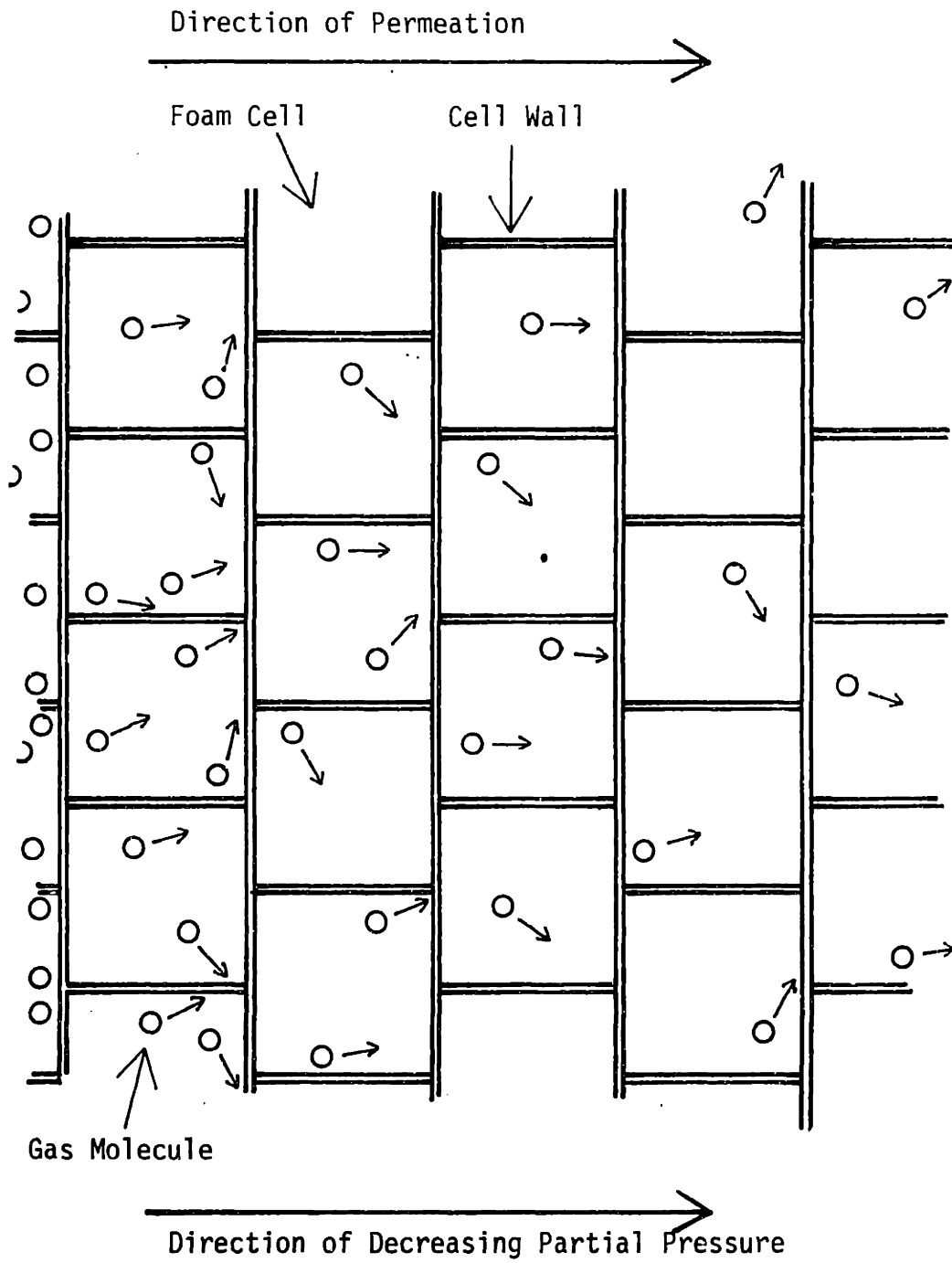


FIGURE 1.3: PERMEATION IN FOAM MODELED AS SUCCESSIVE CELL WALLS

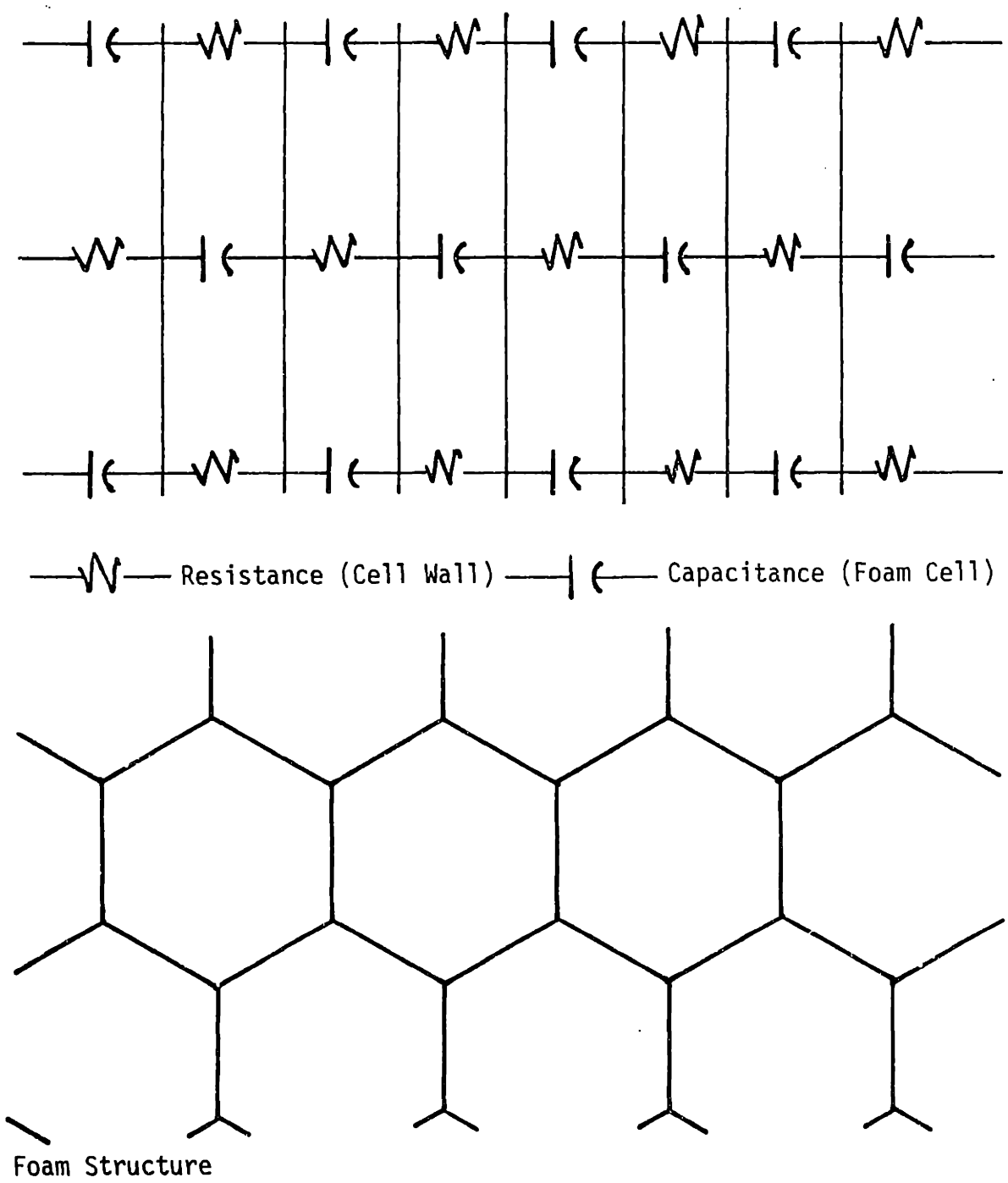


FIGURE 1.4: ELECTRICAL ANALOGY OF FOAM STRUCTURE

Therefore, by increasing the temperature of the foam product, the ability of a gas to permeate through the foam should also increase.

Equation (1-9) will be used to determine the permeability coefficients for the cell walls and for the overall foam insulation. However, in foams, the permeability coefficient is actually considered as an effective permeability, $P_{e_{eff}}$. This accounts for the fact that the foam is not solid polymer and has significant gas storage capacity in the cells. Fick's Law and Henry's Law should apply for both cases; however, homogeneity becomes a major concern - particularly for the foam samples. An inhomogeneous product will become subject to other phenomenon of mass transport such as Knudsen diffusion [11]. Knudsen diffusion occurs when there are openings in the solid of the same length scale as the mean-free path of a gas molecule. (≈ 1 micron). See Figure 1.5. The gas will then diffuse through the solid at much higher flowrates determined by total gas pressure gradients, not according to Fickian diffusion which is independent of total pressures. Although the Knudsen flowrates will be higher than Fickian diffusion flowrates at pressures above atmospheric, they will, however, be many orders of magnitude less than that of a bulk flow leak, and can be confused with permeation-related flow.

1.5 Project Approach

The approach that will be used in this project to determine the aging characteristics of phenolic foam is divided into two methods: a) a direct foam experimental measurement and b) an analytical model. The results of these two methods will then be compared. Figure 1.6 shows a simplified schematic of the approach.

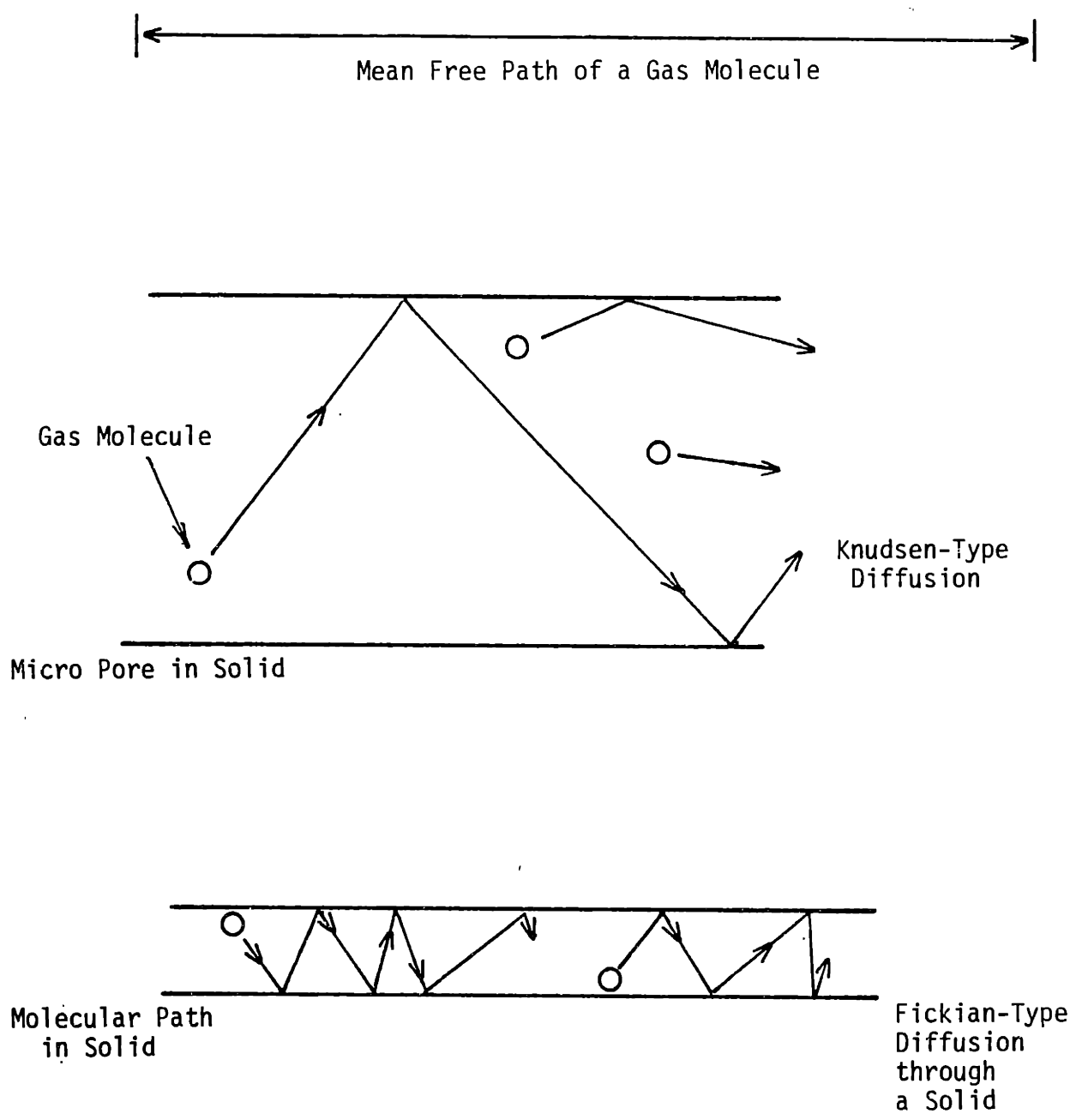


FIGURE 1.5: KNUDSEN AND FICKIAN DIFFUSION OF A GAS THROUGH A SOLID

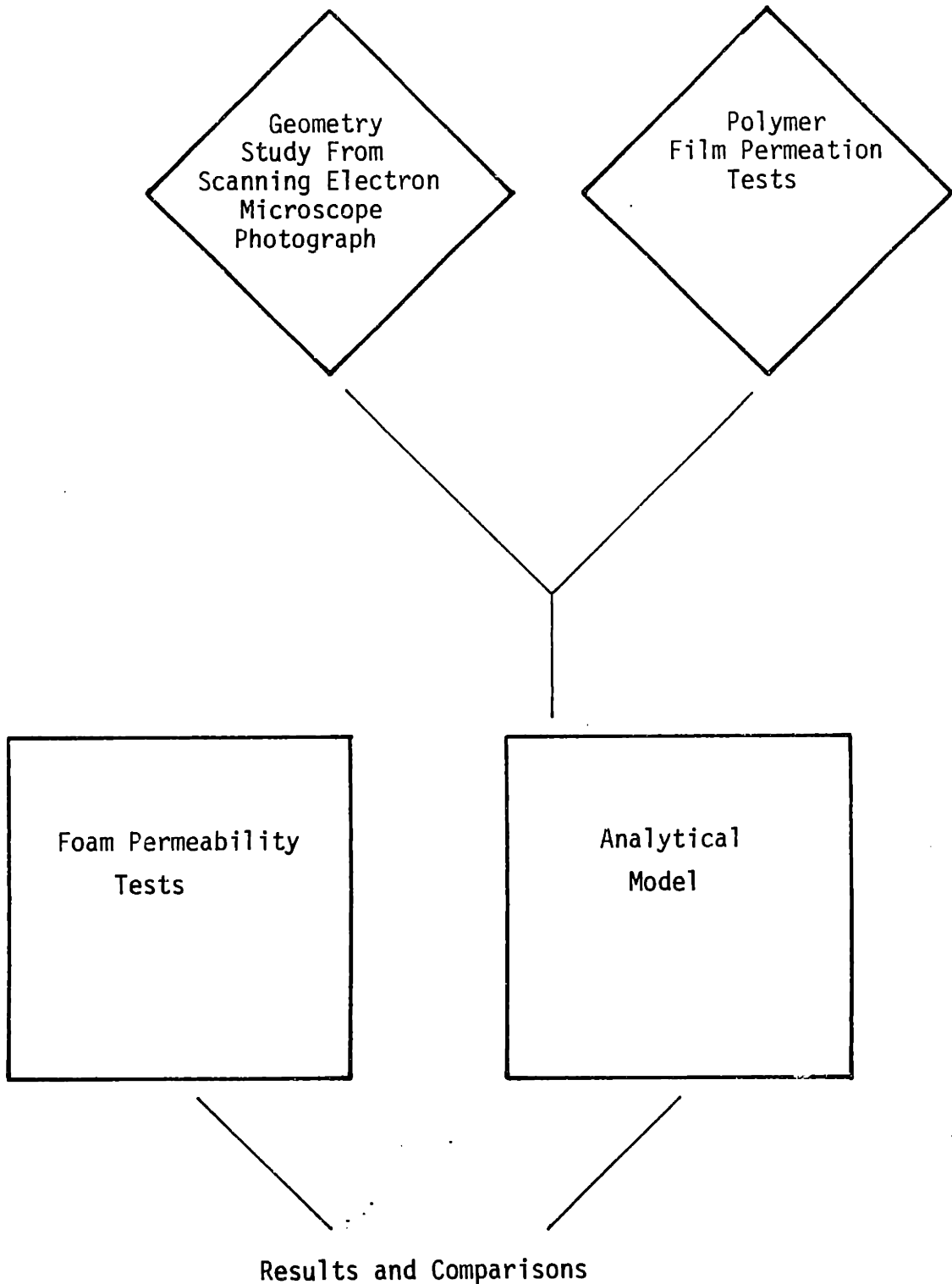


FIGURE 1.6: SCHEMATIC OF PROJECT APPROACH

The direct foam permeability measurement consists of obtaining a manufactured sample of foam product and subjecting it to a partial pressure difference of test gas across its thickness. The volumetric flowrate due to gas permeation through the foam will then be measured on the low pressure side of the sample. The analytical model requires that the permeability of the phenolic polymer be determined by subjecting a film of polymer to a partial pressure difference and again, measuring the resulting volumetric flowrate. Also necessary is a geometric study of the cell formation which includes the cell wall thickness, polymer distribution and cell diameter. Once the foam geometry and polymer permeation characteristics are known, the foam product can be modeled as a succession of cell walls and voids, and the permeation of various gases driven by their own partial pressures can be mathematically predicted.

CHAPTER 2
EXPERIMENTAL APPARATUS AND PROCEDURES

2.1 Introduction

The experimental aspects to this project consisted of three main areas: phenolic foam permeability tests, phenolic polymer film permeability tests, and phenolic foam cell geometry studies. As mentioned in Section 1.5, the film tests and geometry studies will be combined through the use of a mathematical model to confirm the foam permeability results. A description of this model can be found in Chapter 3.

Experimental techniques to measure foam and film permeabilities have been developed throughout industry and research, including MIT. Many of the approaches previously implemented carried with them prohibitively high costs, the use of exotic apparatus, or techniques that produced inaccurate or unrepeatably results (particularly for long term data acquisition periods). Examples include gas spectrometers, transient measurement techniques, and volumetric measurements that are "opened" to the environment and can ultimately be affected by barometric pressure changes. It was the intent of this project to build and utilize an apparatus that would be relatively simple in design and low in cost, but generate the suitable results in a reasonably short period of time that are necessary for future research and development in the foam insulation industry.

One significant improvement for the foam permeability tests was the development of the rapid steady-state technique by Ostrogorsky at MIT [1]. Since a steady-state, or linear, concentration gradient is necessary for

accurate measurements in a foam sample, it is useful to obtain this state as rapidly as possible. From the Arrhenius-type equation for permeability; $P_e = P_{e_0} \exp(-E_p/RT)$, it is evident that permeation is enhanced by an increase in temperature. In fact, Ostrogorsky determined that for polyurethane foams, air components will diffuse approximately 10 times faster with an increase of 50°C above room temperature. The rapid steady-state technique utilizes this temperature dependence by establishing a linear concentration profile at high temperatures and preserving steady-state as the foam is cooled to lower temperatures. To do this, the foam is isolated from the environment after reaching its high temperature steady-state condition. The linear concentration gradient is then maintained as the pressures are altered simultaneously with controlled temperature changes within the foam sample and apparatus through the ideal gas laws. Permeation measurements are then ready to be taken at a desired temperature as soon as thermal equilibrium is established. (Section 2.2.6).

The film tests were used to determine the permeability of the solid phenolic polymer. This was a relatively simple test that, again, used concentration gradients as the driving potential and determined the permeation from measurements of the volumetric flowrates.

The foam cell geometry was found through the use of scanning electron microscope photographs. Important parameters from the geometry studies included cell wall thickness, percentage of polymer in the cell struts versus the cell walls, and foam cell diameter.

2.2 Foam Tests

2.2.1 Introduction

In order to implement the results obtained from the mathematical model, it was necessary to determine the foam permeability coefficients experimentally. Various techniques are described in [9]. Early studies at MIT utilized the volumetric or variable volume method (ASTM D1434-75) due to its relatively low cost and simple design. In this method, a foam sample is sealed between two chambers and subjected to a pressure (i.e., concentration) difference across the sample. The test gas, at high pressure in the lower chamber, then diffuses through the foam and into the upper chamber, which is at atmospheric pressure. The volumetric gas diffusion rate is then measured by the movement of a slug in a capillary tube attached to the upper chamber (Figure 2.1). This method later proved to be inaccurate for long term (over 1 hour) testing due to changes in atmospheric pressure that occurred while taking data [1]. The non-constant ambient conditions would enhance or prevent the upward movement of the slug as the barometric pressure would fall or rise, respectively. It was then decided to measure the volumetric diffusion rates by means of an absolute pressure transducer and correlate the pressure increase in the upper chamber to a constant pressure increase in volume as a function of time. The mass diffusion rate could then be calculated knowing the density of the test gas. Since the absolute transducer measured pressure changes with respect to vacuum, this technique was not affected by changes in ambient pressure.

The approach to this measurement, as mentioned earlier, was to subject a foam sample to a pressure difference across its thickness, and determine

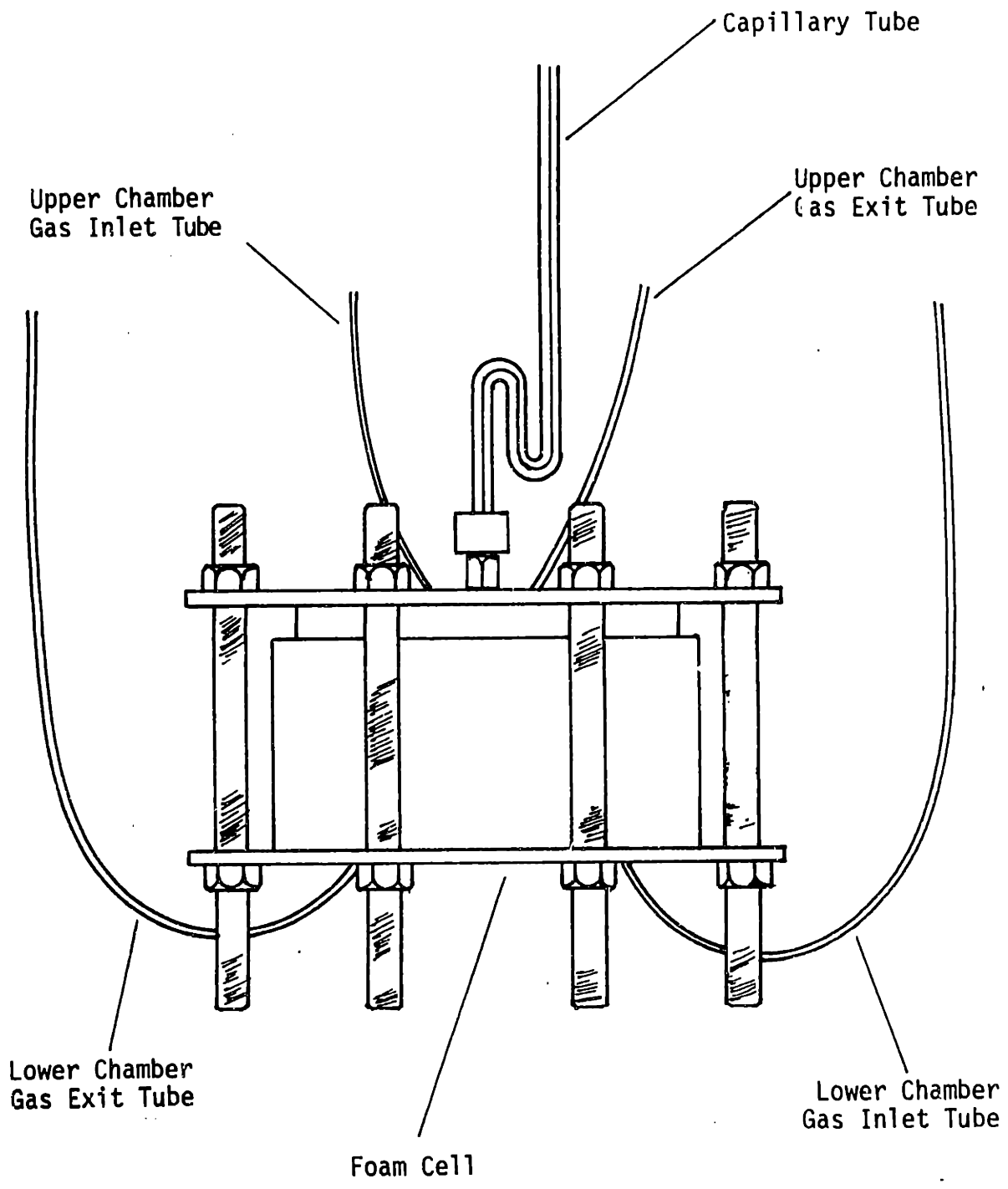


FIGURE 2.1: FOAM TEST CELL WITH CAPILLARY TUBE

the volumetric flowrates as the gas diffuses from the high pressure side to the low pressure side according to Equation (1-9):

$$P_e = \frac{\dot{V}(t)}{(p_1 - p_2)(A)} \quad \text{Also see Figure 2.2.}$$

There were several important points to consider when designing the apparatus:

- The volumetric flowrates were expected to be very small - on the order of $1 \times 10^{-3} \text{ mm}^3/\text{sec}$ ($6.1 \times 10^{-8} \text{ in}^3/\text{sec}$); therefore it was very important to minimize the volume of the upper chamber to increase the sensitivity of the apparatus.
- Due to the very small flowrates, any outgassing effects would prove to be an important source for error in the measurements. To prevent this, the entire apparatus would have to be constructed from stainless steel, and any material possessing capacitive properties for dissolved gases could not be used (e.g., rubber, paper, etc.).
- Extensive cleaning procedures would be necessary to eliminate contaminated surfaces that could become volumetric outgassing sources.
- To minimize the possibility of leakage, the use of solid stock machining should be used wherever possible, and any welding performed should be done in accordance with sophisticated techniques used in vacuum technologies.
- Since rubber seals could not be used, another type of sealing material would be necessary. Indium metal was found to have excellent sealing properties, and could be thoroughly cleaned so as not to become an outgassing source in the apparatus.

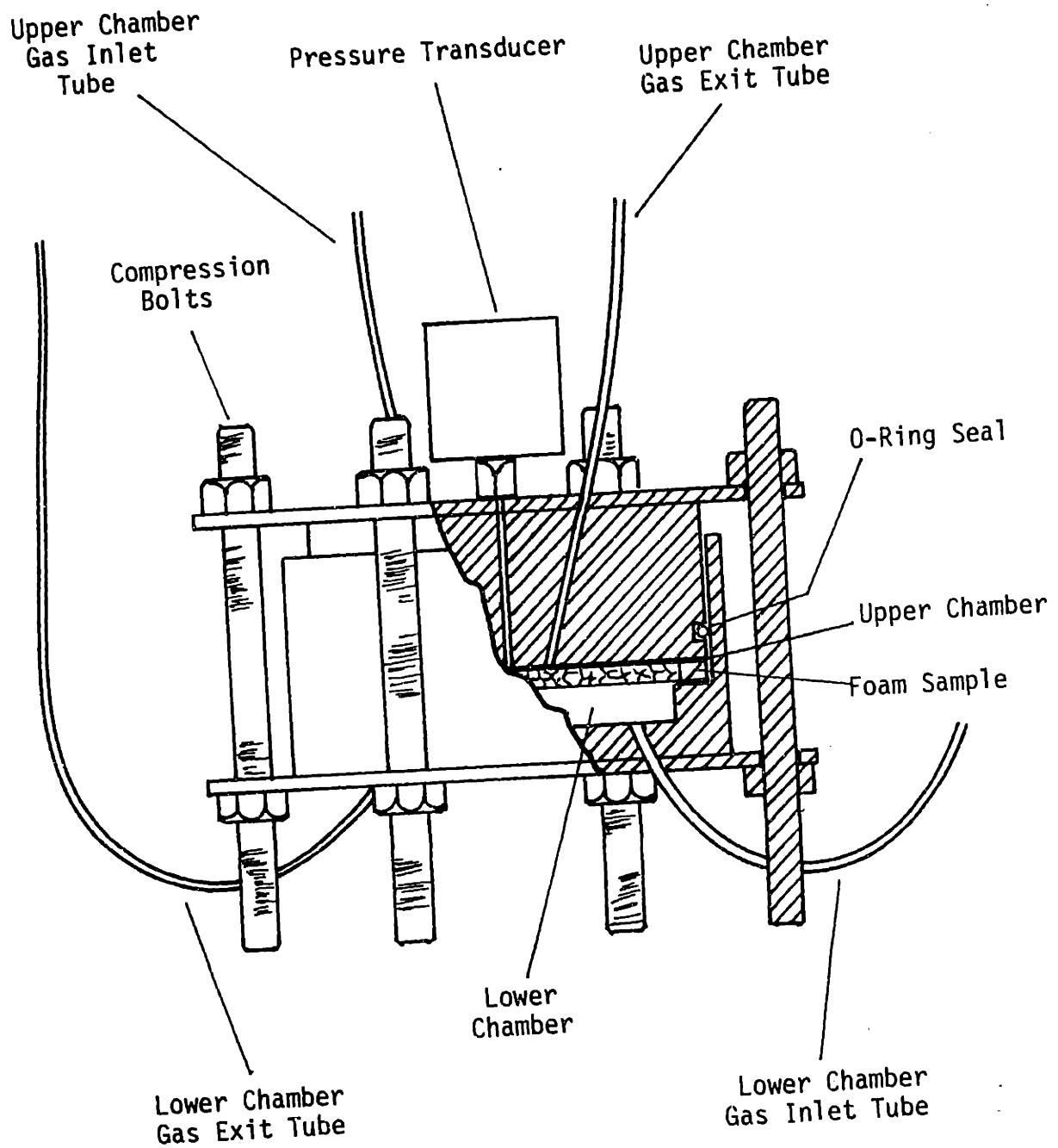


FIGURE 2.2: FOAM TEST CELL WITH PRESSURE TRANSDUCER

- All greases and glues would have very low vapor pressures while maintaining excellent sealing and adhesive properties at accelerated temperatures.
- Since the repeatability of the measurement would require that constant boundary conditions (i.e., pressures) be maintained throughout the experiment, high and low pressure reservoirs would be necessary, so that external barometric pressure effects could be eliminated. Also, the volume of the reservoirs would need to be large enough so that changes in pressure by volumetric flowrates and the ideal gas law would be negligible during testing.
- The absolute pressure transducer was found to be very temperature dependent relative to the sensitivity of the measurements. A constant thermal environment around the transducer would eliminate affects due to changes in the ambient laboratory climate.
- As discussed in Section 1.4, permeation behaves according to an Arrhenius-type expression of the form

$$P_e = P_{e_0} \exp(-E_p/RT) \quad (1-10)$$

where

P_{e_0}	=	experimental constant
E_p	=	activation energy of permeation
R	=	universal gas constant
T	=	absolute temperature

Therefore, close, constant temperature control is necessary throughout the experiment for repeatable and accurate results. Also, according to Ostrogorsky's rapid steady-state procedure [1], temperature control is also necessary so that the sample can quickly establish a linear and steady-state concentration gradient at an elevated temperature, and the linearity of the gradient could then be maintained as the temperature is uni-

formly lowered. (Section 2.1)

The application of the preceding design concerns will become more apparent to the reader and discussed in further detail in the following sections.

2.2.2 Apparatus

2.2.2.1 Introduction

The foam permeability apparatus, shown in Figure 2.3, is comprised of three major components; a) the foam cell, b) the constant temperature bath, and c) the data acquisition system. These parts will be discussed in further detail.

2.2.2.2 Foam Cell

The components of the foam cell include: the lower chamber, the upper chamber, the sample ring, the low pressure reservoir, the high pressure reservoir, and a plexiglas container. These parts are shown in Figure 2.4, and their operational importance will be discussed in Sections 2.2.5 and 2.2.6.

The lower chamber was machined from 5 in. 304 stainless steel round stock to an outer diameter of 4.98 in. and an overall length of 2.50 in. The inner bore dimensions are 4.540 in. diameter x 1.625 in. deep for the upper section and 3.760 in. diameter x 0.535 in. deep for the lower section. This design will accommodate samples ranging in thickness from $\frac{1}{8}$ in. to 1 in. A $\frac{1}{8}$ in. thick piece of 304 stainless steel plate was then cut to a diameter of 7 in. and welded to the bottom of the lower chamber. Six $\frac{5}{8}$ in. diameter holes were drilled symmetrically around the chamber and two $\frac{1}{8}$ in. holes were drilled through the center of the entire piece. Stainless steel

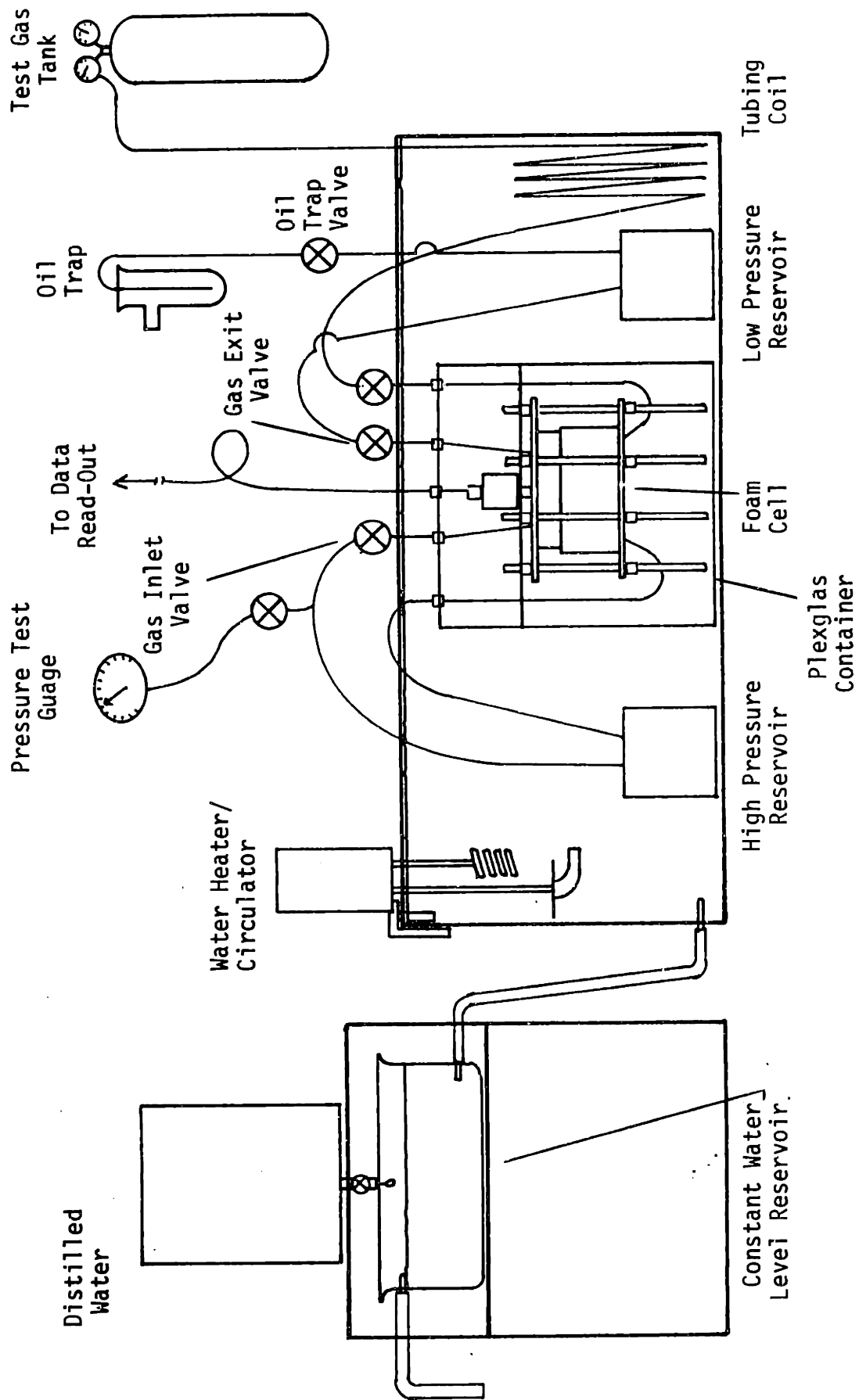


FIGURE 2.3: FOAM TEST APPARATUS

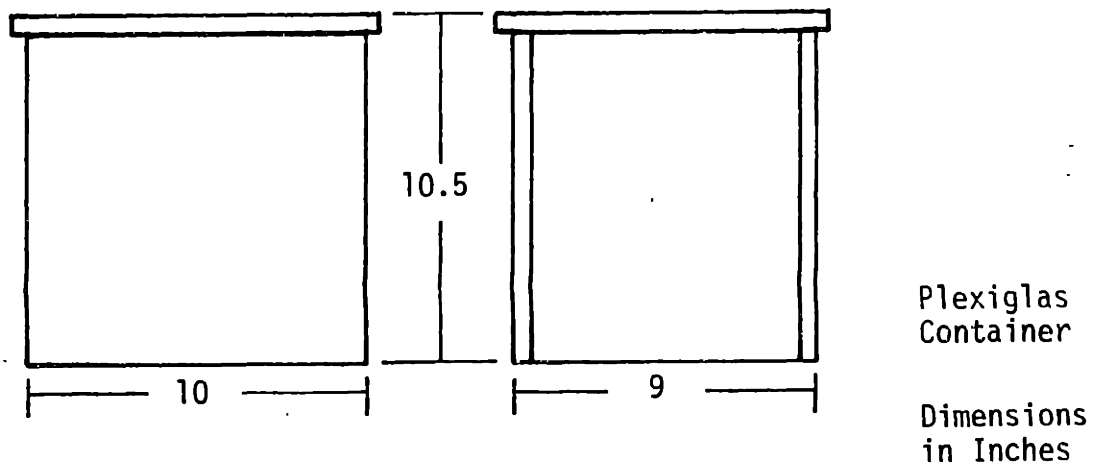
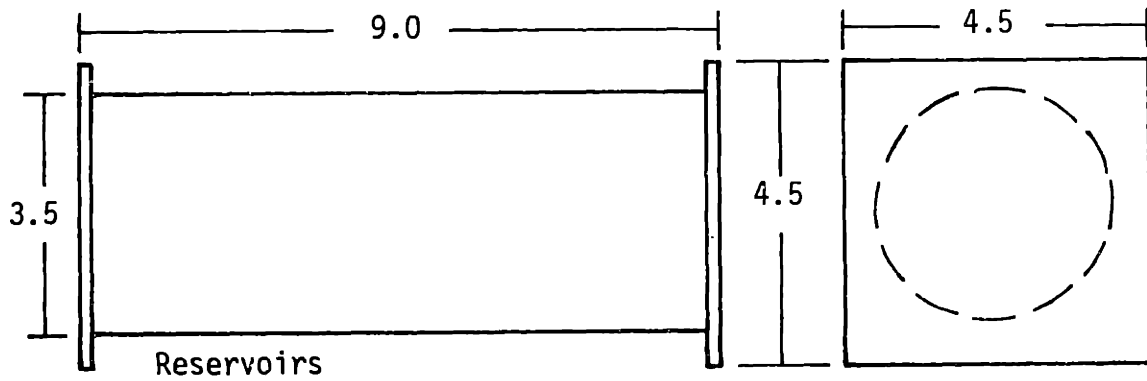
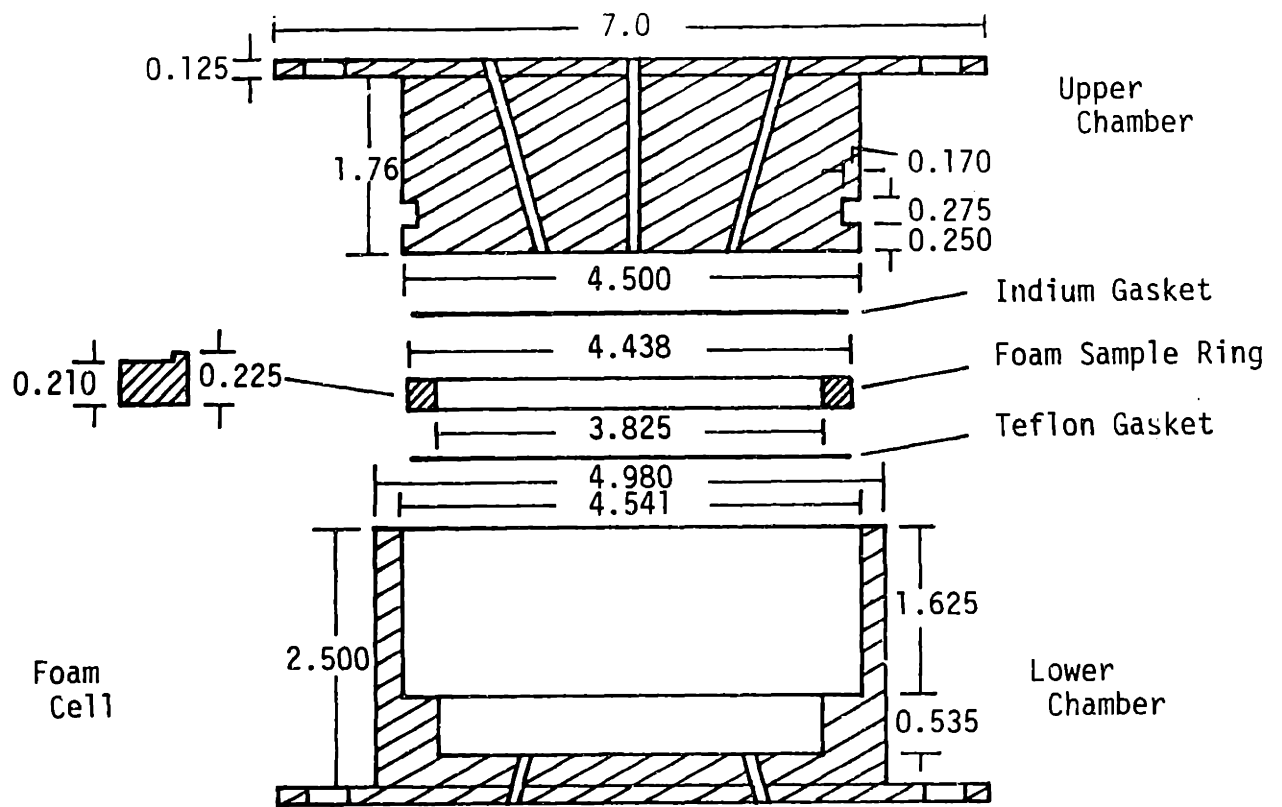


FIGURE 2.4: FOAM TEST COMPONENTS

$\frac{1}{8}$ in. tubing with a 0.035 in. wall was then placed through the holes and heli-arc welded from the inside of the chamber. This welding technique assured that no impurities could be lodged between the outside of the tubing and the $\frac{1}{8}$ in. hole, and that the thorough cleaning of the piece would be simplified. Also included in the lower chamber assembly was a small foam sample support, 3.0 in. diameter x 0.535 in. high, to prevent sample breakage in the event of the upper chamber being over pressurized.

The upper chamber was also machined from 5 in. 304 stainless steel which was turned to a diameter 4.5 in. A 0.275 in. wide by 0.170 in. deep groove was then cut 0.250 in. from the end to accommodate a water-tight rubber O-ring seal. A $\frac{1}{8}$ in. thick piece of 304 stainless steel was again cut to a diameter of 7 in. and welded to the top of the piece, where six $\frac{5}{8}$ in. diameter holes were drilled so as to align with the lower chamber holes. Three $\frac{1}{8}$ in. diameter holes drilled through through the entire upper chamber to fit the stainless steel gas inlet and exit tubes and also the transducer tube. These tubes were also heli-arc welded from the inside in accordance with the same vacuum techniques mentioned earlier.

Although this portion of the cell is referred to as a "chamber", its volume is actually quite small. In fact, foam support against the pressure differential is provided directly by this piece. Therefore, the volume of the upper chamber is simply the inner volume of the inlet and exit tubing and the sensing chamber of the pressure transducer. There is also a minute volume contribution associated with the foam/steel interface as shown in Figure 2.5. The total volume of the upper chamber is estimated to be 1100 mm³ with a foam surface area/upper chamber volume ratio of 6.7. This ratio was an important consideration in the cell design as a larger ratio

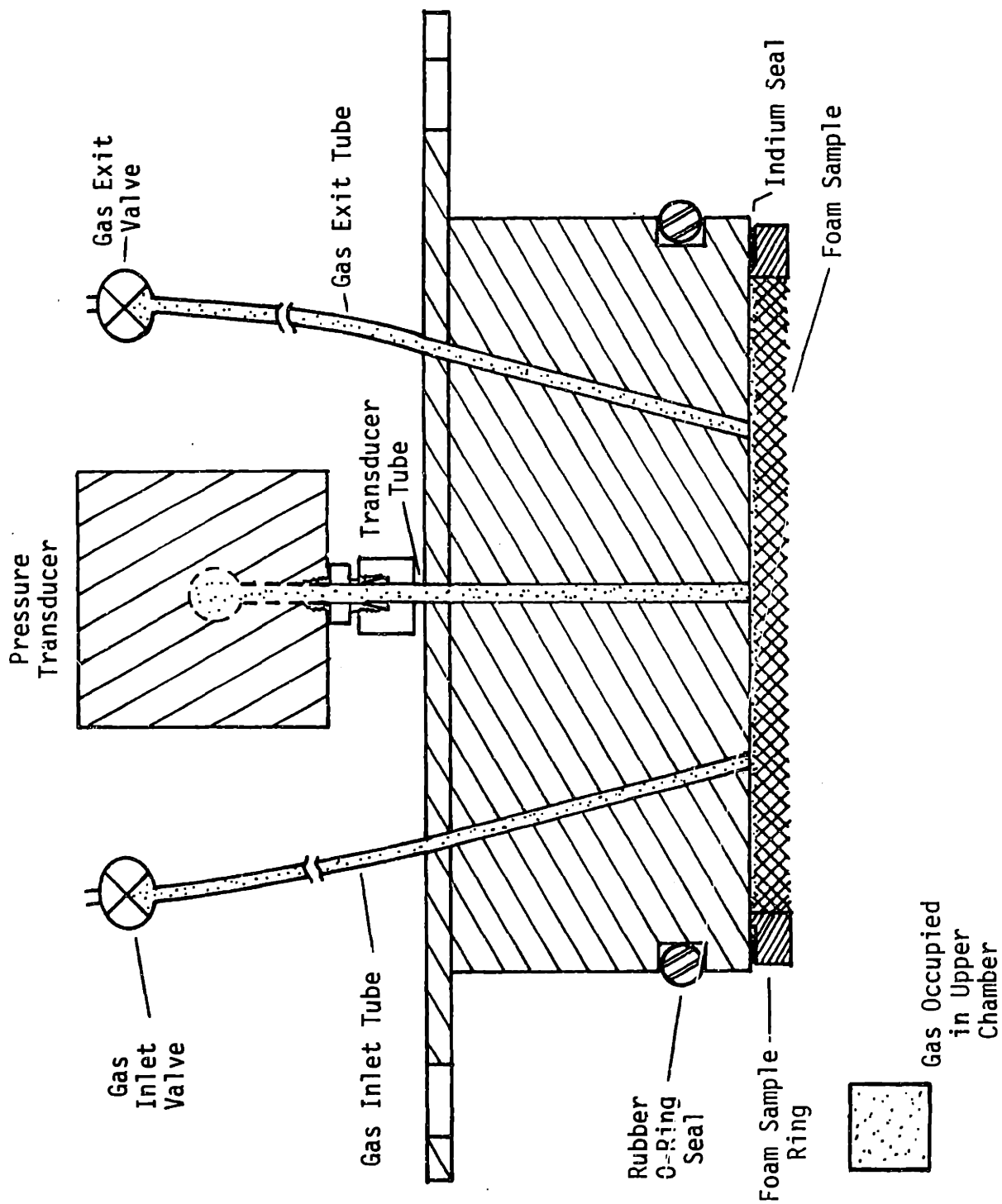
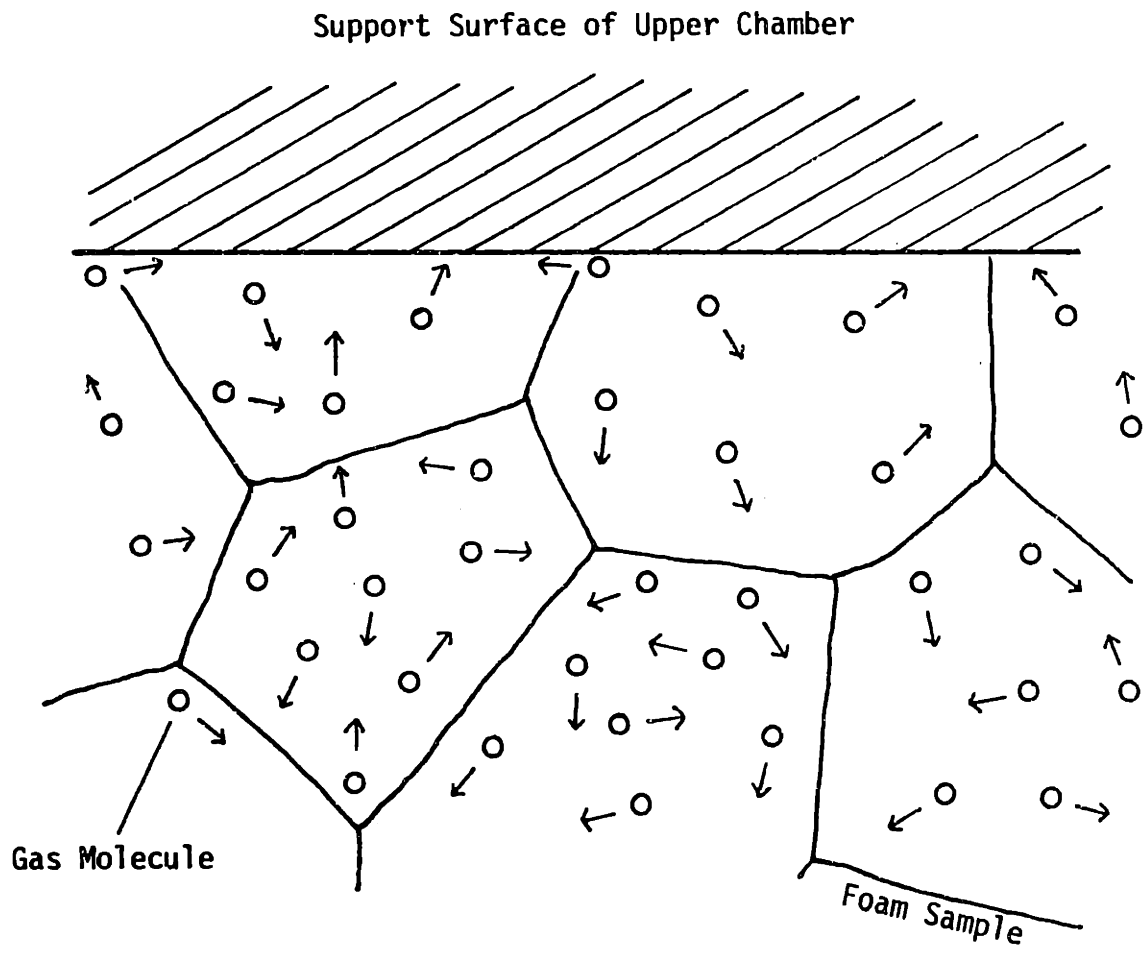


FIGURE 2.5: VOLUME OF UPPER CHAMBER

will result in a more pressure sensitive foam cell. It should be noted that there was concern over whether such a design (no separate upper support) would affect the pressure measurements, considering that the foam sample directly covered the transducer port and the inlet and exit tube openings. This concern was alleviated after considering that the cell size of the phenolic foam varied from 70 to 300 microns and that the initial layer of foam resting against the upper chamber consisted of broken cells and a non-uniform surface having voids of the same order of magnitude (say, 100 microns). The mean free path of a gas molecule at atmospheric pressure is on the order of 1-10 microns [12], therefore, a negligible resistance occurs between the foam interface and the upper chamber (Figure 2.6).

The foam sample ring was cut from a piece of 4.5 in. 304 stainless steel tubing. The finished dimensions are inside diameter, 3.825 in., and outside diameter, 4.438 in. The overall thickness (and, consequently, the foam sample thickness) is 0.225 in. A small indentation was cut into the upper surface of the ring to accept an indium gasket. This permitted a tight seal with the indium upon compression, but eliminated the volume associated with the gasket thickness (Figure 2.5). Indium metal was utilized for its excellent sealing characteristic and its very low outgassing properties.

The low pressure and high pressure reservoirs were similarly constructed from 3.5 in. diameter 304 stainless steel tubing, each 9.0 in. in length. Two holes of $\frac{1}{8}$ in. diameter were drilled through the sides of each tube and $\frac{1}{8}$ in. stainless steel tubing was inserted and welded. The entire inner surface was cleaned with successive applications of acetone and 200-proof ethyl alcohol and then placed in an ultrasonic cleaner filled with distilled water. The reservoirs were then heated to approximately



—| Mean Free Path of a Gas Molecule

—| Length Scale of Openings at Foam/Support Interface

FIGURE 2.6: MEAN FREE PATH ANALYSIS AT FOAM/SUPPORT INTERFACE

800°F and then cooled. These techniques assured that no outgassing would occur from the inner surfaces. Endcaps constructed of $\frac{1}{8}$ " stainless steel plate were similarly cleaned and welded into place.

The plexiglas container, with outer dimensions of 10 in. length by 10.5 in. height by 9 in. width was fabricated from $\frac{1}{2}$ in. plexiglas plate. The sides and bottom were attached by means of stainless steel allen bolts and the necessary water seal was assured by using $\frac{1}{16}$ in. rubber gaskets and General Electric RTV 106 high temperature silicon rubber adhesive sealant. The top piece was bolted into place and sealed with a one-piece rubber gasket. Since the box would be opened and closed many times throughout the test program, the adhesive sealant was replaced with vacuum grease. Sealing around the stainless steel tubing was achieved by use of compression fittings and number 6 O-Rings.

2.2.2.3 The Constant Temperature Bath

The constant temperature bath was constructed from an 18 gallon glass aquarium tank measuring 30 in. long x 12 in. wide x 12 in. deep. Two holes were drilled into the lower portion of the tank - one for drainage; the other connecting to the constant water level reservoir. This reservoir assured that the amount of water in the tank would remain steady without heating excessive amounts of make-up water. (Figure 2.7) To minimize heat loss, the sides of the tank were covered with foam board insulation, and the top was fitted with a $\frac{3}{16}$ in. plexiglas cover. The cover greatly reduced the heat and mass losses associated with testing at the elevated (above 50°C) temperatures. Distilled water was used for the bath and make-up water to keep the apparatus clean and free of mineral deposits.

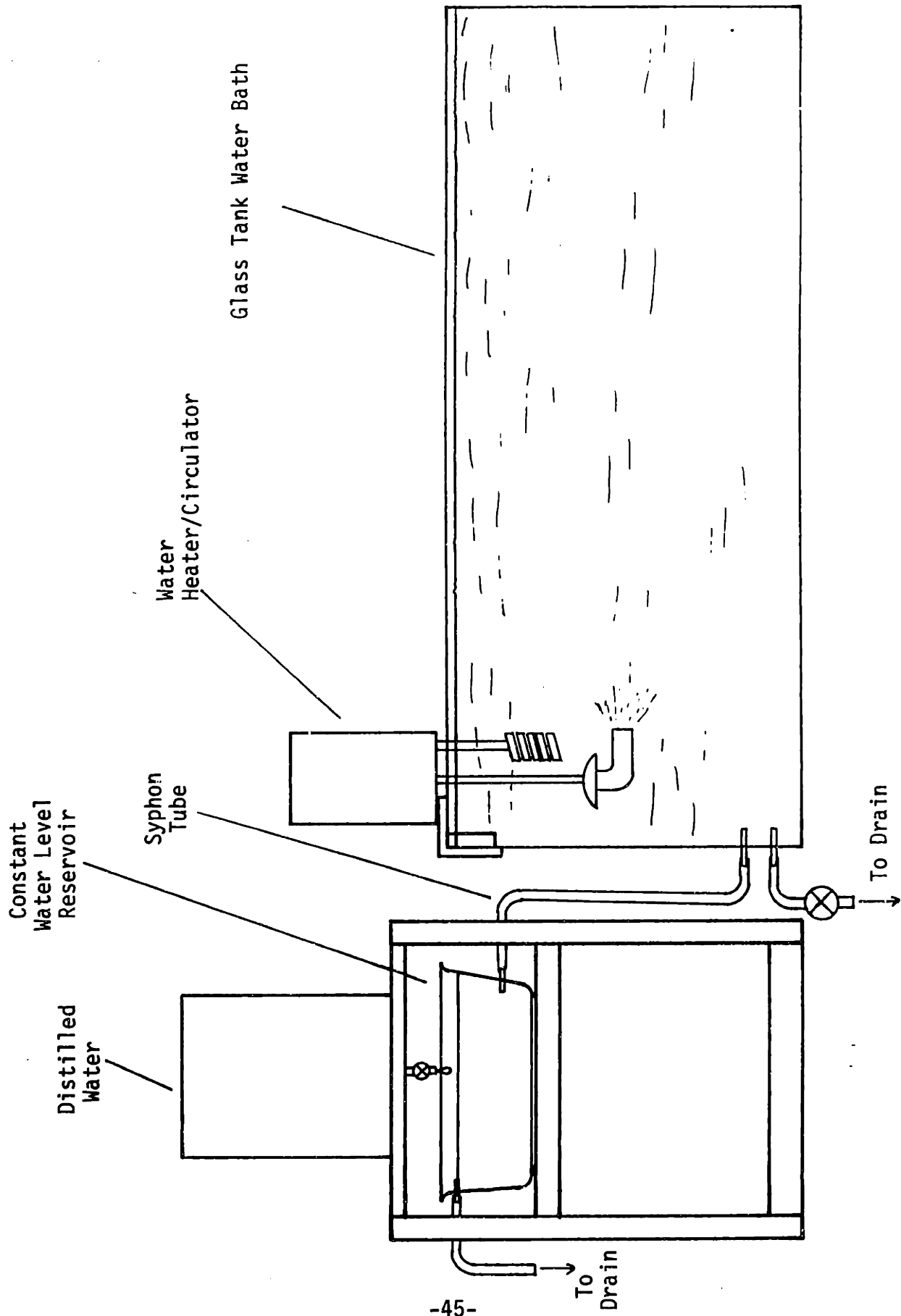


FIGURE 2.7: CONSTANT TEMPERATURE BATH ASSEMBLY

It also prevented the hose connecting the constant level reservoir to the bath from experiencing vapor locks that occur when the dissolved gases in normal tap water are released after heating. The bath temperature was maintained with a Fisher Model 73 immersion circulator to an accuracy of $\pm 0.02^{\circ}\text{C}$. Temperature was monitored with two type K thermocouples placed in the bath and inside the foam cell container. Close temperature control was necessary to produce accurate, repeatable measurements, and to eliminate any transient thermal effects; also, the pressure transducer was found to be very temperature sensitive for this experiment, as explained in the next section.

2.2.2.4 Data Acquisition

Volumetric flowrates (i.e., permeation rates) were measured through the use of a Validyne Model AP-1042 absolute pressure transducer and calibration correlations between pressure increases and changes in volume (see Section 2.2.2.7). While being non-responsive to changes in ambient pressure, the absolute transducer proved to be temperature sensitive. Manufacturer's specifications estimated the temperature sensitivity as 0.01% full scale per $^{\circ}\text{F}$. This corresponds to a 1 mV shift for every $^{\circ}\text{F}$ change in temperature given a 10 volt span; however, early tests revealed a somewhat larger dependency.

With typical data acquisition comprising of 25 mV increases, this temperature dependency would cause considerable errors in the measurement if the environment around the transducer was not carefully controlled. For this reason, it was decided to enclose the transducer within the plexiglas container where the temperature would remain constant. Initial

testing showed that the presence of excessive moisture condensing on the electrical connection of the transducer would cause shorting between the pins of the connector. This problem was resolved by removing the entire Bendix-type connection from the top of the transducer, thus exposing the four pins extruding from the transducer case. The signal lead wires were soldered directly to the pins, then the entire connection was potted using General Electric RTV 118 translucent self-leveling silicon rubber adhesive sealant and allowed to cure for several days. The signal wires connected to a Validyne Model 15 carrier demodulator which converted the AC signals from the transducer to DC voltage. (Figure 2.8) The demodulator also controlled span adjustment and zero shifting. The D.C. voltage was measured by a digital voltmeter and then sent to a Gould Model 2200 strip chart recorder for hard copy recording. It should be noted that the cable shield for the signal wires were disconnected and the transducer was grounded directly through the plumbing connection to the foam cell. This prevented any type of ground loop that could result in signal zero instabilities.

2.2.3 Foam Samples

Foam samples for the permeability tests were obtained from standard production 1.2 in. phenolic foam boards manufactured by Koppers Co., Inc., Pittsburgh, PA. Appendix A lists the properties of the foam. The foam was cut into 4.5 in. diameter circles and then sliced in half to reduce the thickness and expose the interior of the foam. This permitted a visual check for any unordinary voids or imperfections inside the foam. One of the halved sections was then trimmed to snugly fit inside the sample ring.

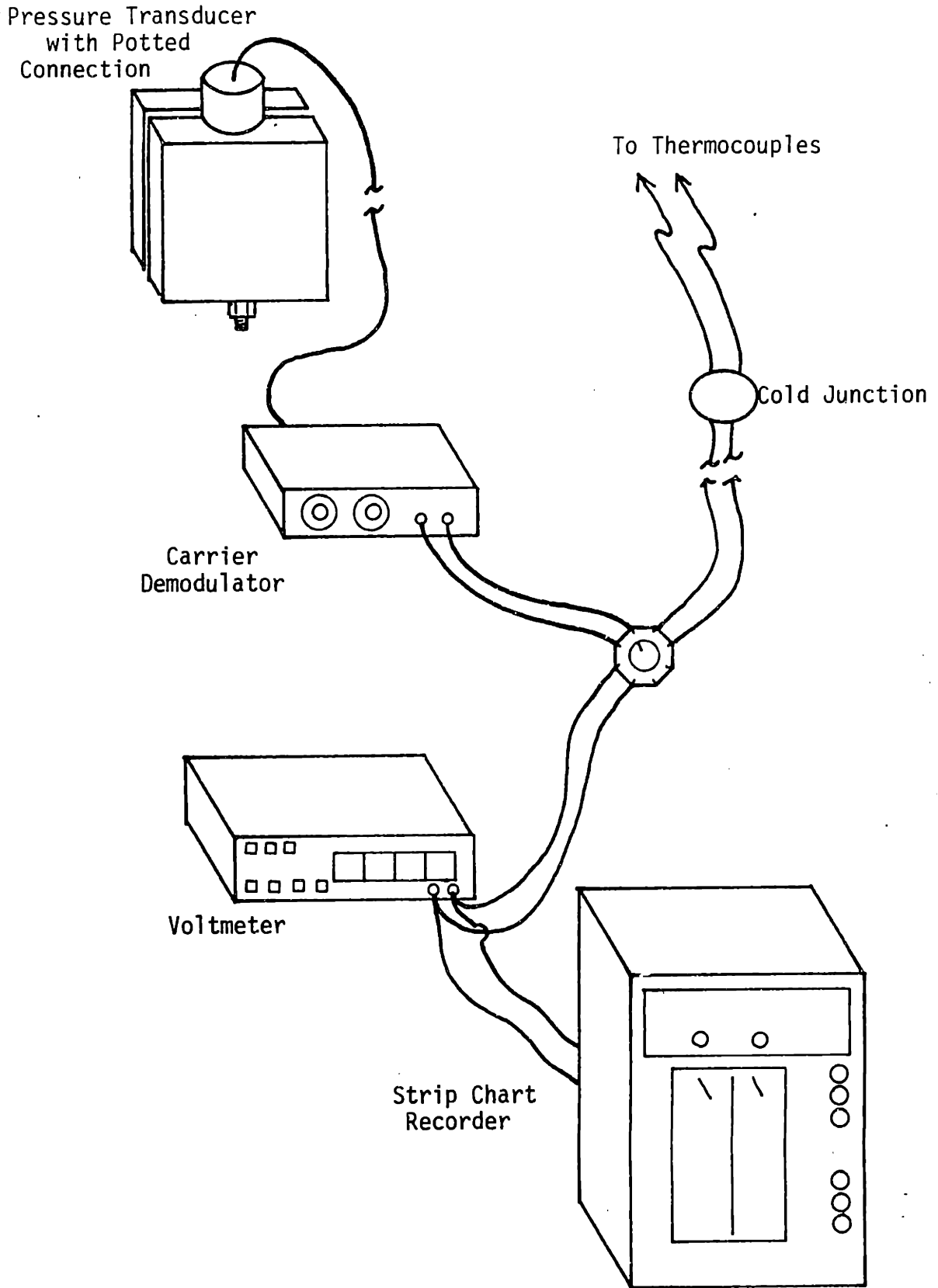


FIGURE 2.8: DATA ACQUISITION SCHEMATIC

The sample ring was cleaned using successive applications of acetone and 200 proof ethyl alcohol and then ultrasonically cleaned in distilled water. The ring was heated in an oven to approximately 500°F and allowed to cool. This procedure assured that any outgassing impurities due to machining and general handling would not affect the measurements. Although the ring would again be handled while the sample was being sealed inside the ring, a final cleaning with acetone and 200 proof ethyl alcohol would eliminate any contamination.

The foam was cemented into the sample ring by applying DER 331 Epoxy (Allied Resin Corporation) to the outer edge of the foam and to the inner surface of the ring. The foam was fitted into the ring and allowed to cure overnight. The DER 331 epoxy was chosen for its very low vapor pressure characteristics, thus eliminating any outgassing effects on the measurements. Finishing was performed by sanding the foam sample flush with the face of the ring to a finished thickness of 5.72 mm (0.225 in) and cleaning up any unnecessary glue present on the sealing faces. Leaks were detected by placing the sample into the foam cell and sealing it with 4.5 in. rubber O-Rings. A capillary tube was placed onto the transducer tube connection and the inlet and exit gas tubes were sealed with valves. A slug of ethyl alcohol was placed in the top of the capillary tube and allowed to fall. If the slug stopped and remained motionless, the sample was then assumed to be sealed within the ring. It was removed, the ring was again cleaned with acetone and 200 proof ethyl alcohol and covered until the cell was ready to be assembled. A continuously falling slug, when monitored over a period of several minutes, indicated that there was a leak, and the sample was removed and discarded. The entire procedure was repeated until a good

sample was obtained. It should be noted that, depending on the size of the capillary tube, a slug could fall to the bottom of the tube, thus, giving the appearance as if the sample was leaking; however, this could be due to the compressibility of the air inside the upper chamber. When this occurred, one of the valves was opened as the slug was falling and the chamber was slightly pressurized so as to stabilize the slug. The valve was then closed and the slug was observed for any type of motion.

2.2.4 The Outgassing Phenomenon

The phenomenon of outgassing is a very important consideration when performing the foam permeability tests. Any surface that is not properly cleaned will outgas and affect the sensitive permeability measurements substantially. This became evident in early work at MIT [13]. For this reason, all surfaces associated with the measurements were constructed from stainless steel, and only greases or seals with very low vapor pressures were used. The valves used in this experiment were also of high quality stainless steel and were thoroughly cleaned before use.

2.2.4.1 Cleaning Procedures

Components of the foam cell were cleaned using acetone and 200 proof ethyl alcohol. The acetone was applied first, being strong enough to dissolve and remove any greases or oily films. The pure ethyl alcohol was then used as it evaporated completely from the surface and left no residue. After an ultrasonic cleaning in distilled water, the components were heated in an oven to 500°F. The excessive heating will allow the first few molecular layers of the surface to expand and release any impurities that may be present. Great effort was taken not to handle any surface without

the use of plastic surgical gloves.

2.2.4.2 Seals and Greases

The problem of outgassing prevented the use of rubber seals for any surface associated with data acquisition. It was discovered that indium metal would provide an excellent seal without the negative outgassing effects. For this reason, the seal between the sample ring and the upper chamber was constructed from indium metal and covered with a thin film of high quality vacuum grease having a very low vapor pressure. To seal the lower side of the sample ring, a teflon seal was constructed, cleaned and coated with vacuum grease.

2.2.5 Cell Assembly

This section describes the procedures followed to assemble the foam cell for permeability measurements. The lower chamber was first fitted with the lower foam support and the teflon seal was seated into place. After inserting the foam sample, the indium gasket coated with vacuum grease was placed on top of the sample ring. The 4.5 in. rubber O-Ring was inserted into the groove of the upper chamber and small amounts of vacuum grease were applied as a lubricant. The O-Ring acts as a water seal keeping the internal parts of the cell dry. The upper chamber was then fitted on top of the gasket and sample ring and tightened down with the stainless steel threaded rod and nuts. To assure even compression around the gasket, a torque wrench was used to tighten the nuts to 120 in-lbs. The pressure transducer was connected to the cell using $\frac{1}{8}$ in. stainless steel swagelok fittings. After placing the entire cell assembly in the plexiglas box, it was filled

with distilled water to a point just below the transducer. This permitted an increased heat transfer coefficient around the cell without allowing the transducer to be totally immersed. The top of the box was bolted into place and sealed, and the entire container was placed into the constant temperature bath. Additional connections were made as shown in Figure 2.3 using $\frac{1}{8}$ in. stainless steel tubing.

2.2.6 Testing Procedures

Permeability data were required at three temperatures: 75°C, 50°C and room temperature. The apparatus was first heated to 75°C according to the accelerated temperature method described by Ostrogorsky [1]. A pressure of 8 psig was maintained in the lower chamber and in the high pressure reservoir with a gas regulator and was monitored with a test gauge. The exit valve was fully opened and the inlet valve was slightly opened to permit small amounts of gas to flush across the sample into the low pressure reservoir. This allowed any impurities other than the test gases permeating from the foam, to be cleaned from the measurement area. An oil trap provided a visual check of gas flow and maintained atmospheric pressure in the pressure reservoir. The sample was flushed for a few days in this mode and then the inlet valve and oil trap valve were closed to establish the concentration boundary condition on the upper side of the foam. To determine when the sample had reached steady-state, transient charts, developed by Ostrogorsky [1] and similar to the Heisler Charts of heat conduction, were used by periodically taking data and comparing the results.

Data were taken by closing the exit valve of the upper chamber and

recording the upper chamber pressure increase with the strip chart recorder. At the end of a 25 mV span, the recording was stopped and the exit valve reopened. A period of time (usually $\frac{1}{2}$ hour to 2 hours) was allowed to elapse between each data acquisition run to reestablish the original boundary conditions.

Once repeatable data were obtained at 75°C, the supply valve was securely closed and the bath cooled to 50°C. With this technique, the linear concentration gradient established across the sample at 75°C is maintained as the pressure conditions within the entire apparatus change proportionally with temperature (See Section 2.1). Therefore, once a new steady temperature is obtained both inside and outside of the cell, the data can be taken immediately. After taking data at 50°C, the temperature was dropped to room temperature and the recording procedure was repeated.

It should be noted that the volumes of the high and low pressure reservoirs must be great enough for pressure changes (concentration changes) caused by permeation to be negligible while achieving steady-state and during the cooling periods between data temperatures.

2.2.7 Calibration

The calibration of the foam cell permitted a correlation between the increase in pressure for the closed volume and the volumetric flow-rate which would occur at constant pressure. A calibration constant was required at each data temperature due to the thermal sensitivity of the pressure transducer. To accomplish this, a capillary tube with an internal bore diameter of 0.5 mm was attached with Swagelok fittings to the top of the inlet gas valve as shown in Figure 2.9. A scale graduated in

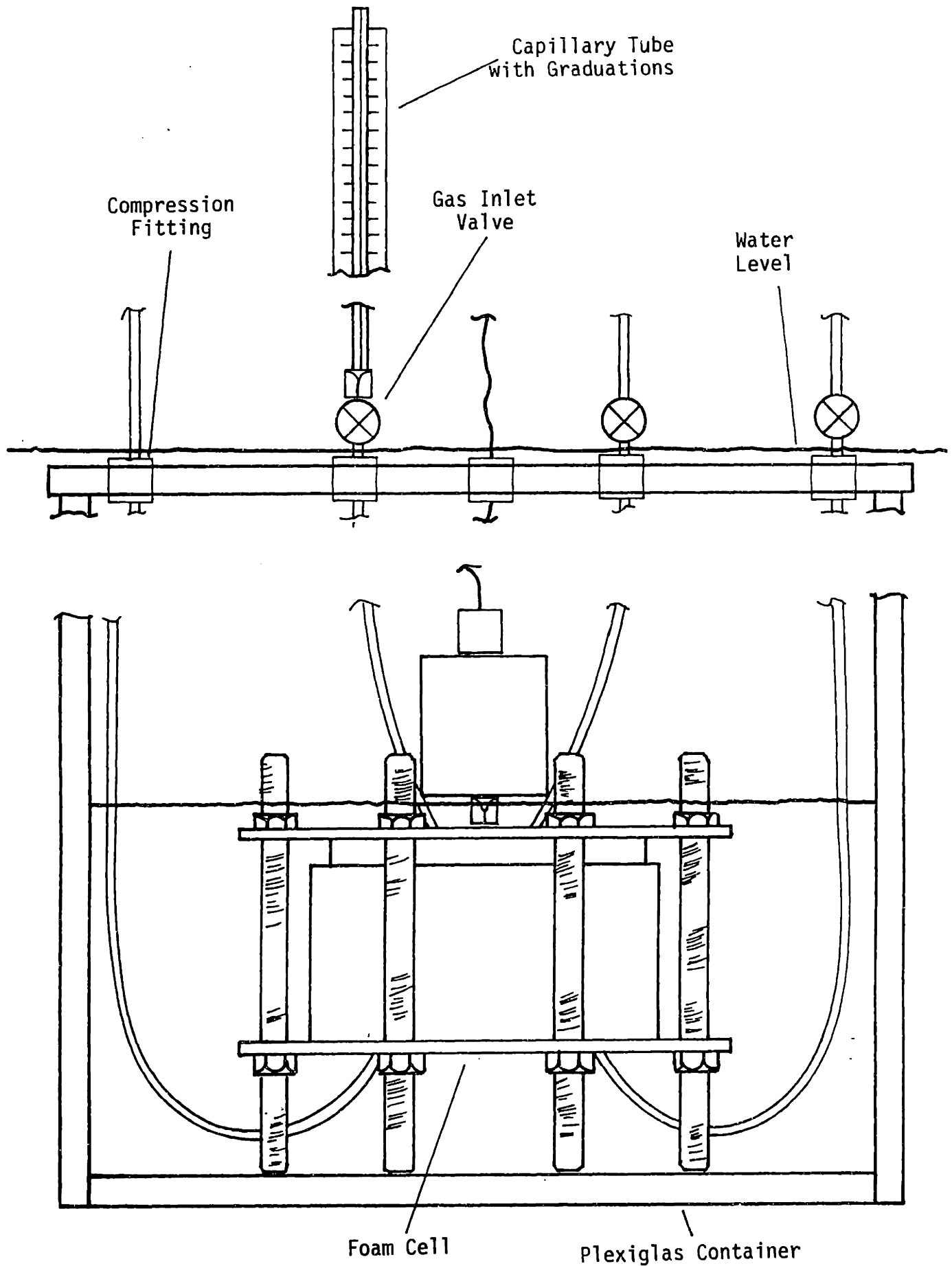


FIGURE 2.9: CALIBRATION SET-UP OF FOAM CELL

millimeters was attached to the tube to measure slug displacements. The inlet valve was opened $\frac{1}{2}$ turn and an ethyl alcohol slug was injected with a small syringe into the top of the tube. The length of the slug was recorded along with the change in voltage from the transducer. This process was repeated using various lengths of slugs. The correlation between the transducer output and volumetric change can be calculated knowing a) the capillary tube cross-sectional area, b) the slug displacement, and c) the change in the transducer output. The data were then plotted and a least squares fit determined the calibration constant. The results of the calibration are shown in Figure B-1 of Appendix B.

2.3 Film Tests

2.3.1 Introduction

To better understand the properties of the phenolic polymer, permeability coefficients of the polymer film would be determined experimentally. The approach to this test is similar to that of the foam tests. A film sample would be subjected to a concentration difference of a test gas across its thickness, and the permeability coefficient for the gas would be determined by measuring the volumetric flowrate through the sample. Again, the upper and lower chambers would be separated and sealed by the sample; but rather than place a large pressure difference across the thin film, the concentration difference could be achieved by the use of two different gases. In the upper chamber, the test gas at one atmosphere absolute pressure would be present, while Freon 12 at one atmosphere absolute pressure would occupy the lower chamber. This would permit a partial pressure difference of test gas equal to 1 atmosphere. Freon gas is known to permeate at least one order of magnitude slower than nitrogen, oxygen

or carbon dioxide; therefore the permeation rates of Freon through the sample and into the upper chamber would be negligible. Volumetric flow-rates could then be determined by measuring the decrease in volume in the upper chamber as a function of time. See Figure (2.10). The early apparatus at MIT used a liquid slug in a capillary tube and monitored the fall of the slug over time. This method proved to be inadequate for long term testing as mentioned in Section 2.2.1. Therefore, an absolute pressure transducer was mounted to the upper chamber, and the decrease in volume was determined through a decrease in pressure and the correlation constant found by calibrating the film cell. The permeability coefficient could then be calculated through the use of Equation (1-9).

Design considerations for the film cell were very much similar to those of the foam cell described in Section 2.2.1.

- The volume of the upper chamber should be minimized to increase the sensitivity of the apparatus.
- Outgassing effects would need to be eliminated through the use of stainless steel construction, the use of glues and greases with very low vapor pressures, and the thorough cleaning of all surfaces.
- All welding would utilize vacuum techniques and be kept to a minimum.
- Seals would be formed from indium metal.
- Close and constant temperature monitoring would be necessary for accurate and repeatable results. This would be required due to the temperature dependence on permeation and the pressure transducer sensitivity.

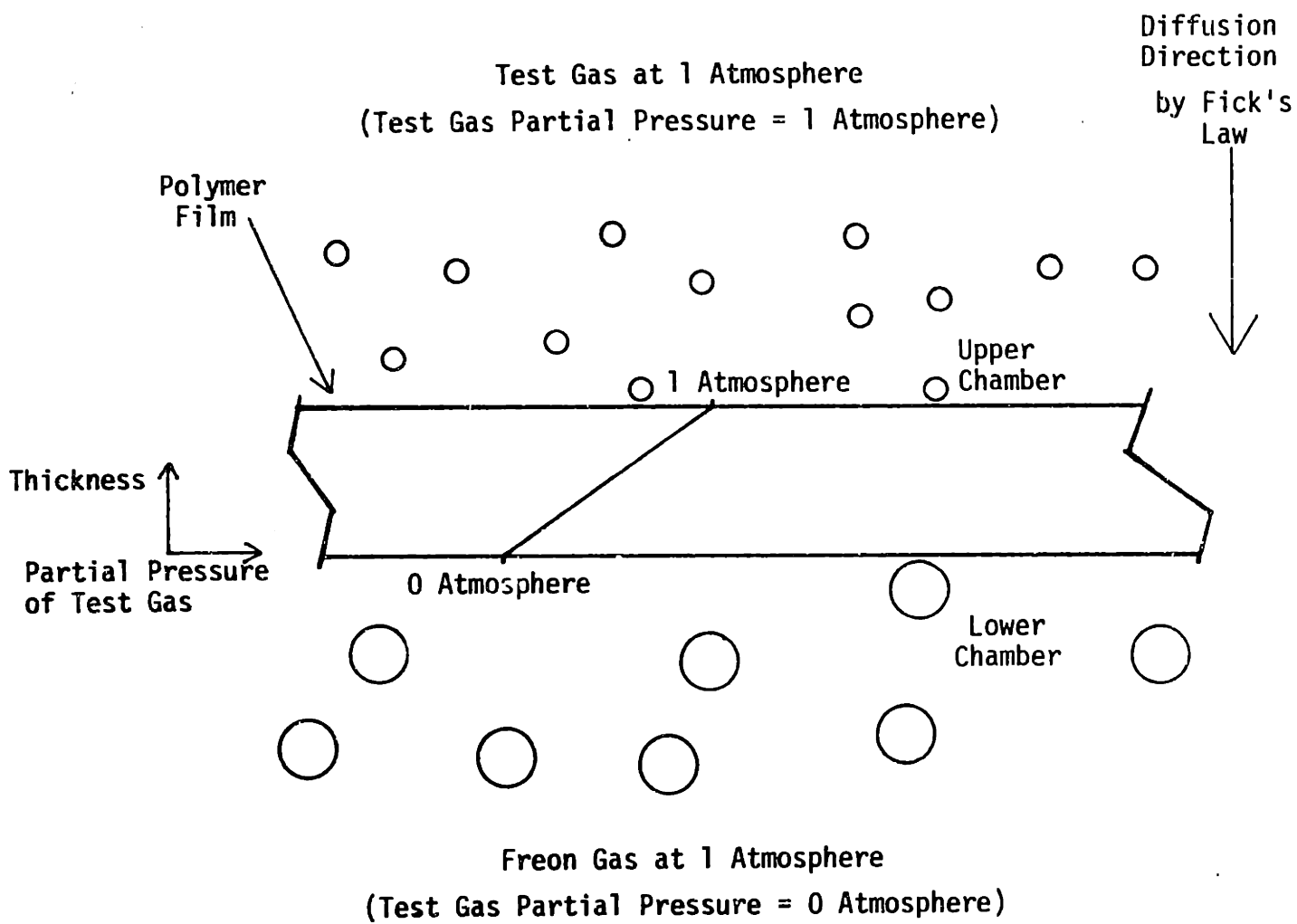


FIGURE 2.10: PERMEATION IN THE FILM TEST CELL

2.3.2 Apparatus

The film permeability test apparatus is very similar in nature to the foam apparatus described in Section 2.2.2. For the film test, the three major components include: a) the film test cell b) the constant temperature bath and c) the data acquisition system. The apparatus set-up is shown in Figure 2.11 and will be discussed in slightly more detail.

2.3.2.2 The Film Cell

The film cell consists of 4 parts: the upper chamber, the lower chamber, the sample mounting ring, and the plexiglas container. See Figure 2.12. The upper chamber was machined from 2 in. 304 stainless steel round stock to a length of 0.545 in. and a diameter of 1.970 in. The internal volume of the upper chamber was determined by machining a 0.010 deep cavity into the lower face of the upper chamber. By including the valves, tubing, and pressure transducer chamber, the total volume was approximately 900 mm^3 (0.055 in^3). Three $\frac{1}{8}$ in. diameter holes, one for gas inlet, one for gas exit and one for the transducer fitting were drilled through the upper chamber and fitted with $\frac{1}{8}$ in. diameter stainless steel tubing. These were then heliarc welded into place from the lower face of the upper chamber so as to facilitate the thorough cleaning of this part and prevent outgassing.

The lower chamber consists of a 2 in. diameter piece of 304 stainless steel round stock cut to 1.990 in. in length with an internal bore diameter of 0.650 in. and a depth of 1.575 in. A small indentation was cut on the upper face to accommodate the mounting ring and hold it into

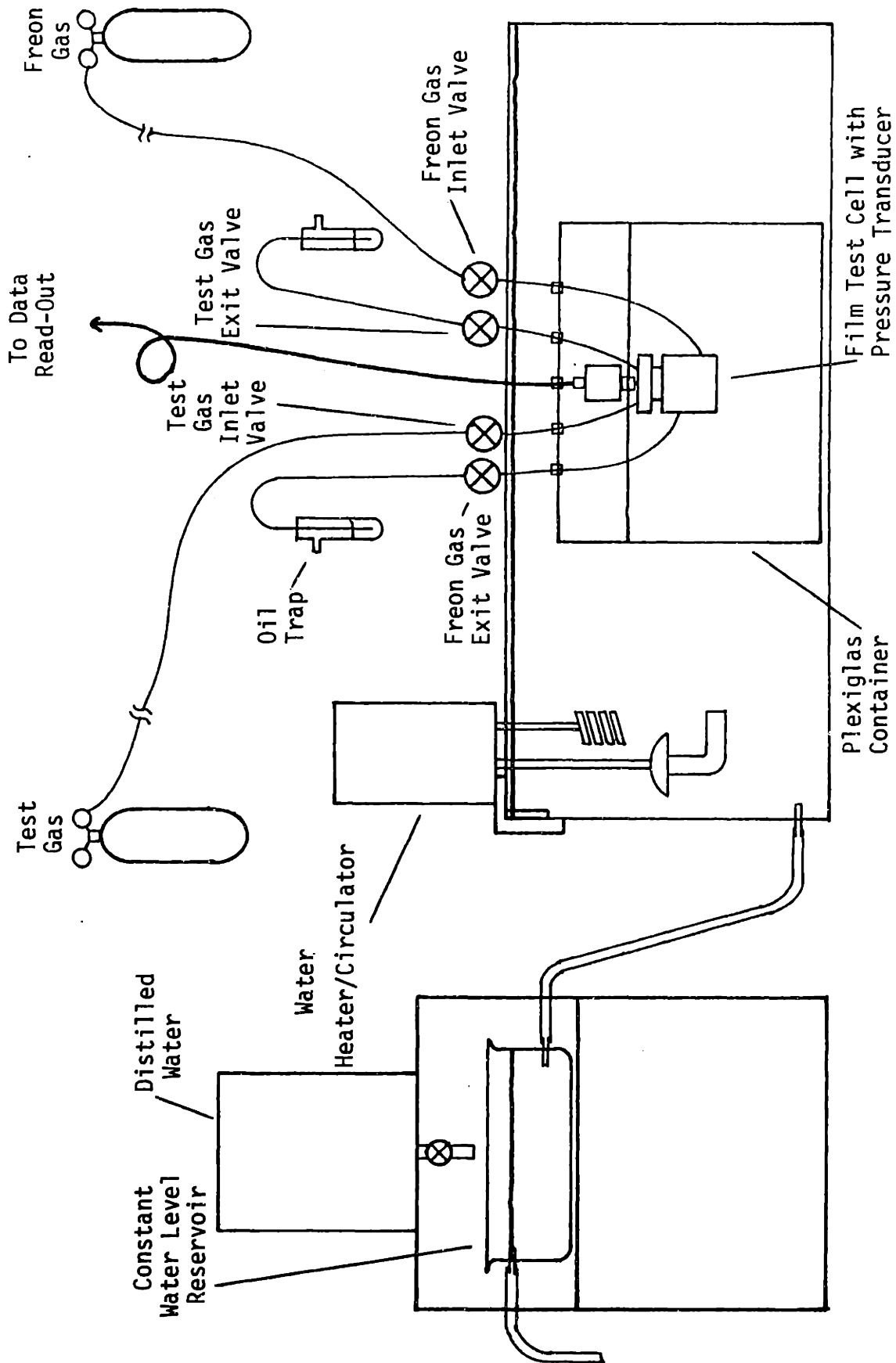


FIGURE 2.11: FILM TEST APPARATUS

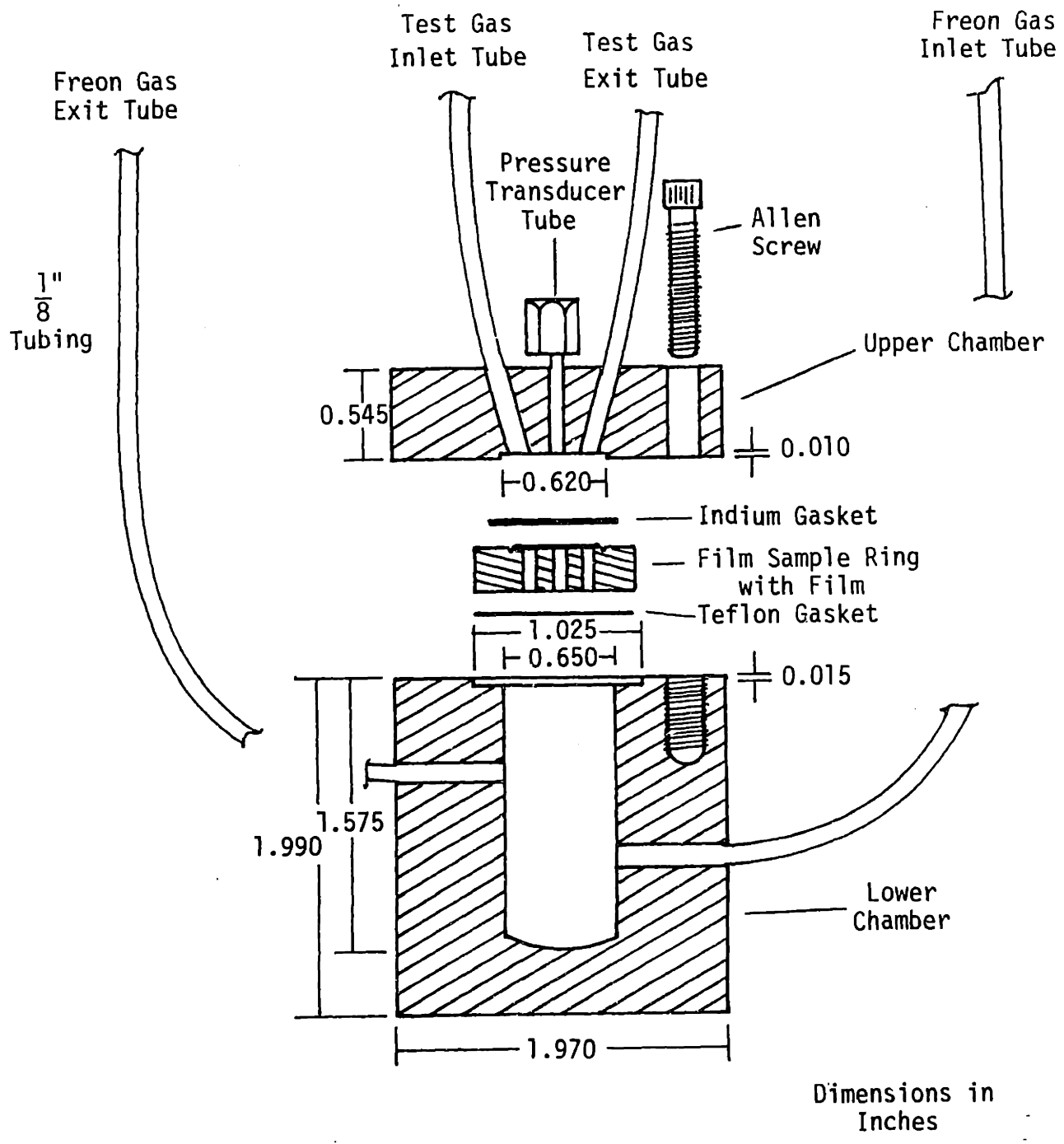


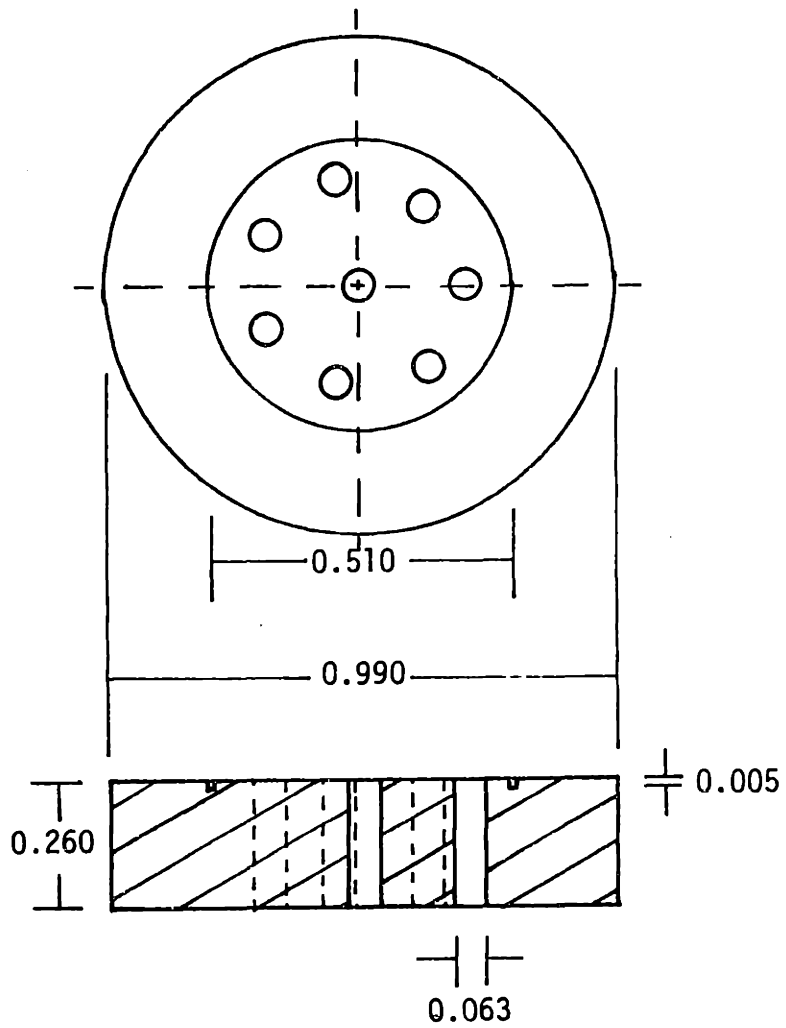
FIGURE 2.12: FILM TEST CELL

place as the cell is being assembled. Three holes were then symmetrically drilled through the upper chamber into the lower chamber, and the lower chamber was then tapped so that the two halves could be bolted together with $\frac{3}{4}$ in. #10 stainless steel allen bolts. Inlet and exit gas tubes were then attached to the lower chamber by drilling through the side of the piece and welding them into place.

The sample mounting ring is shown in Figure 2.13. The outer diameter is 0.990 in. and the thickness is 0.260 in. It also was machined from 304 stainless steel. A shallow groove 0.510 in. in diameter was cut into the upper face of the ring so as to center the sample while gluing it into place. The $\frac{1}{16}$ " holes provided gas access to the sample surface and also sample support.

The plexiglas container has outer dimensions of $9\frac{1}{4}$ in. height, 11 in. length and $4\frac{1}{2}$ in. in width and was constructed from $\frac{1}{2}$ in. plexiglas plate. Since the testing would not be performed at temperatures above 50°C, the bottom and sides of the container were simply joined by plexiglas cement. The top of the box was drilled and tapped for #8-32 stainless steel allen screws and fitted with a one-piece rubber seal coated with vacuum grease. This would allow repeated openings of the container while assuring a water-tight seal.

As mentioned in Section 2.3.1 and Section 2.1, permeation through any solid is an exponential function of temperature: $P_e = P_{e_0} \exp(-E_p/RT)$. Therefore, the thermal environment around the film cell and transducer required constant control and stability through the use of a water bath. The constant temperature bath for the film tests was similar to the bath



Dimensions in
Inches

FIGURE 2.13: FILM SAMPLE RING

for the foam tests (Section 2.2.2.3). An 18-gallon glass aquarium tank was connected to a constant water level reservoir, insulated on the sides and fitted with a plexiglas cover. The water temperature was maintained with a heater/circulator to an accuracy of $\pm 0.03^{\circ}\text{C}$. To maintain cleanliness inside the bath and reduce mineral deposits on the apparatus, distilled water was used in the tank and for the make-up water. This also prevented vapor-lock in the hose connecting the reservoir to the bath due to dissolved gases being released after heating.

2.3.2.3 Data Acquisition

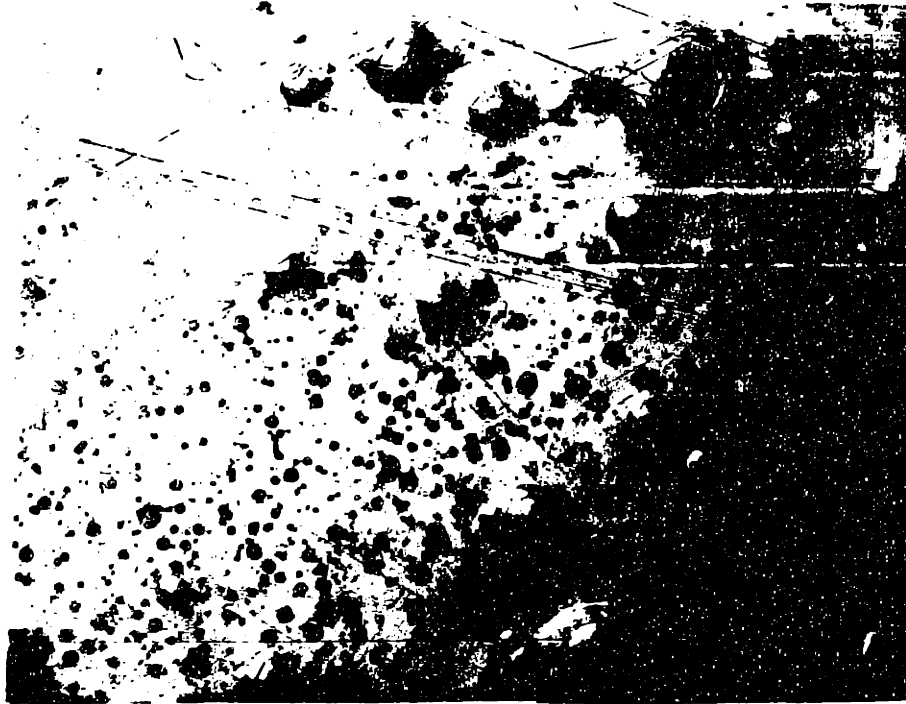
Pressure readings from the absolute pressure transducer were conditioned and recorded in a manner similar to Section 2.2.2.4. The Validyne AP10-42 transducer was placed inside the plexiglas container so as to maintain a constant temperature around it, and the signal was sent through the Validyne Model 15 carrier demodulator and on to the digital voltmeter where it was measured in D.C. volts. The Gould Model 2200 strip chart recorder provided a printed copy of the voltage change as a function of time. As in the foam tests, the Bendix connector between the transducer and the cable was eliminated, and the wires were soldered directly to the pins extruding from the transducer case. This connection was potted in General Electric RTV 118 translucent self-leveling silicon rubber adhesive sealant to prevent moisture build-up between the pins that could cause electrical shorting.

2.3.3 Film Samples

Phenolic polymer, in the form of a thin film, is used to determine the permeability characteristics of the solid material in foam. Samples

were obtained from Koppers Co., Inc., Pittsburgh, PA. In order to create a representative film with respect to the polymer in the actual foam product, concern was focused to the areas of thermal history and blowing environment. Thermal history is important in the production of foam insulation as the diffusion properties of the polymer are directly related to this parameter. The blowing environment, in this case Freon 11 and Freon 113, was maintained so as to most closely match the conditions under which the insulation is blown. It was confirmed that the film samples should adequately represent the polymer found in the phenolic insulation [14].

One problem of major concern when testing film samples is the presence of any micro-holes, cracks or small micro-bubbles in the solid. (Figure 2.14) These are difficult, is not impossible, to detect with the naked eye and each sample must be scanned with a high power optical microscope. Micro-holes and cracks will severely alter the permeation test results since the volumetric flowrate measured with such a sample will be a contribution from bulk flow through these passages and not mass diffusion. An open path on the order 1-10 microns (the mean free path of a gas molecule) is all that is necessary to establish bulk flow. Micro-bubbles within the solid enhance the volumetric flowrate since there is a void of zero resistance to diffusion within the film, thus, the actual polymer thickness through which the gas passed through cannot be determined. These defects can also be detected during testing if the permeation results appear to be totally independent of temperature and test gas.



Micro-bubbles Entrapped in Polymer Film Sample



Micro-cracks on Surface of Polymer Film Sample

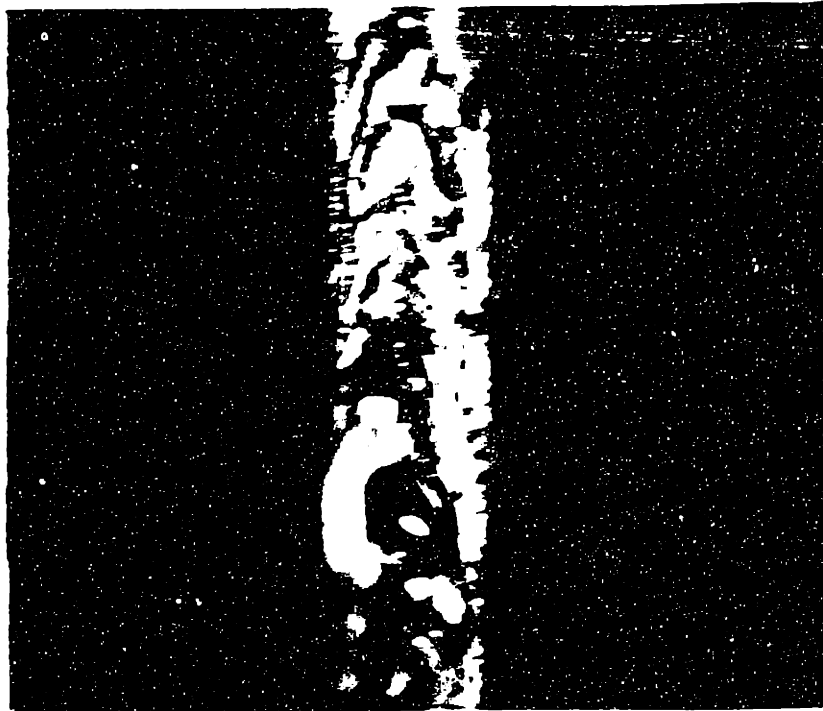
FIGURE 2.14: OPTICAL MICROSCOPE PHOTOS OF MICRO-BUBBLES AND MICRO-CRACKS IN PHENOLIC POLYMER FILMS (50x)

In previous testing with polyurethanes at MIT, films were obtained from large bubbles that formed on the top of free rise foam buns. These films were very thin and difficult to work with. This method did not prove to be viable with phenolic foam, however, due to the foam's free rise inability to create large bubbles of a consistent nature. Therefore, the films were made in the laboratory at Koppers Co. by forming thin films on glass plates. These samples were then carefully cured. Although the phenolic films were thicker than the polyurethanes, they proved to be much easier to handle and less brittle.

According to Equation (1-9), the two physical parameters of the sample necessary to calculate the permeability are the film area and the film thickness. Each film sample was cut by using a cork borer and the surface diameter was simply measured with a ruler followed by an area calculation. The exact thickness of the films was determined by using an optical microscope equipped with a camera. Thickness photographs were then taken at various points around the edges of the sample and averaged. Figure 2.15 shows a typical photograph.

2.3.4 Cell Assembly

After the thorough cleaning of all film test cell parts with acetone and ethyl alcohol, the cell was placed in a bath of distilled water and ultrasonically cleaned. It was then kept under vacuum for at least 1 day to aid in the elimination of any outgassing. A sample from the phenolic film was cut and the necessary measurements taken for thickness and surface area. The film was mounted on the sample ring by using Sealstik cement which has a vapor pressure of 10^{-3} mm/hg. This solid cement must be



—| |—
Film Thickness

—| |—
100 Microns

FIGURE 2.15: OPTICAL MICROSCOPE PHOTO OF POLYMER FILM THICKNESS (100x)

melted into liquid form to become adhering, so the ring was first heated to the cement's melting point, 140°C, by placing it on an electric hot plate. Small pieces of the cement were then melted onto the mounting ring face and the sample was sealed into place and allowed to cool. Leaks along the glued edges were detected by sealing the sample in the test cell using rubber O-Rings, and a capillary tube was then connected to the transducer tubing. The inlet and exit tubes were sealed with valves. A slug of ethyl alcohol was placed in the capillary tube and observed for movement. A falling slug indicated a leak upon which the entire sample mounting procedure was repeated.

After obtaining a non-leaking film sample, the test cell was assembled as shown in Figure 2.12. The sample ring was sealed between the upper and lower chambers by using a teflon seal on the bottom and an indium metal seal on the top. Again, the indium was used for its excellent sealing qualities and non-outgassing properties. The indium seal was checked for leaks by using a liquid slug in the capillary tube mentioned earlier. After mounting the pressure transducer, the entire cell was placed into the plexiglas container and filled with distilled water to a point just below the transducer. The use of the water would increase the heat transfer coefficient to the cell to more quickly and accurately maintain a constant temperature around the cell. The top of the container was sealed with the rubber gasket and vacuum grease, the valves fitted onto the inlet and exit tubes, and the entire container was placed into the constant temperature bath and connected to the test gases.

2.3.5 Testing Procedures

The following section will describe the test procedures to obtain data to determine the permeability of the solid polymer. After assembling the test cell as described in Section 2.3.4, the container was placed in the constant temperature bath and heated to the desired temperature (in this case, 25°C and 50°C). The test gas, either carbon dioxide, oxygen or nitrogen, was allowed to enter the upper chamber and flush through to the oil trap as shown in Figure 2.11. The oil trap not only provided a visual check of the gas flow, but acted as a pressure relief valve so as not to overpressurize the chamber and break the film. The maximum pressure permissible in the upper chamber was therefore the pressure head associated with the depth of the oil in the trap. The lower chamber was similarly flushed with Freon 12 exiting through an oil trap to the atmosphere. Note that this method maintains atmospheric pressure on both sides of the film (or zero pressure difference across the sample), but allows an effective partial pressure difference of the test gas equal to one atmosphere across the film. The apparatus was maintained in this mode for approximately 24 hours to assure that a linear concentration gradient has been established and that any foreign gas released from the film has been flushed out. The inlet valves were then closed, and after a period of several minutes, the exit valves were also sealed. The strip chart recorder then plotted the decrease in pressure of the upper chamber as a function of time. This indicated the volumetric permeation flowrate of the test gas in the upper chamber through the film to the lower chamber. As mentioned earlier, the diffusion rate of the Freon gas when compared to the test gases was assumed negligible so that

no error was encountered from reverse flow (i.e., Freon gas from the lower chamber to the upper chamber). The time rate of decrease in pressure was then converted to a volumetric flowrate by means of a correlation constant obtained from the calibration of the test cell (Section 2.3.6). This procedure was then repeated for the remaining test gases and at different temperatures.

2.3.6 Calibration of the Film Test Cell

Calibration of the film test cell was necessary to obtain the correlation constant between the change in voltage from the pressure transducer and the change in volume. A precision bore capillary tube 0.5 mm \pm 0.005 mm in diameter was placed on the upper chamber inlet gas valve. The outlet valve was sealed and a slug of ethyl alcohol was placed in the tube and permitted to fall by gravity until it was stable. The slug position along with the change in voltage was then recorded. The change of volume could then be calculated knowing the bore diameter and the slug position measurement. This process was repeated many times with various length slugs and a straight line fit using linear regression was plotted. The slope of the curve then became the correlation constant having units of mm³/millivolt.

2.4 Foam Geometry Studies

2.4.1 Introduction

As mentioned in Section 1.5, foam geometry studies were necessary to analytically model the aging in phenolic foam. Previous work by Reitz [9] with polyurethanes provided the techniques to determine three main geometric parameters: 1) polymer distribution in the struts and

cell walls 2) cell wall thickness and 3) cell diameter.

In order to conduct the analysis, scanning electron microscope (SEM) photographs of the actual foam product were required. However, when obtaining samples to be photographed, the following constraints had to be considered:

- The samples must be from the same production lot as the foam used in the foam permeability tests
- The sections of the sample to be photographed must be from the interior of the foam board and not near the surface where the facers were applied. The cells close to the facer surface could be altered by the manufacturing processes implemented when applying the facers.
- The foam structure must be fairly homogeneous with respect to cell size and shape.

Further details of the geometry study are found in the following sections with the results being presented in Section 4.1.

2.4.2 SEM Techniques

2.4.2.1 Previous Techniques

The process of obtaining suitable scanning electron microscope (SEM) photos was the most important aspect of the study. Early work at MIT with polyurethanes revealed that 2-dimensional planar views of the foam were required, but were difficult to obtain. (The necessity of these 2-dimensional views is discussed later). The delicate nature of the foam structure prohibited the simple slicing of samples with a knife without damage to the exposed first layer of cells. Microtomes with glass knives were then used, but under SEM magnification, the third dimension was

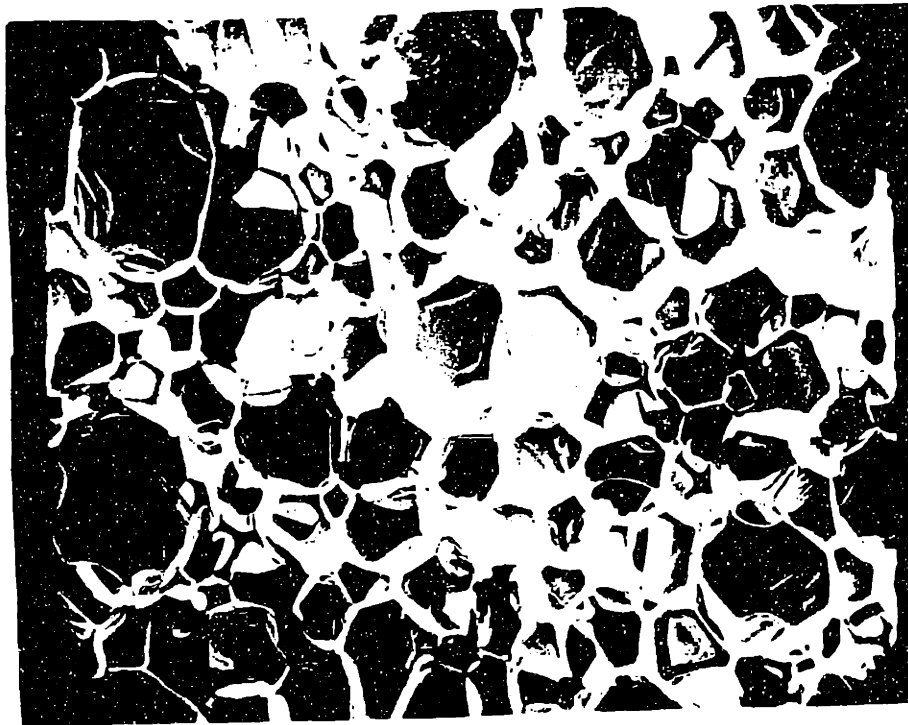
superimposed on the cross-sectional view. (See Figure 2.16) It was then discovered that the foam could be successfully embedded with a resin that would permeate the first layer of the foam and cure to a workable hardness. Thin slices of the impregnated foam were then sliced with a microtome, thus exposing a true planar cross-section without damage to the foam structure (see Figure 2.17).

Before applying the embedding technique to any type of foam, the following considerations were first evaluated,

- 1) the ability of resin to fully impregnate the exposed layers of the foam and
- 2) the chemical affects of the resin on the polymer before and after curing. The most significant chemical affects considered are the swelling of the cell walls and the expansion of the curing resin. In the polyurethanes, there appeared to be no resin expansion but significant polymer swelling. This was accounted for by experimentally determining the percentage of swell in the polymer before and after curing.

2.4.2.2 Current Project Technique

For the phenolic foam used in this project, it was decided to first consult with the manufacturer for the experience they have obtained during the development stages of their product. A factory expert in SEM photography revealed that they have tried embedding resins on the phenolic foam but with very limited success [15]. He felt that the resin's inability to fully occupy the cell voids was the major drawback of this method. He also stated that, due to the physical nature of the phenolic foam structure, suitable photographs could be obtained by simply slicing




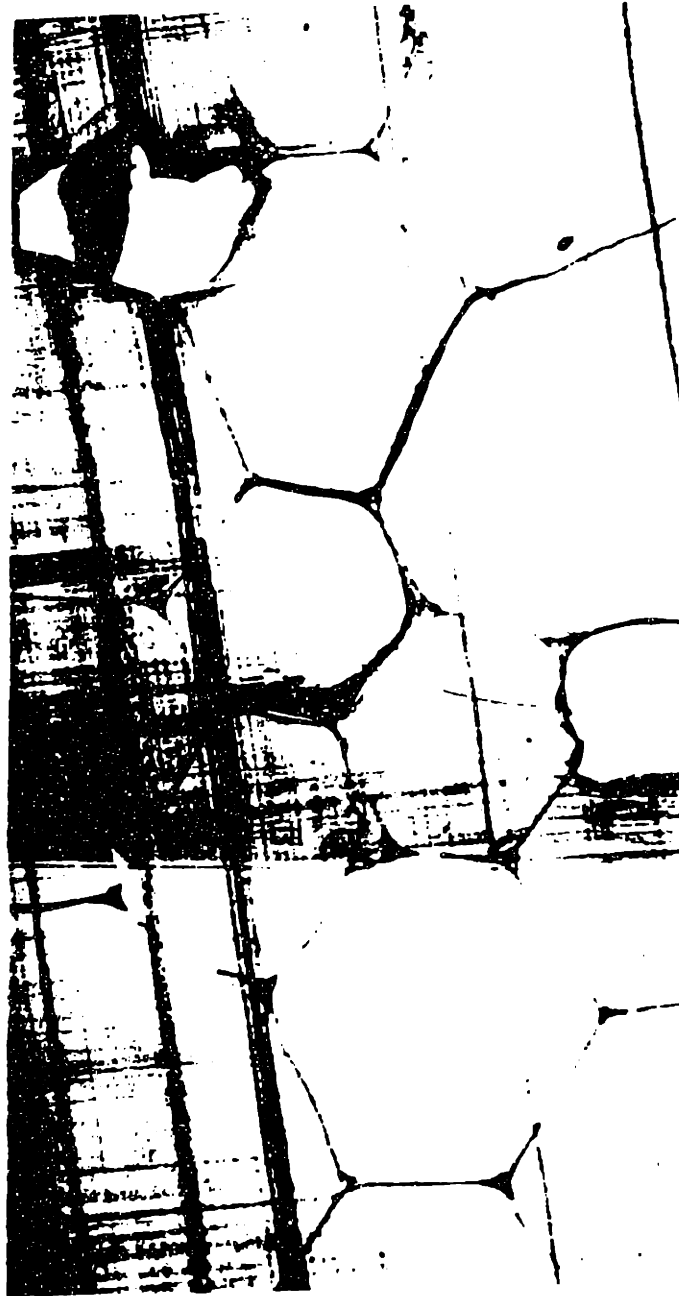

100 Microns

FIGURE 2.16: 3-D SEM PHOTO OF PHENOLIC FOAM (100x)



100 Microns

FIGURE 2.17: SEM PHOTO OF EMBEDDED POLYURETHANE FOAM (100x)

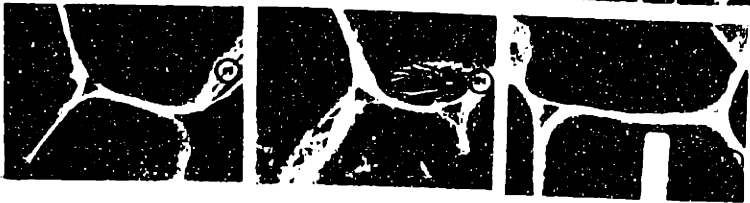
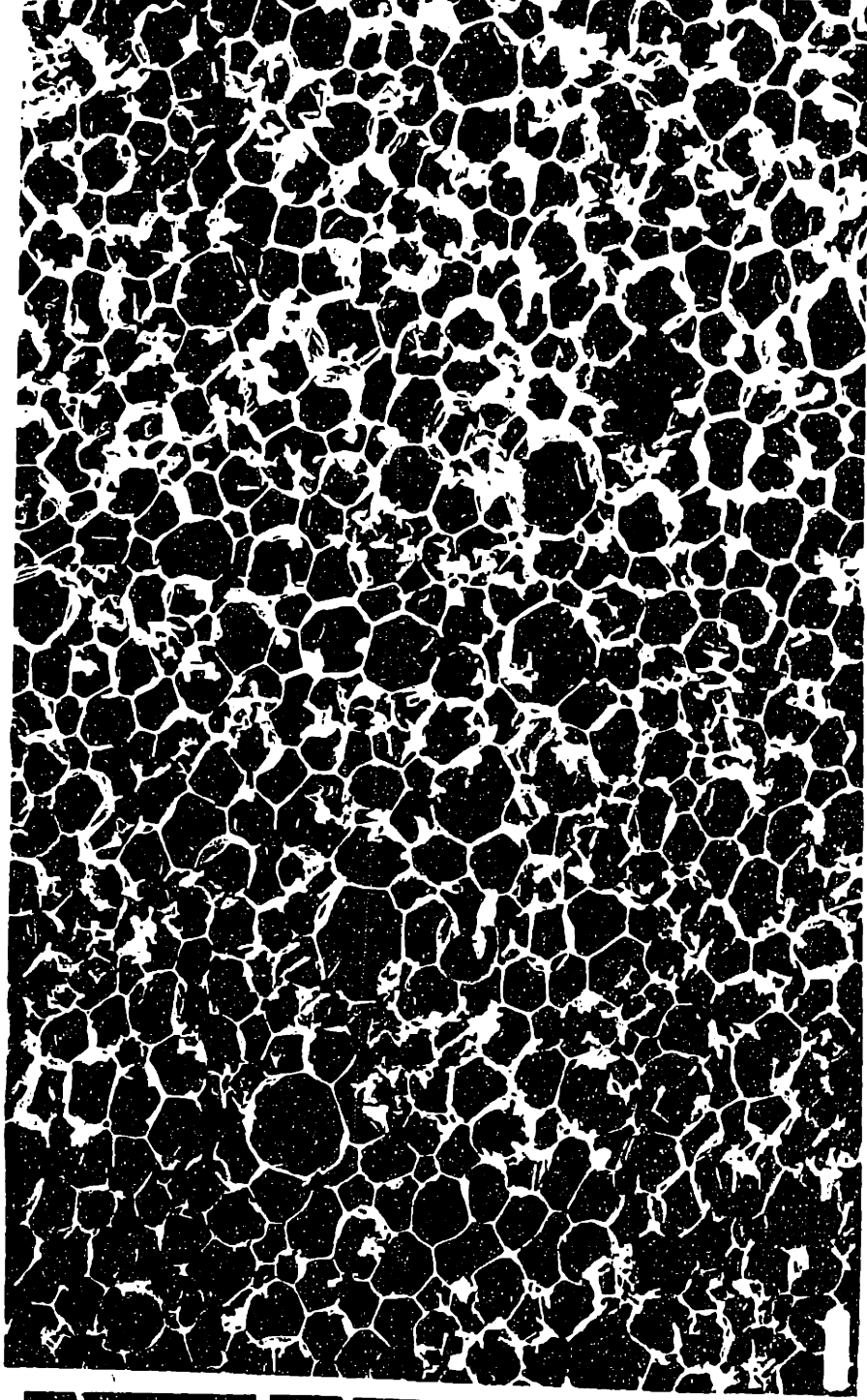
the foam with a high quality microtome. It was then decided that the most efficient method of obtaining the photographs was to send the foam samples to the manufacturer and have all the SEM work performed there.

The foam samples were obtained from the same shipment of foam used in the permeability tests. They were then forwarded to the manufacturer where a small section was cut from the center of the foam board and finishing cuts were performed on the microtome. The sample was then coated with gold according to standard SEM techniques. Photographs were then taken at various magnifications and a montage was also assembled creating a large cross-sectional area. (See Figure 2.18) Although the views obtained were not totally 2-dimensional, they were adequate enough for the the geometric study without the complexities of the embedding techniques.

2.4.3 Polymer Distribution Within Foams

When analyzing a foam product for aging characteristics, one of the most important parameters determined was the polymer distribution in the struts and in the cell walls. This indicated how efficiently the polymer was being used to prevent permeation and R-value degradation. Obviously, the more polymer allotted to the cell walls, the better the aging performance. However, Schuetz showed that increasing the material in the cell walls also increased the available pathways for heat transfer by conduction through solid material, thus decreasing the R-value of the foam [6]. Ideally, an optimum polymer distribution provided good initial insulating performance, but was capable of maintaining that R-value with suitable polymer in the cell walls that resisted the gas diffusion into and out of the product.

1000x



4000x

10,000x

200x

FIGURE 2.18: SEM PHOTO ASSORTMENT OF CLOSED-CELL PHENOLIC FOAM

In order to determine polymer distribution, metallography measurements were implemented with the SEM photos. The first property necessary, the surface area to volume ratio, (S_V), proved to be very important and relatively simple to obtain. This parameter was calculated from

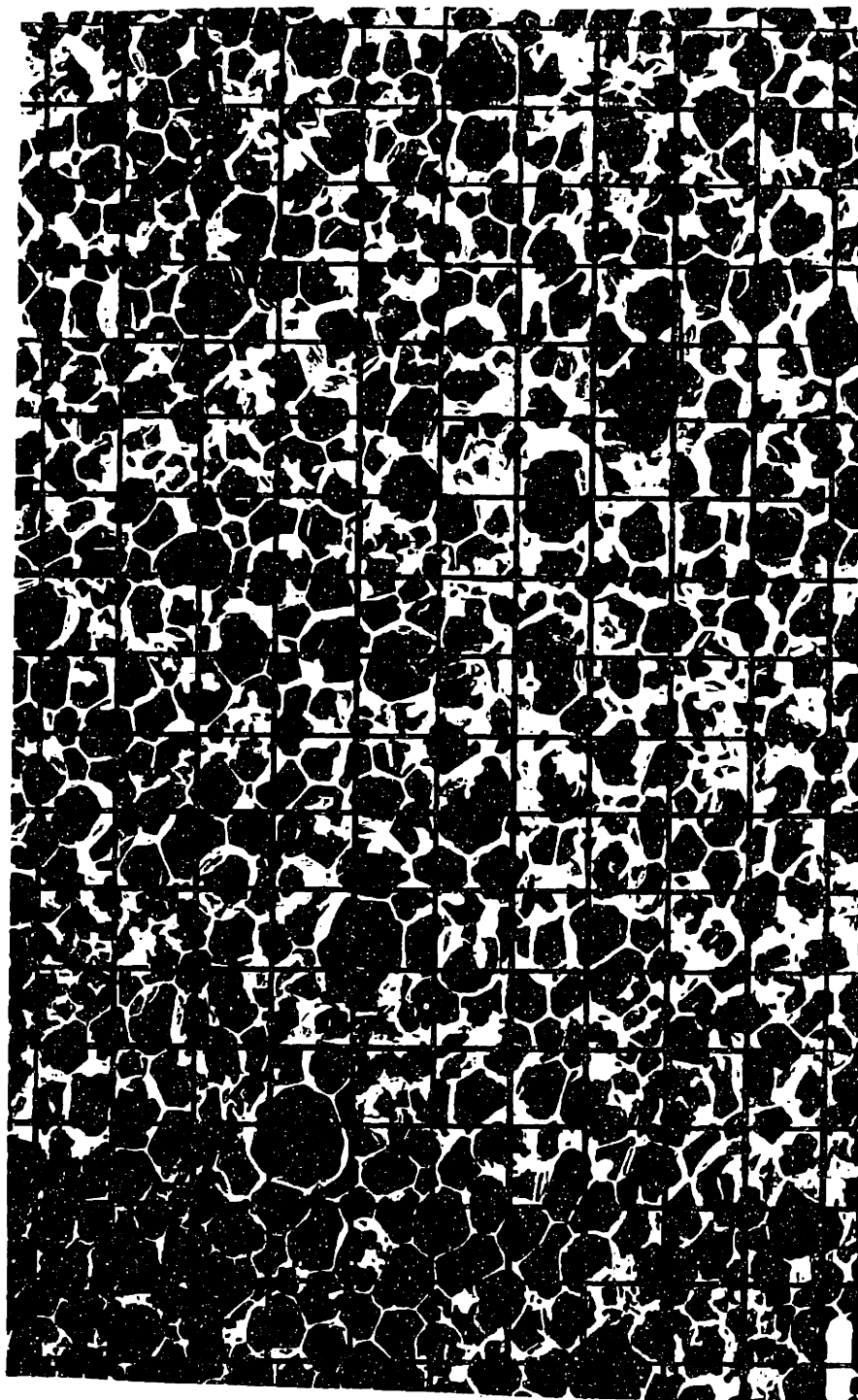
$$S_V = 2 N_L \quad (2-1)$$

where N_L is the number of intersections per unit length created by a test line drawn across a 2-dimensional photograph of the polymer material. This is one reason why the planar cross-sectional photos discussed in Section 2.3.2 were necessary. For the case of the phenolic foam, the large SEM photo montage was sectioned with a uniform grid as shown in Figure 2.19. The number of polymer-test line intersections were then counted and divided by the length of the test line. It was assumed that a non-oriented (i.e., no cell elongation) geometry on the plane was present and was verified by comparing the SEM photos of the different planes shown in Figure 2.20. Although slight cell elongation was detected, it was assumed to be negligible. A more dramatic example of an oriented structure was seen with the polyurethanes in Figure 2.21. For cases such as this, Equation (2-1) became

$$(S_V)_{OR} = 1.571(N_L)_1 + 0.429(N_L)_{11} \quad (2-2)$$

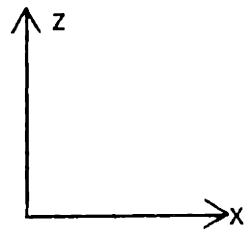
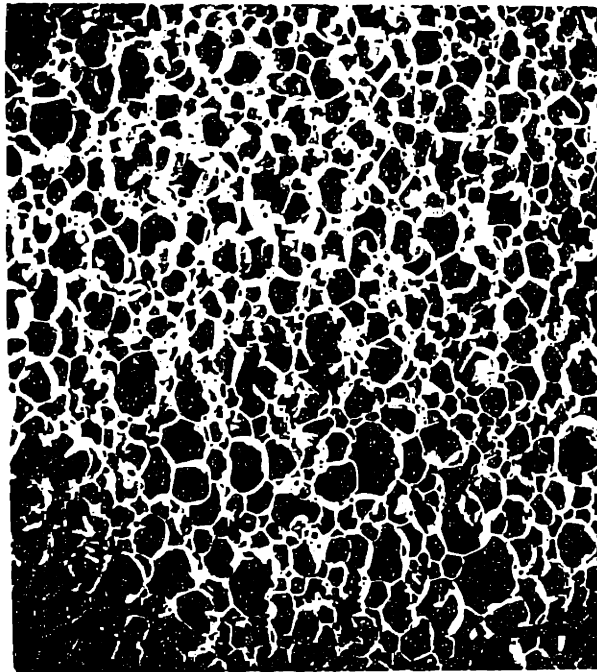
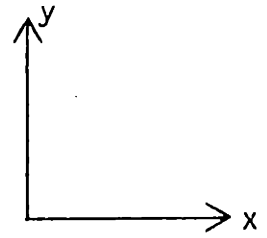
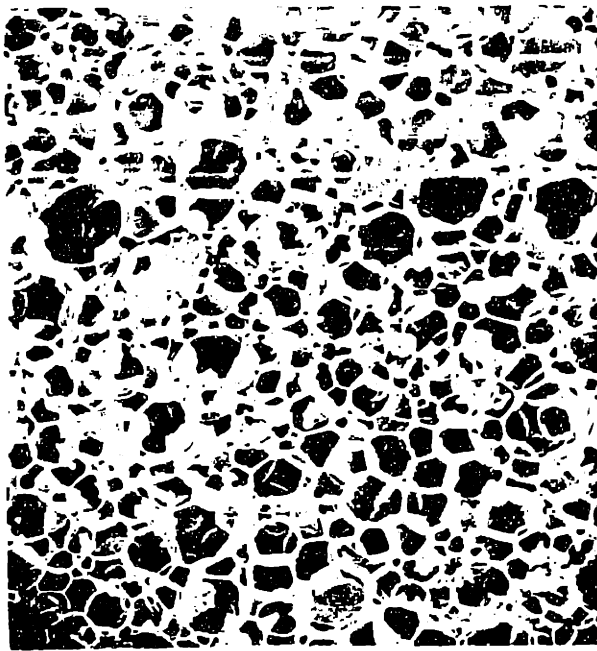
where $(N_L)_1$ is calculated perpendicular to the direction of elongation and $(N_L)_{11}$ along the direction of elongation. A more detailed description for oriented structures can be found in [9].

The second parameter necessary for polymer distribution was the actual cell wall thickness. This was directly measured from high mag-



50
Microns

FIGURE 2.19: SEM PHOTO MONTAGE WITH GRID (200x)



Foam Board

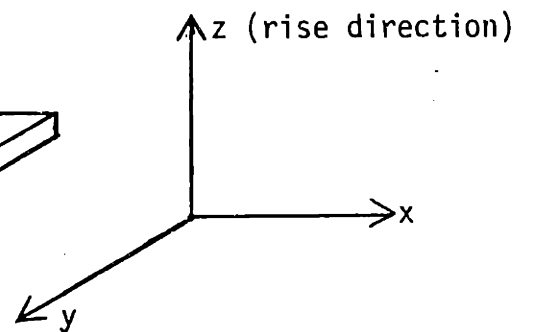
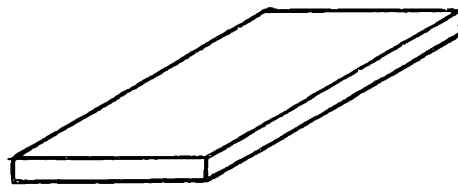


FIGURE 2.20: PHENOLIC FOAM CELL ELONGATION AND ORIENTATION



↑
Rise
Direction

FIGURE 2.21: CELL ELONGATION IN POLYURETHANE FOAM (100x)

nification (10,000x) photographs of the foam cell walls.

The third parameter calculated was the cell wall thickness assuming 100% of the polymer was contained in the cell walls. This was given by:

$$t_{100\% \text{ walls}} = (1-\delta)(1/S_v) \quad (2-3)$$

where

$$\delta = \text{foam void fraction} = \frac{\rho_s - \rho_f}{\rho_s - \rho_g} \quad (2-4)$$

ρ_s = density of solid polymer

ρ_f = density of foam

ρ_g = density of insulating gas

S_v = surface to volume ratio (Equation (2-1))

Therefore, the actual percentage of material in the cell walls was then

$$\% \text{ walls} = \frac{t_{\text{actual}}}{t_{100\% \text{ walls}}} \quad (2-5)$$

where t_{actual} = thickness measured from SEM photos.

Likewise, the percentage of polymer in the struts,

$$\% \text{ struts} = 100 - \% \text{ walls} \quad (2-6)$$

One important assumption was made in order to perform this analysis: the cell wall thickness was so small when compared to the length scale of the cell dimensions that the cell can be treated as having only one surface area. This supposition combined with the assumption of foam structure uniformity (oriented or not) permitted the use of Equations (2-1) and (2-2).

2.4.4 Determination of Cell Size and Shape

As stated previously, the three main goals of the geometry study was to determine the polymer distribution, the cell wall thickness and the cell diameter. The first two parameters were found by methods in the preceding section. The final dimension, cell diameter, required an assumption of the foam geometry and a subsequent calculation. Although cell diameters can easily be seen and measured from SEM photos, it was not known whether the cross-section shown was one that exactly bi-sectioned the cell, thus exposing the correct diameter. If the cell diameters were totally uniform, the proper cell diameter could be assumed as the largest cell diameter visible on the photographs. However, this assumption could not be made for the phenolic foam since cell sizes were known to vary by approximately $\pm 50\%$.

From earlier work with the polyurethanes, four polyhedran structures were chosen to best model any foam material [9]. These were determined in part, by the 3-dimensional geometric possibilities that would exist knowing that the walls of the cells intersect at approximately 120° and that each cell cross-section creates either a 5 or 6-sided figure. These polyhedra include:

rhombic dodecahedron, pentagonal dodecahedron and truncated octahedron. The fourth shape chosen was the cube due to its simplistic shape and ease of modeling.

The approach to the cell diameter calculation was to compute the foam density using the four polyhedra and compare it to the actual foam density. The cell diameter was also calculated for each polyhedra and the results were evaluated based on the actual foam density.

According to reference [9], it was known that the volume of solid polymer was either contained in the cell walls or in the struts. Therefore,

$$1 - \delta = \frac{V_{\text{solid}}}{V_{\text{total}}} = \frac{V_{\text{strut}}}{V_{\text{total}}} + \frac{V_{\text{walls}}}{V_{\text{total}}}, \quad (2-7)$$

where δ , the foam void fraction is defined in Equation (2-4). For each cell,

$$1 - \delta = (A_{\text{strut}}) \left(\frac{L_{\text{edge}}}{V_{\text{model}}} \right) + (t_{\text{wall}})(S_v) \quad (2-8)$$

where, A_{strut} = cross-sectional area of the struts

$\frac{L_{\text{edge}}}{V_{\text{model}}}$ = the total edge length of a given polyhedron per volume according to an aggregate arrangement.

Using Equation (2-4) and solving for the foam density, ρ_f ,

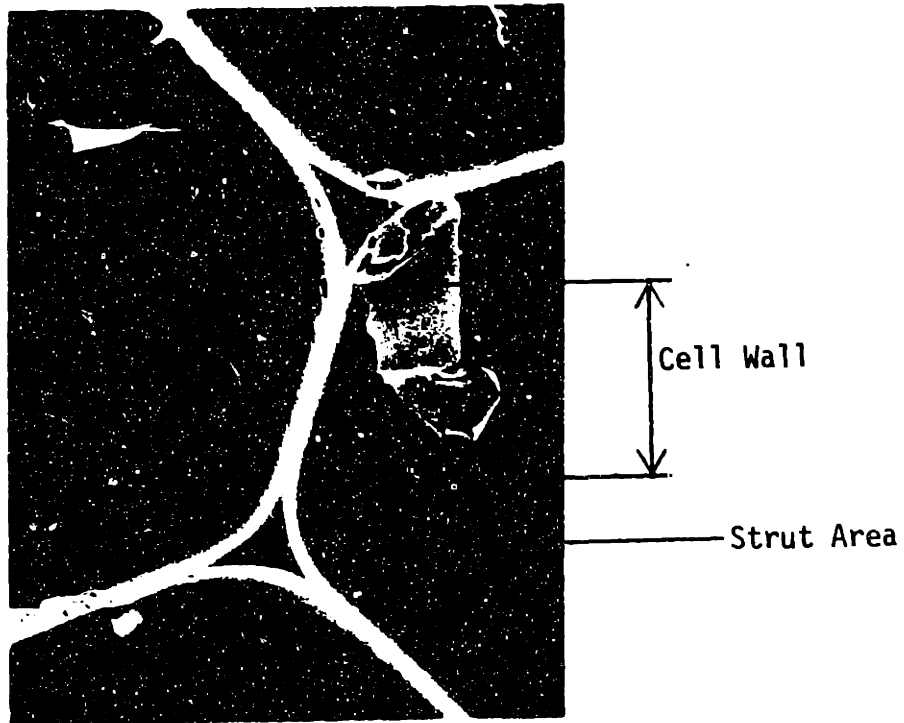
$$\rho_f = (\rho_s - \rho_g) \left[(A_{\text{strut}}) \left(\frac{L_{\text{edge}}}{V_{\text{model}}} \right) + (t_{\text{wall}})(S_v) \right] + \rho_g \quad (2-9)$$

The two quantities not previously determined in Equation (2-9) were A_{strut} and $\frac{L_{\text{edge}}}{V_{\text{model}}}$. The edge length to volume ratio for each polyhedra was found in Table 2-1.

The average cross-sectional area for the struts were found through the use of a Magiscan Image Analyzer computer at MIT. SEM photos that clearly distinguish the struts from the cell walls were used to trace an outline of the strut area on white paper using a dark lead pencil.

TABLE 2.1: GEOMETRIC PARAMETERS OF VARIOUS POLYHEDRA WHEN COMBINED IN AGGREGATE FORM

Polyhedron	# Faces	# Edges	Surface Area	Volume	Surface Area/ Volume Ratio (S_v)	Edge Length/ Volume Ratio	Diameter (d)
Cube	6	12	$3a^2$	a^3	$\frac{3}{a}$	$\frac{4}{a^2}$	a
Pentagonal Dodecahedron	12	30	$10.323a^2$	$7.663a^3$	$\frac{1.347}{a}$	$\frac{1.305}{a^2}$	2.57a
Truncated Octahedron	14	36	$13.393a^2$	$11.314a^3$	$\frac{1.184}{a}$	$\frac{1.06}{a^2}$	3.0a
Rhombic Dodecahedron	12	24	$4.243a^2$	$2a^3$	$\frac{2.121}{a}$	$\frac{4}{a^2}$	2.0a



10 Microns

FIGURE 2.22: SEM PHOTO SHOWING CELL WALL - STRUT DISTINCTION FOR STRUT AREA SURVEY (1000x)

The polymer was not assumed to be in the strut once a uniform wall thickness was obtained. (See Figure 2.22). This was repeated for various cross-sections and the outlines were filled solid with a lead pencil. The Magiscan computer then photographed the traced areas, and, once given a scaling factor, detected the total lead-filled area by the distinction of black and white on the paper. A statistical analysis was generated which determined the average cross-sectional area of the strut. The process was repeated to check for the degree of human error present when tracing the struts. The data are presented in Appendix C.

The geometric parameters for each polyhedra are shown in Table 2-1. These were based strictly on the analysis of the geometric shape and presented as functions of a constant denoted as "a". The parameters include:

- number of faces
- number of edges
- surface area
- volume
- surface area to volume ratio
- edge length to volume ratio
- cell diameter

Of these parameters, the only one previously found was the surface area to volume ratio, S_v . Therefore, "a" was determined from the definition of S_v for each polyhedra and applied to the calculation of the other parameters, including cell diameter. It should be noted, however, that the definition of the parameters are based on an aggregate of successive polyhedra cells. Therefore, each cell shares common

polymer with the other cells around it, and thus alters the calculated parameters (e.g., the surface area of a cube is not $3(\text{diameter})^2$ unless it shares half with a neighboring cube). See Reference [9] for more details. The results are presented in Section 4.1.

CHAPTER 3

THE FOAM MODELS

3.1 Introduction and Background Work

The analytical modeling of the diffusion through phenolic foam was performed through the use of previous models developed at MIT. The earliest models consisted of a simple cubical structure that assumed 100% of the polymer in the cell walls. (See Figure 3.1) The extremely thick cell walls resulted in a gross underestimate of the diffusion coefficient. Further work by Valenzuela and Glicksman [16] suggested that additional modifications were necessary to account for cell stagger and cell elongation. (See Figure 3.2) Reitz later developed a suitable model based on the polyhedra shapes of Section 2.3 and obtained reasonable agreement with experimental polyurethane foam data [9]. More recently, Ostrogorsky suggested that the polyurethane foam would be accurately modeled as closed-packed spheres [1]. The disagreement between his analytical values and the measured values ranged from 23.7% to 0.3%.

This project will utilize the foam models developed by Reitz and Ostrogorsky. The details of the models will not be discussed and only the basics of each technique will be presented in Sections 3.3 and 3.4. Detailed analysis and derivations of the previous work can be found in the references.

3.2 Project Modeling Approach

After reviewing the results of earlier studies, it was decided to implement both modeling techniques (polyhedra and closed-packed spheres) with the phenolic foam. The polyhedra models tended to under predict

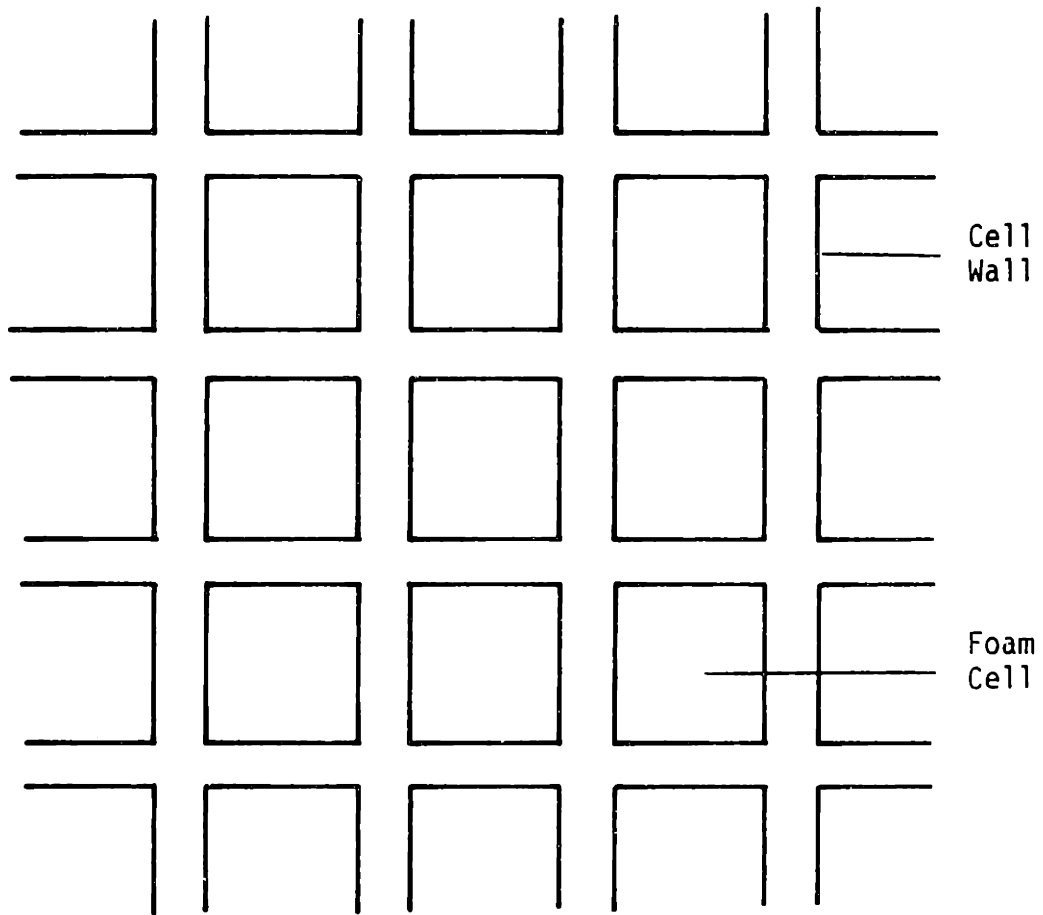
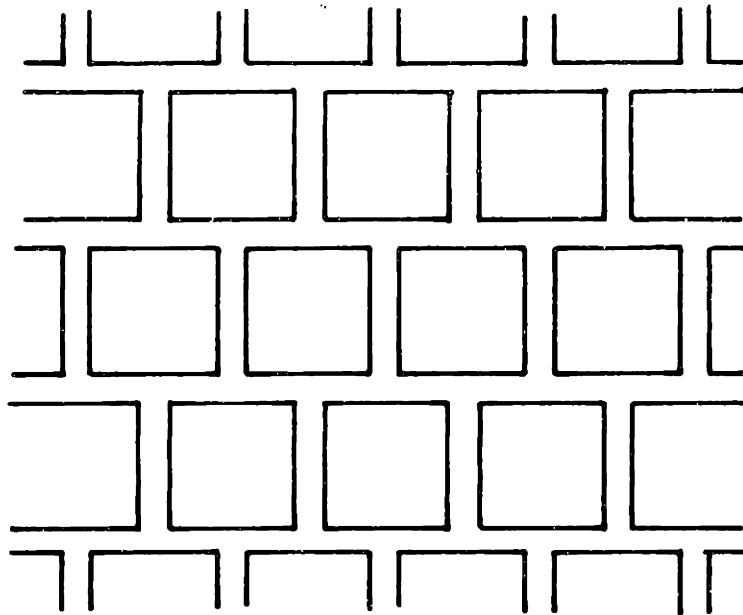
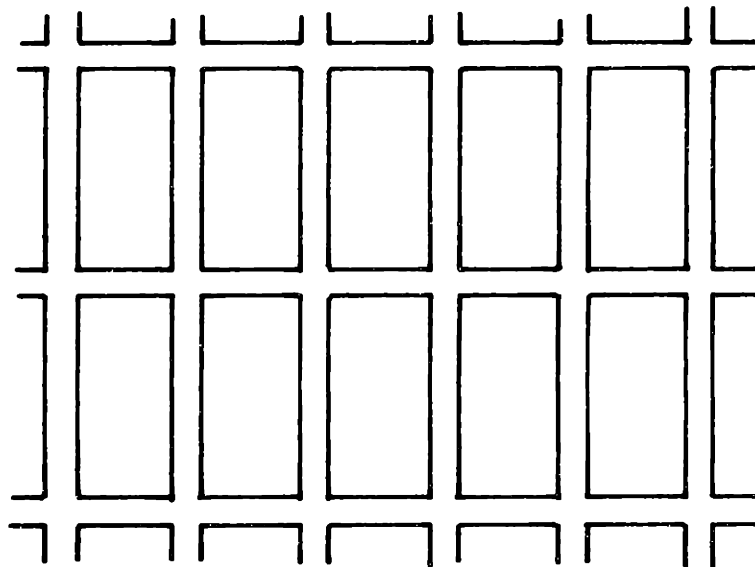


FIGURE 3.1: SIMPLE CUBIC FOAM STRUCTURE



STAGGERED CUBIC CELL STRUCTURE



ELONGATED CELL STRUCTURE

FIGURE 3.2: STAGGERED CUBIC AND ELONGATED CELL STRUCTURES

the measured foam diffusion coefficient while the closed-packed sphere predictions were also less than the experimental results. The closed-packed sphere model was also confirmed through the use of an electrical analogy [1]. By applying both criterion, it was felt that an appropriate range for diffusion coefficients would be found. Also, after encountering difficulties in obtaining experimental polymer film permeability coefficients, it was necessary to use the equations for the foam diffusion coefficient along with the measured values to calculate an approximate polymer permeability coefficient. This will be discussed later in Chapter 4.

Before using either method, the following assumptions were made:

- the cell wall thickness was uniform
- the resistance to diffusion occurred only in the cell walls and resistance within each cell was neglected
- no pinholes or cracks were present in the cell walls
- the direction of diffusion was always parallel to the direction of the gas concentration gradients.

The next two sections will briefly describe each technique and conclude with the equations necessary to predict the foam diffusion coefficients.

3.3 Foam Modeled as Various Polyhedra

In order to define a diffusion coefficient for foam in terms of measurable quantities, the relationship between the diffusion coefficient and the permeability coefficient had to be established. The correlation was found by beginning with the volumetric flux relation of

Equation (1-8).

$$\frac{\dot{V}}{A} = P_e \frac{(p_1 - p_2)}{t}$$

This equation was valid for both foams and films, however, the subsequent analysis applied only to foams. Due to the gas storage capacity of the foam cells and the geometry, the permeability coefficient was redefined as an effective permeability coefficient, $P_{e\text{eff}}$. The mass flux through the foam was then

$$J = \frac{V}{A} \rho_{\text{gas}} = P_{e\text{eff}} \frac{(p_1 - p_2)}{t} \rho_{\text{gas}} \quad (3-1)$$

The partial pressures of the gas species in question, p_1 and p_2 , were then defined through the ideal gas law

$$pV = nRT$$

to obtain

$$p = RT \frac{n}{V} = \frac{RT}{M_{\text{gas}}} C \quad (3-2)$$

where

- p = gas partial pressure
- R = universal gas constant
- T = absolute temperature
- M = molecular weight of the gas
- C = gas concentration

Equation (3-1) then becomes

$$J = \frac{C_1 - C_2}{t} \rho_{\text{gas}} \frac{RT}{M_{\text{gas}}} (P_{e\text{eff}}) \quad (3-3)$$

The effective diffusion coefficient, D_{eff} , was defined based on Equation (3-3) to simply be the multiplicand with $\frac{C_1 - C_2}{t}$, or

$$D_{\text{eff}} \equiv \rho_{\text{gas}} \frac{RT}{M_{\text{gas}}} (P_{e\text{eff}}) \quad (3-4)$$

Therefore,

$$J = D_{\text{eff}} \left(\frac{C_1 - C_2}{t} \right) \quad (3-5)$$

which restated Fick's Law.

Also, by the ideal gas law,

$$p_{\text{gas}} \frac{RT}{M_{\text{gas}}} = \frac{n_{\text{gas}} RT}{V} = p_{\text{gas}} \quad (3-6)$$

Or, combined with Equation (3-4) yielded that, for each specific gas,

$$D_{\text{eff}} = p_{\text{gas}} (P_{e_{\text{eff}}}) \quad (3-7)$$

Now, what remained to be determined was the value of p_{gas} . However, since the low pressure side of the foam was maintained at ambient pressure and the high pressure side was measured with respect to ambient pressure, p_{gas} was simply atmospheric pressure. Therefore:

$$D_{\text{eff}} = p_{\text{gas,atm}} P_{e_{\text{eff}}} \quad (3-8)$$

for each gas considered.

As shown in Section 3.4, Ostrogorsky determined that $p_{\text{gas,atm}}$ is analogous to the effective solubility of foam. In that foam, Equation (3-8) would closely follow Equation (1-7).

In order to model the foam structure, each cell wall was considered to be a resistance to diffusion as

$$R = \frac{t}{A P_{e_{\text{cell wall}}}} \quad (3-9)$$

For the simple cubic structure of thickness L and walls of thickness t (Figure 3-3), the overall resistance was given by summing the individual resistances,

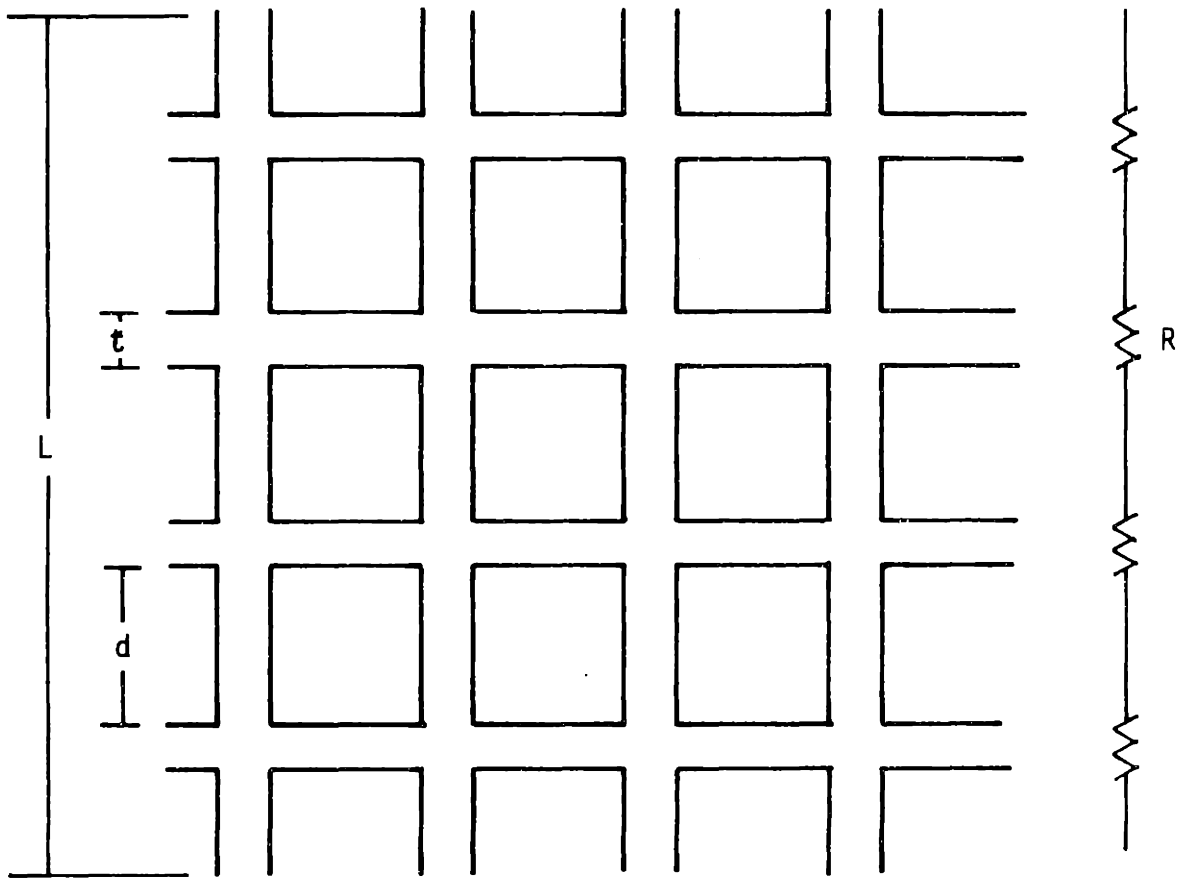


FIGURE 3.3: CUBIC CELL FOAM MODELED AS A SUM OF RESISTANCES

or,

$$R = n \frac{t}{A Pe_{\text{cell wall}}} = \frac{L}{A Pe_{\text{eff}}} \quad (3-10)$$

where

n = number of cell walls for thickness L

t = wall thickness

A = cross-sectional area

L = sample thickness

Pe_{eff} = the effective permeability coefficient for the foam which accounts for the foam geometry and the gas storage in the cells.

• Solving for Pe_{eff} yielded:

$$Pe_{\text{eff}} = \frac{L}{nt} Pe_{\text{cell walls}} \quad (3-11)$$

but n is calculated by

$$n = \frac{L}{t+d} \quad (3-12)$$

where d = cell diameter.

Combining Equations (3-11) and (3-12), resulted in

$$Pe_{\text{eff}} = \frac{t+d}{t} Pe_{\text{cell wall}} \quad (3-13)$$

and for $t \ll d$,

$$Pe_{\text{eff}} \approx \frac{d}{t} Pe_{\text{cell wall}} \quad (3-14)$$

Equation (3-14) exposed a very useful result: the effective permeability coefficient for a foam of thickness t can be calculated by determining only two parameters; the cell diameter, d , and the polymer permeability coefficient, $Pe_{\text{cell wall}}$. Therefore, it was easy to model any of the

foam polyhedra discussed in Section 2.3 by simply substituting the relationship for surface area to volume ratio, S_v , and the cell diameter (found in Table 2-1) into Equation (3-14) for each shape:

$$\text{Cube: } Pe_{\text{eff}} = \frac{3Pe_{\text{cell wall}}}{(S_v)t} \quad (3-15)$$

Pentagonal Dodecahedron:

$$Pe_{\text{eff}} = \frac{3.46 Pe_{\text{cell wall}}}{(S_v)t} \quad (3-16)$$

Truncated Octahedron:

$$Pe_{\text{eff}} = \frac{3.55 Pe_{\text{cell wall}}}{(S_v)t} \quad (3-17)$$

Rhombic Dodecahedron:

$$Pe_{\text{eff}} = \frac{4.24 Pe_{\text{cell wall}}}{(S_v)t} \quad (3-18)$$

Note that it was assumed that for Equation (3-15) to (3-18) there was no cell stagger in the models and no cell elongation. Reference [9] contains the details for these slight variations. The results of the modeling are presented in Chapter 4.

3.4 Foam Modeled as Closed-Packed Spheres

The "successive membrane", or closed-packed sphere model suggested by Ostrogorsky [1] was similar in principle to the polyhedron models of Section 3.3. In order to model the foam as a succession of cell walls, the first parameter determined was the average distance between the cell

walls. This was calculated from the SEM photos of Section 2.3 by computing.

$$\langle \ell \rangle = 1/N_L \quad (3-19)$$

where,

$\langle \ell \rangle$ = average distance between cell walls

N_L = number of polymer test line intersections per length of test line from Section 2.4.3.

or, for the overall foam structure of Figure 3.4,

$$\langle \ell \rangle = L/n \quad (3-20)$$

The resistance of each cell wall was defined as:

$$R_{\text{cell wall}} = \frac{t}{A_{\text{act}} Pe_{\text{cell wall}}} \quad (3-21)$$

where A_{act} = the actual polymer permeation of the cell

t = cell wall thickness

For a foam structure consisting of n successive membranes, the overall foam resistance became:

$$R_{\text{foam}} = n R_{\text{cell wall}} = \frac{nt}{A_{\text{act}} Pe_{\text{cell wall}}} \quad (3-22)$$

The next point recognized was that, due to cell curvature, the actual polymer area involved in the permeation process was not necessarily equal to the cross-sectional area of the cell. In fact, the only case where they were equivalent was for a cubical model. To account for this, an effective permeability coefficient was defined from Equation (3-21):

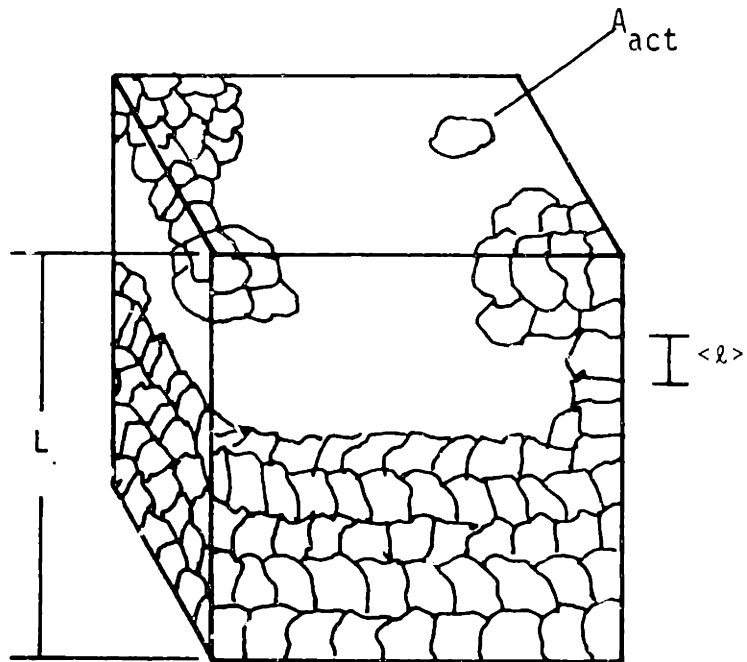


FIGURE 3.4: CLOSED PACKED SPHERE MODEL OF FOAM

$$R_{\text{foam}} = \frac{L}{A P_{\text{eff}}} \quad (3-23)$$

where L = thickness of foam
 A = foam cross sectional area

Therefore, from Equations (3-22) and (3-23)

$$P_{\text{eff}} = \left(\frac{L}{nt}\right) \left(\frac{A_{\text{act}}}{A}\right) Pe_{\text{cell wall}} \quad (3-24)$$

By combining Equation (3-20),

$$P_{\text{eff}} = \frac{\langle l \rangle}{t} (\epsilon) Pe_{\text{cell wall}} \quad (3-25)$$

where, $\epsilon \equiv \frac{A_{\text{act}}}{A}$ (3-26)

In Equation (3-26), ϵ is defined as the enhancement parameter and described in greater detail in [1]. Also presented is an electrical analogy technique which determines ϵ for structures of various shapes and complexities.

If we assumed the foam to be modeled as closely packed spheres, ϵ simply becomes the area of a hemisphere divided by its cross-sectional area, or $\epsilon = \left(\frac{1}{2}\right) 4 \pi R^2 / (\pi R^2) = 2$ (3-27)

Therefore, Equation (3-25) becomes:

$$P_{\text{eff}} = \frac{2\langle l \rangle}{t} (Pe_{\text{cell wall}}) \quad (3-28)$$

To convert the effective permeability coefficient to an effective diffusion coefficient, Equation (1-7) was rewritten as:

$$D_{\text{eff}} = \frac{P_{\text{eff}}}{S_{\text{eff}}} \quad (3-29)$$

where S_{eff} = the effective solubility of the foam due to the cell voids.

Ostrogorsky showed that the effective solubility is a function of temperature only and that in this form, the solubility of air component gases at STP is $1 \frac{\text{cm}^3_{\text{STP}}}{\text{cm}^3\text{-atm}}$. Therefore, for convenience, a temperature correction was added to Equation (3-29).

$$D_{\text{eff}} = \frac{P_{\text{eff}}}{S_{\text{eff,STP}} (T_{\text{STP}}/T)} \quad (3-30)$$

where T = absolute temperature

By combining Equation (3-28) with Equation (3-30) and using

$$S_{\text{eff}} = 1 \frac{\text{cm}^3_{\text{STP}}}{\text{cm}^3\text{-atm}},$$

$$D_{\text{eff}} = 2 \frac{\langle l \rangle (P_{\text{cell wall}})}{t} \left(\frac{T}{T_{\text{STP}}} \right) \quad (3-31)$$

In review, Equation (3-31) provided an effective diffusion coefficient for a foam at temperature T when modeled as a succession of closed-packed spheres. The three physical parameters necessary for the calculation are 1) the thickness of the cell walls, 2) the permeability of the polymer and 3) the average distance between the cell walls.

3.5 Polymer Distribution Effects on Foam Permeability

In order to analytically determine the effects of polymer distribution on the effective permeability coefficient, P_{eff} , a foam sample of thickness, L , and cross-sectional area, A , (Figure 3-4) was considered.

The amount of polymer in the cell walls was defined as:

$$\% \text{ wall} = \frac{V_{\text{wall}}}{V_{\text{wall}} + V_{\text{strut}}} = \frac{V_{\text{wall}}}{V_{\text{polymer}}}$$

where, V_{wall} = total volume of polymer in the cell walls

V_{polymer} = total volume of polymer in the foam

or, $V_{\text{wall}} = (\% \text{ wall}) V_{\text{polymer}}$ (3-32)

Also, the mass of the foam was given by

$$M_{\text{foam}} = M_{\text{polymer}} + M_{\text{gas}}$$

where, M_{foam} = mass of foam

M_{polymer} = mass of polymer

M_{gas} = mass of insulating gas

but, $M_{\text{gas}} \ll M_{\text{polymer}}$

so, $M_{\text{foam}} \approx M_{\text{polymer}}$ (3-33)

The foam density then became:

$$\rho_f = \frac{M_{\text{foam}}}{V_{\text{foam}}} \approx \left(\frac{M_{\text{polymer}}}{V_{\text{polymer}}} \right) \left(\frac{V_{\text{polymer}}}{V_{\text{foam}}} \right) \quad (3-34)$$

where, $V_{\text{foam}} = (A)(L)$ (3-35)
 = volume of the foam sample

Therefore, from Equation (3-32),

$$\frac{V_{\text{wall}}}{V_{\text{foam}}} = (\% \text{ wall}) \frac{V_{\text{polymer}}}{V_{\text{foam}}} \quad (3-36)$$

The volume of polymer in the walls is equal to:

$$V_{\text{wall}} = n A_{\text{act}} t \quad (3-37)$$

where, n = number of cell walls
 A_{act} = actual area of cell wall
 t = cell wall thickness

so,

$$\frac{V_{\text{wall}}}{V_{\text{foam}}} = \frac{n A_{\text{act}} t}{A L} \quad (3-38)$$

Equating (3-36) and (3-38) results in:

$$\frac{nt}{L} = (\% \text{ wall}) \frac{\rho_{\text{foam}}}{\rho_{\text{polymer}}} \left(\frac{A}{A_{\text{act}}} \right) \quad (3-39)$$

Combining Equations (3-39), (3-24) and (3-20) and letting $Pe_{\text{cell wall}} =$

Pe_{polymer}

$$Pe_{\text{eff}} = \left(\frac{A_{\text{act}}}{A} \right)^2 \frac{\rho_{\text{polymer}}}{\rho_{\text{foam}}} \frac{(Pe_{\text{polymer}})}{(\% \text{ walls})} \quad (3-40)$$

and by the definition of the enhancement parameter, ϵ ,

$$Pe_{eff} = (\epsilon)^2 \frac{\rho_{polymer}}{\rho_{foam}} \frac{(Pe_{polymer})}{(\% \text{ walls})} \quad (3-41)$$

Equation (3-41) suggests that the resistance to gas permeability in a foam can be improved by a) utilizing polymer resins that have lower permeability coefficients, and b) placing a larger percentage of polymer in the cell walls. It is interesting to note that simply increasing the thickness of the cell walls is not necessarily beneficial to the aging phenomenon if the struts are thickened by a corresponding amount. The most important aspect of foam development is efficiently making use of the total polymer present by shifting it from the struts to the cell walls.

CHAPTER 4

RESULTS AND OBSERVATIONS

4.1 The Foam Geometry Study

The foam geometry study was performed by using scanning electron microscope (SEM) photographs of the foam and the various metallography measurements discussed in Section 2.4. The surface area to volume ratio, S_v , was determined from the photo montage and grid arrangement shown in Figure 4.1. The average number of polymer - test line intersections per length of test line was 12.0 mm^{-1} . Using Equation (2-1), the surface area to volume ratio was then 24.0 mm^{-1} .

In order to calculate the percentage of polymer contained in the cell walls, Equations (2-3), (2-4) and (2-5) were combined to yield:

$$\% \text{ Walls} = \frac{t_{\text{actual}}(S_v)}{(1 - \delta)} \times 100 \quad (4-1)$$

where t_{actual} = actual wall thickness

$$\delta = \frac{\rho_s - \rho_f}{\rho_s - \rho_g} \quad (2-4)$$

The void fraction, δ , is the percentage of the foam, by volume, occupied by the insulating gas. The following values were used to calculate δ :

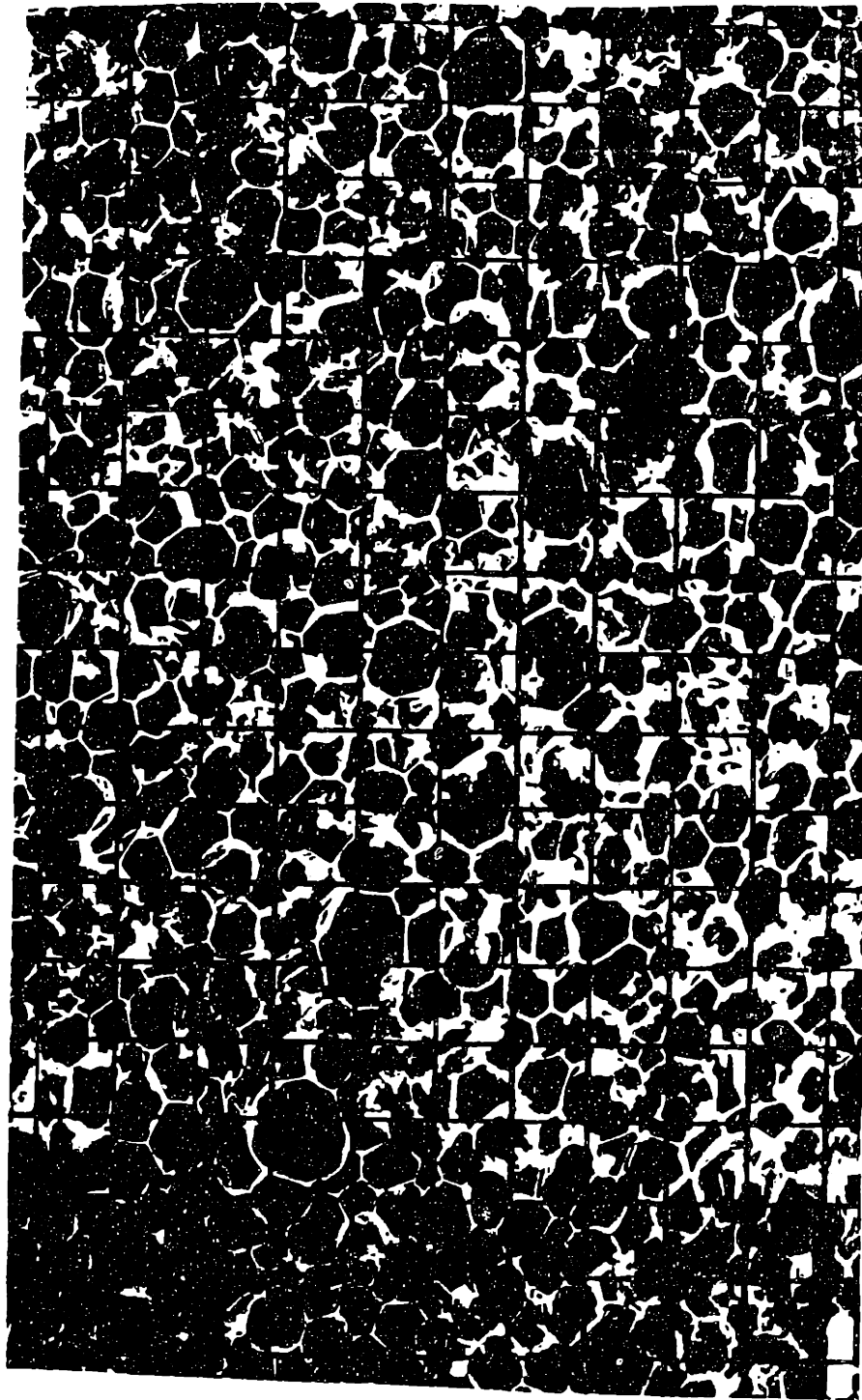
$$\rho_s = \text{density of the solid polymer} = 1200.0 \text{ kg/m}^3 \text{ (74.9 lb/ft}^3\text{)}$$

$$\rho_f = \text{density of the foam} = 40.0 \text{ kg/m}^3 \text{ (2.50 lb/ft}^3\text{)}$$

$$\rho_g = \text{density of insulating gas} = 5.04 \text{ kg/m}^3 \text{ (0.315 lb/ft}^3\text{)} \\ \text{(50/50 mixture of Freon 11 and 113 in vapor form)}$$

The void fraction was then computed to be:

$$\delta = 0.971 = 97.1\%$$



50
Microns

FIGURE 4.1: SEM PHOTO MONTAGE TO DETERMINE: S_V (200x)

The actual wall thickness was measured from SEM photographs (see Figure 4.2) to be an average value of 0.5 microns.

Therefore, the percentage of polymer in the cell wall was calculated as

$$\% \text{ walls} = 41.4\%$$

Likewise,

$$\% \text{ struts} = 58.6\%$$

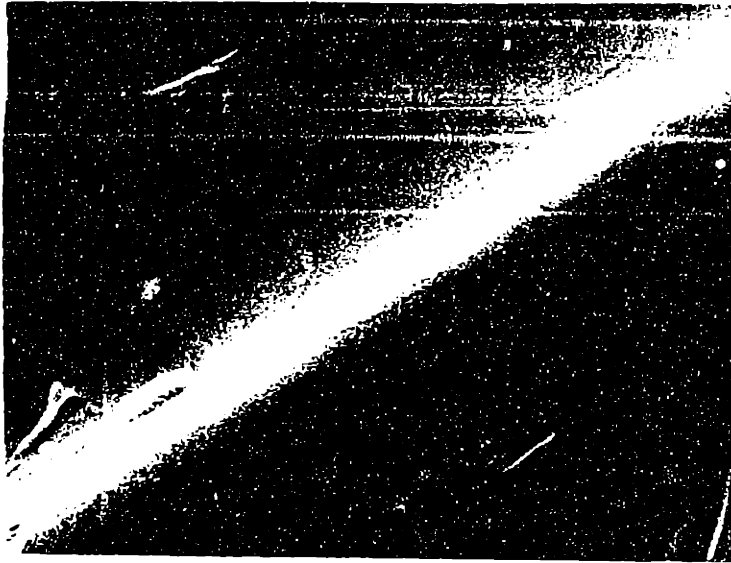
For comparison, in the reported results of polyurethane foams, 15% - 20% of the material is in the cell walls, while 80% - 85% is contained in the struts. The void fraction of polyurethane foam was approximately that of the phenolic [9].

To predict the foam density through the use of the polyhedra models, the cross-sectional area of the struts needed to be determined. The Magiscan Image Analyzer computer analysis revealed the average cross-sectional area of the struts to be

$$A_{\text{struts}} = 3.86 \times 10^{-5} \text{ mm}^2 \quad (5.98 \times 10^{-8} \text{ in}^2)$$

and a measurement repeatability of 3.2%.

The results of applying Equation (2-9) to the four polyhedra discussed in Section 2.4.4 are presented in Table 4.1. The actual foam density, calculated from parallelepiped foam samples of various sizes, was found to be 40.0 kg/m^3 (2.50 lb/ft^3). This value corresponded well with the manufacturer's density range of $38.5 - 41.7 \text{ kg/m}^3$ ($2.40 - 2.60 \text{ lb/ft}^3$). Table 4.1 shows that the cubic model under predicted the density by 22%. However, excellent agreement, - 3.75% and + 7.5%, occurs when using the pentagonal dodecahedron and rhombic dodecahedron



2.5
Microns

(4000x)



1.0
Microns

(10,000x)

FIGURE 4.2: SEM PHOTOS OF PHENOLIC CELL WALL THICKNESS

TABLE 4.1: RESULTS OF FOAM DENSITY PREDICTIONS USING VARIOUS POLYHEDRON AGGREGATES

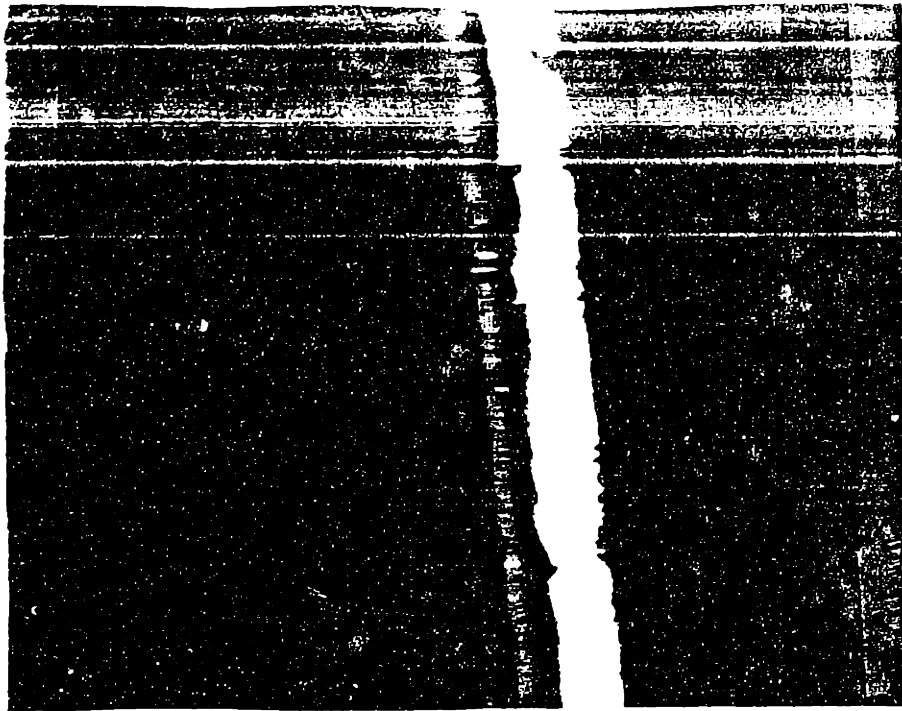
POLYHEDRON SHAPE	CALCULATED CELL DIAMETER, (d) (Microns)	PREDICTED FOAM DENSITY kg/m^3 (1b/ft ³)	ACTUAL FOAM DENSITY kg/m^3 (1b/ft ³)	% ERROR
Cube	125	31.2 (1.95)	40.0 (2.50)	-22.0
Pentagonal Dodecahedron	144	38.5 (2.40)	40.0 (2.50)	- 3.75
Truncated Octahedron	148	39.5 (2.46)	40.0 (2.50)	- 1.25
Rhombic Dodecahedron	177	43.0 (2.68)	40.0 (2.50)	+ 7.5

models, respectively. The closest approximation (-1.25%) was achieved through the use of the truncated octahedron. Table 4.1 also shows the cell diameters were estimated to range from 125 to 177 microns.

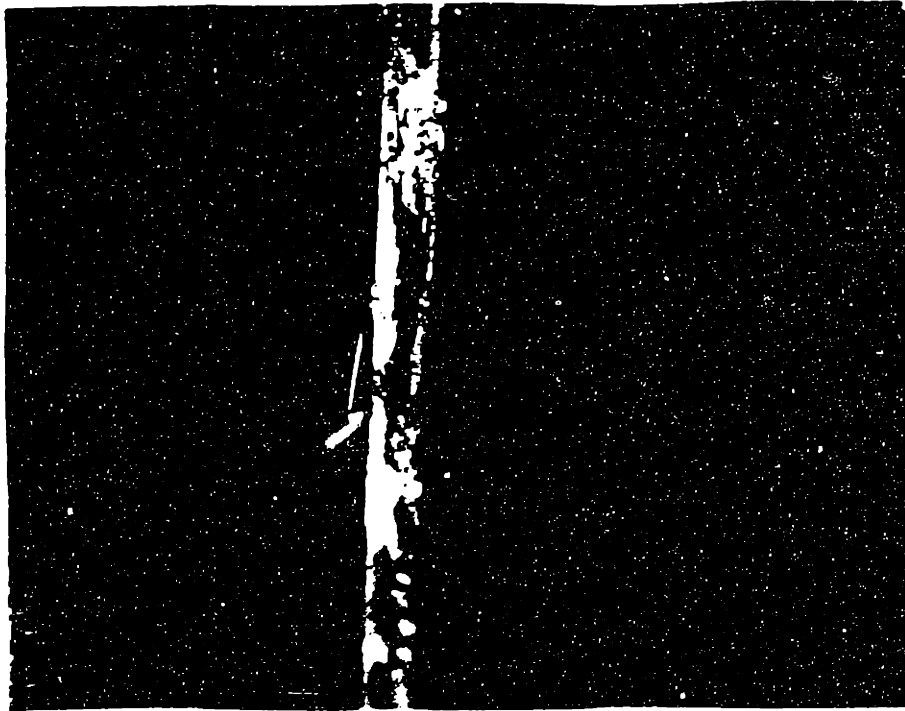
4.2 The Polymer Film Tests

The polymer film tests were performed according to the procedures of Section 2.3. The initial tests were conducted with a cell similar to Figure 2.12; however, the pressure transducer was not incorporated into the design. Instead, a methyl isobutyl ketone slug in a capillary tube was used to indicate the volumetric flow due to permeation. The film samples obtained from the manufacturer appeared to be adequate for testing. The film thicknesses were measured from optical microscope photographs (Figure 4.3) and varied from 30 to 70 microns. Table 4.2 shows the permeability coefficients of these initial tests along with values obtained from polyurethane films. The fact that the phenolic permeability coefficients were approximately equal to those of the polyurethane, and that they appeared to be fairly independent of test gas and temperature, prompted further examination into the film samples. Optical microscope surveys revealed the presence of micro-holes and cracks in the polymer surface. Therefore, the polymer films were determined inadequate for testing.

The film test cell apparatus using the pressure transducer (shown in Figures 2.11 and 2.12) was constructed while various methods for generating improved film samples were investigated. A polymer scientist at the manufacturer stated that to eliminate the formation of micro-holes that occurred during resin curing, the thickness of the films would have to



65 Microns



35 Microns

FIGURE 4.3: OPTICAL MICROSCOPE PHOTOS TO DETERMINE POLYMER FILM THICKNESS (200x)

TABLE 4.2: INITIAL RESULTS OF PHENOLIC POLYMER FILM TESTS
USING DEFECTED FILM SAMPLES

FILM SAMPLE	TEST GAS	TEMPERATURE °C	PERMEABILITY COEFFICIENT, Pe $\left(\frac{\text{cm}^3}{\text{cm} \cdot \text{s} \cdot \text{atm}}\right)_{\text{STP}}$
Phenolic #2	CO ₂	27	26.6 x 10 ⁻¹⁰
Phenolic #2	CO ₂	27	35.0 x 10 ⁻¹⁰
Phenolic #2	CO ₂	27	23.6 x 10 ⁻¹⁰
Phenolic #4	CO ₂	27	24.3 x 10 ⁻¹⁰
Phenolic #5	CO ₂	50	25.8 x 10 ⁻¹⁰
Phenolic #10	CO ₂	50	44.1 x 10 ⁻¹⁰
Polyurethane ⁽¹⁾ (Methane Diisocyanate)	CO ₂	27	16.9 x 10 ⁻¹⁰
Phenolic #6	O ₂	27	17.5 x 10 ⁻¹⁰
Phenolic #6	O ₂	27	10.6 x 10 ⁻¹⁰
Polyurethane ⁽¹⁾ (Methane Diisocyanate)	O ₂	27	4.26 x 10 ⁻¹⁰

(1) Ostrogorsky

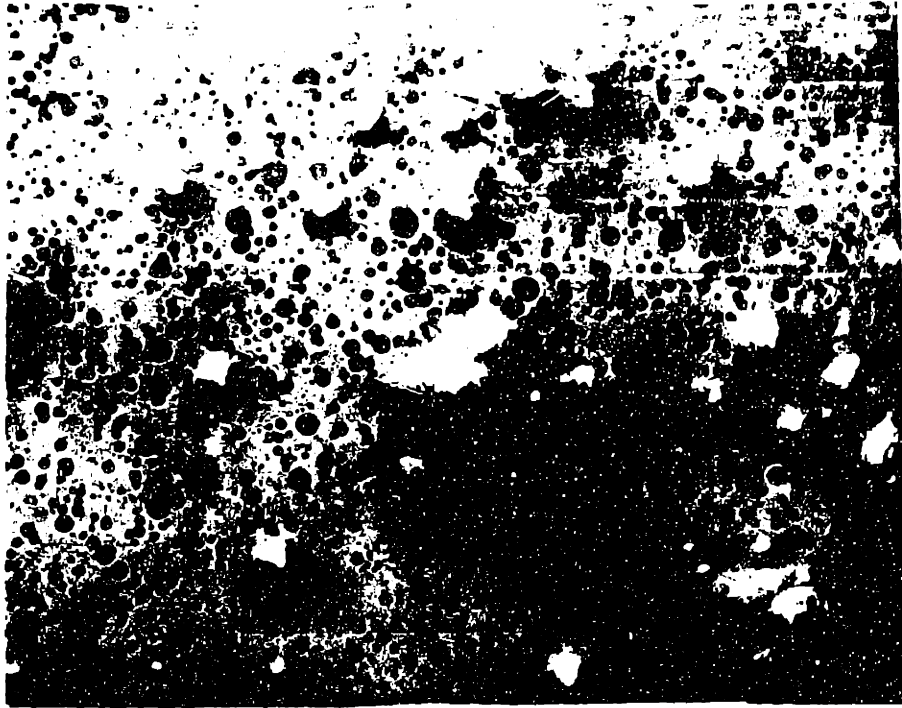
be increased [14].

Two new series of film samples were made that ranged in thickness from 100 to 650 microns. The thinner specimens (100 to 200 microns) consisted of the proper phenol polymer but was not mixed with the formaldehyde additive used in the actual foam product. These films entrapped an unacceptable amount of micro-bubbles during curing as shown in Figure 4.4. The thicker specimens (400 to 650 microns) did include the formaldehyde additive, but also contained micro-bubbles and some surface cracks (Figure 4.5). In addition, the excessive polymer thickness prevented any practical permeation measurements.

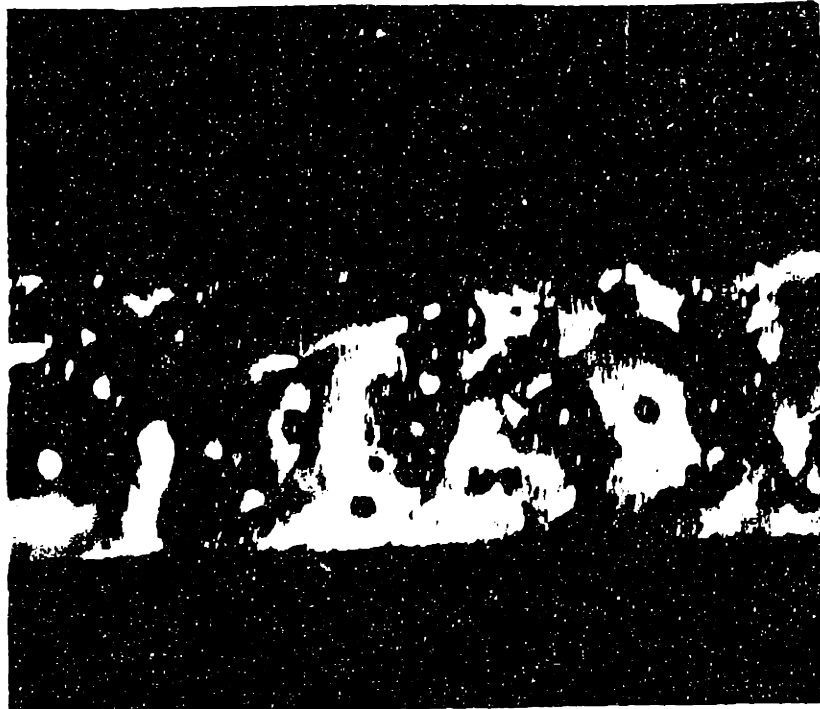
Further consultation with the manufacturer revealed that, at the present time, all conceivable ideas for creating suitable film samples, without severely altering the polymer characteristics, have been exhausted. Therefore, it was decided to calculate the film permeability coefficients by use of the models presented in Chapter 3 and the measured foam permeability coefficients. These results are shown in Section 4.4.

4.3 The Phenolic Foam Tests

The phenolic foam permeability tests were completed by using the apparatus and techniques described in Section 2.2. A 0.57 cm (0.225 in) thick foam sample was tested at 75°C, 50°C and room temperature. The test gases used were carbon dioxide, oxygen and nitrogen. The volumetric flowrates due to the permeation of the test gas through the foam were measured by detecting a pressure increase in the upper chamber with a pressure transducer. Typical strip chart data are shown in Figure 4.6. The results of the tests, i.e., the permeation coefficients, are shown



Surface View (50x)

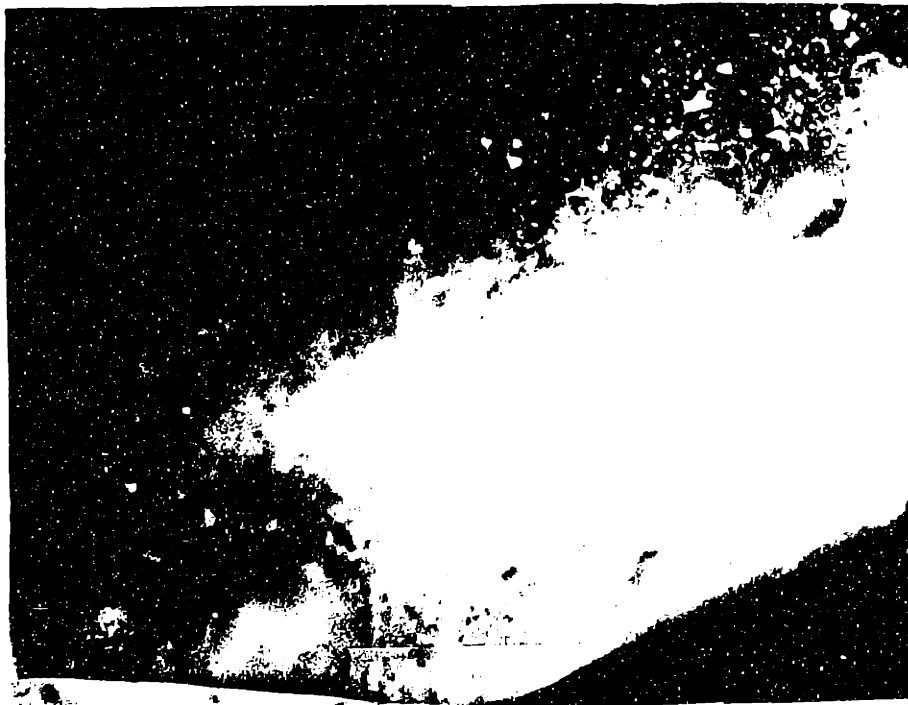


Cross Sectional View (100x)

FIGURE 4.4: OPTICAL MICROSCOPE PHOTOS OF DEFECTS IN PHENOLIC POLYMER WITHOUT FORMALDEHYDE ADDITIVE



Surface View (50x)



100
Microns

Cross Sectional View (100x)

FIGURE 4.5: OPTICAL MICROSCOPE PHOTOS SHOWING DEFECTS AND EXCESSIVE THICKNESS IN PHENOLIC POLYMER WITH FORMALDEHYDE ADDITIVE

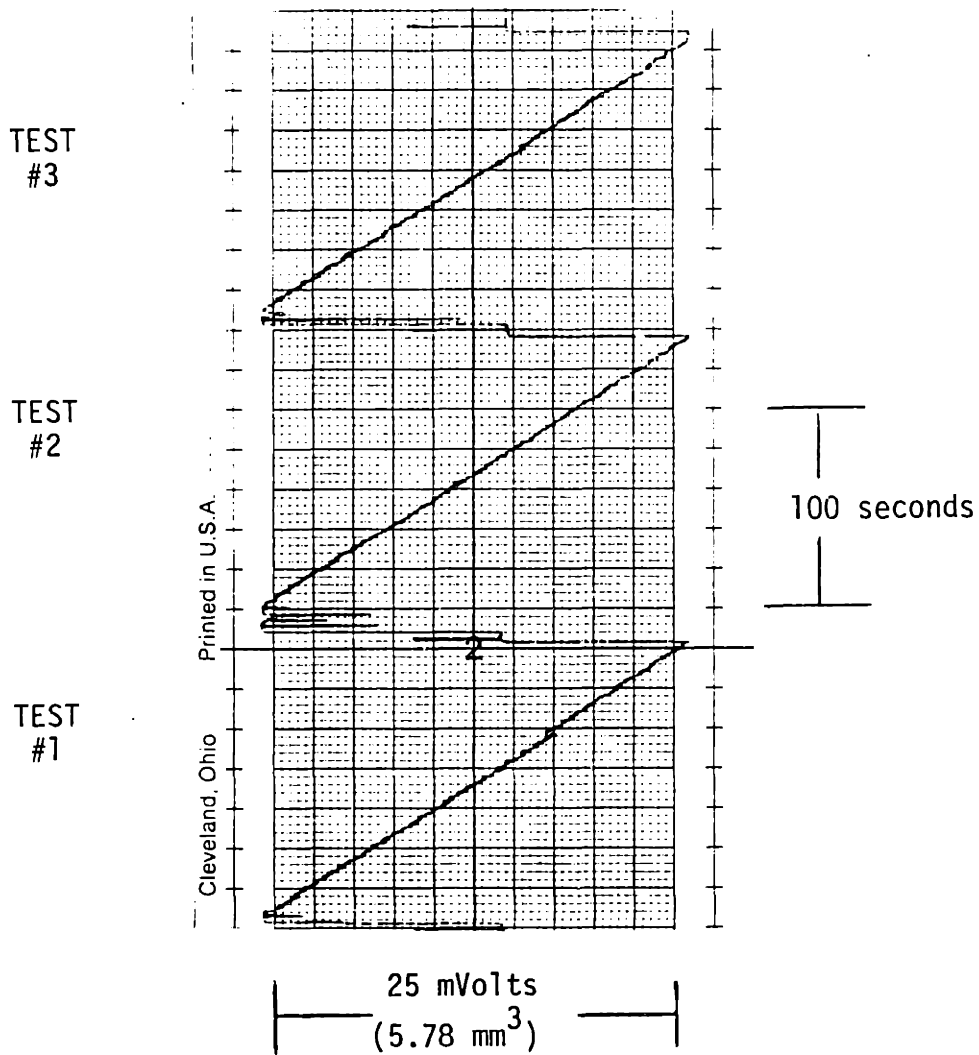


FIGURE 4.6: STRIP CHART DATA OF INITIAL FOAM TESTS SUGGESTING KNUDSEN DIFFUSION (CO₂ at 25°C)

in Figure 4.7 and presented as an inverse function of temperature according to the Arrhenius expression:

$$P_e = P_{e_0} \exp(-E_p/RT) \quad (1-10)$$

Figure 4.7 suggests that the permeability of the foam is independent of both temperature and test gas. This result was inconsistent with reported polyurethane foam data. Apparently, a mass transport phenomenon other than Fickian diffusion was present. The volumetric flowrates were too small to suggest a bulk flow leak, but Knudsen-type diffusion appeared possible. The sample was removed and inspected. There were no visible cracks in the sample, however, after careful measurements, the thickness of the sample was found to have decreased by 13%. Therefore, cell damage was suspected.

In order to further investigate the sample tested, a thermal conductivity test was performed by a local testing firm [17]. A k-value of $0.028 \frac{\text{Watts}}{\text{m}^\circ\text{K}}$ ($0.197 \frac{\text{BTU(in)}}{(\text{hr})\text{ft}^2^\circ\text{F}}$) was determined which is an increase of 79% above the reported conductivity of $0.016 \frac{\text{Watts}}{\text{m}^\circ\text{K}}$ ($0.11 \frac{\text{BTU in}}{\text{hr ft}^2 \text{ }^\circ\text{F}}$) for this particular phenolic foam. This change could be accounted for by assuming the cell walls were damaged during the foam permeability tests and the insulating gas was permitted to escape, thus increasing the thermal conductivity of the foam.

In response to the previous results, a subsequent foam test was performed. It was felt that the cell damage in the previous tests was due to the high temperatures, the 8 psi pressure difference imposed on the foam, or a combination of these conditions. Therefore, a new foam sample was tested using carbon dioxide at 30°C. After two weeks testing

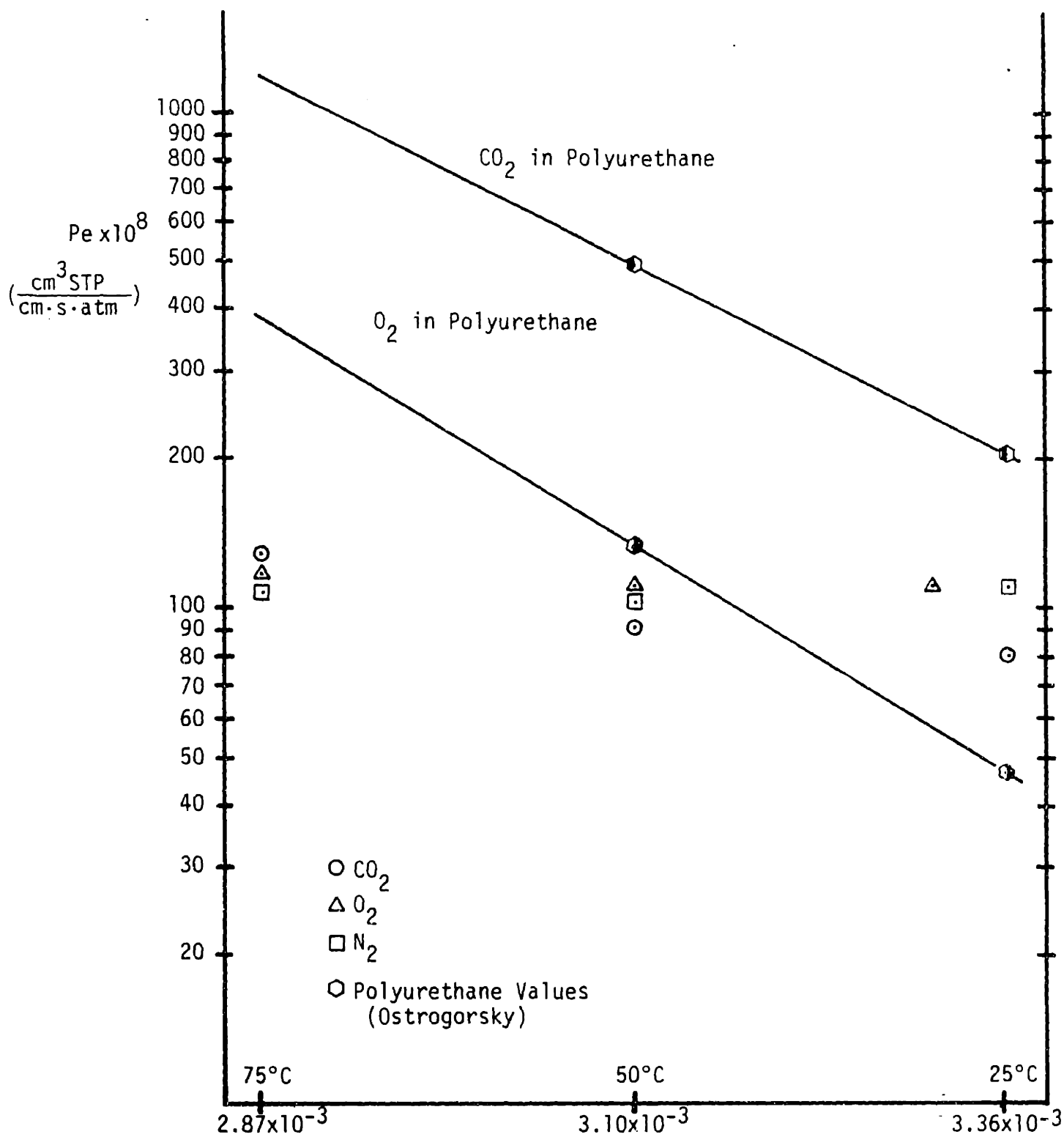


FIGURE 4.7: INITIAL RESULTS OF FOAM TEST SUGGESTING THE PRESENCE OF KNUDSEN DIFFUSION

time, the data were used with the transient charts for mass flux and it was indicated that the sample was not yet at steady-state [1]. Time constraints prohibited continuing the test, so additional Heisler-type charts were used to determine the steady-state values. (See Appendix D)

The permeability coefficient was found to be $8.40 \times 10^{-8} \left(\frac{\text{cm}^3 \text{STP}}{\text{cm-s-atm}} \right)$.

This value was approximately 30 to 45 times less than the published values for polyurethanes under the same condition. Project time constraints also prohibited further testing at low temperatures with other test gases. A sample of the raw data is shown in Figure 4.8.

4.4 Determination of the Polymer Permeability from the Foam Models

As mentioned in Section 4.2, the inability to manufacture adequate phenolic films prevented the attainment of a polymer permeability coefficient by the experimental methods in Section 2.3. Therefore, the film permeability was calculated through the use of the experimental foam permeability (Section 4.3) and the various analytical foam models described in Chapter 3. By rearranging Equations (3-15), (3-16), (3-17), (3-18) and (3-28), the following equations for polymer permeability were obtained according to geometric cell shapes assumed:

$$\text{Cube:} \quad P_{e_{\text{cell wall}}} = \frac{(P_{e_{\text{eff}}}) t(S_v)}{3} \quad (4-2)$$

$$\text{Pentagonal Dodecahedron:} \quad P_{e_{\text{cell wall}}} = \frac{(P_{e_{\text{eff}}})(t)(S_v)}{3.46} \quad (4-3)$$

$$\text{Truncated Octahedron:} \quad P_{e_{\text{cell wall}}} = \frac{(P_{e_{\text{eff}}})(t)(S_v)}{3.55} \quad (4-4)$$

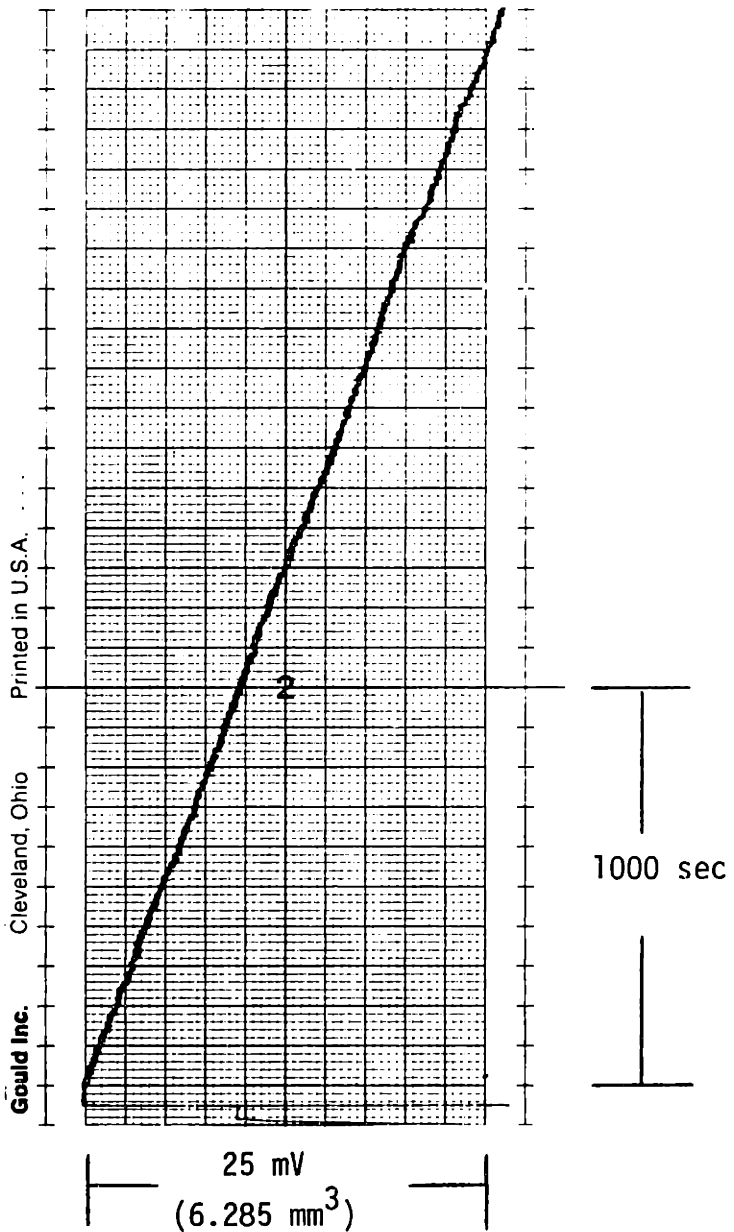


FIGURE 4.8: TYPICAL STRIP CHART DATA FROM CO₂ FOAM TEST AT 30°C

$$\text{Rhombic Dodecahedron: } P_{e_{\text{cell wall}}} = \frac{(P_{\text{eff}})(t)(S_v)}{4.24} \quad (4-5)$$

$$\text{Close Packed Sphere: } P_{e_{\text{cell wall}}} = \frac{(P_{\text{eff}})t}{2\langle \ell \rangle} \quad (4-6)$$

where $P_{e_{\text{eff}}}$ = effective foam permeability (measured value)
 t = cell wall thickness
 S_v = surface area to volume ratio
 $\langle \ell \rangle$ = average distance between cell walls (Equation 3-19)

The actual values used to determine the permeability coefficient of phenolic polymer for carbon dioxide at 30°C were:

$$P_{e_{\text{eff}}} = 8.40 \times 10^{-8} \frac{\text{cm}^3 \text{STP}}{\text{cm-s-atm}}$$

$$t = 0.0005 \text{ mm}$$

$$S_v = 24.0 \text{ mm}^{-1}$$

$$\langle \ell \rangle = 0.083 \text{ mm}$$

The results, shown in Table 4.3, suggest a range in polymer permeability coefficients from $2.38 \times 10^{-10} \left(\frac{\text{cm}^3 \text{STP}}{\text{cm-s-atm}} \right)$ to $3.36 \times 10^{-10} \left(\frac{\text{cm}^3 \text{STP}}{\text{cm-s-atm}} \right)$. As was anticipated, the cubic structure overpredicted the cell wall permeability coefficient due to its inherent underprediction of the overall foam permeability caused by the ideal shape. The cubic prediction will therefore be ignored. Based on the excellent agreement obtained in the density studies, the remaining 3 shapes are assumed to accurate predictions of the foam structure. Also, the packed sphere model was proven by Ostrogorsky to be a very close approximation to closed cell foam geometry. Therefore, the remaining results of Table 4.3 are assumed to

be valid, and the phenolic polymer permeability coefficient is estimated to be in the range of $2.38 \times 10^{-10} \left(\frac{\text{cm}^3 \text{STP}}{\text{cm-s-atm}} \right)$ to $2.91 \times 10^{-10} \left(\frac{\text{cm}^3 \text{STP}}{\text{cm-s-atm}} \right)$. By comparison, the polyurethane films (methane diisocyanate) were reported to have values of $16.7 \times 10^{-10} \frac{\text{cm}^3 \text{STP}}{\text{cm-s-atm}}$ to $17.5 \times 10^{-10} \frac{\text{cm}^3 \text{STP}}{\text{cm-s-atm}}$. This results in the permeability coefficient of the phenolic polymer being approximately 7 times less than the polymer in polyurethane foams for CO_2 at room temperature.

TABLE 4.3: PREDICTED PERMEABILITIES OF PHENOLIC POLYMER WITH CO₂ AT 30°C USING VARIOUS POLYHEDRON SHAPES²

POLYHEDRON SHAPE	PREDICTED PERMEABILITY, $P_{e_{cell\ wall}}$ ($\frac{cm^3_{STP}}{cm-s-atm}$)
Cube	3.36×10^{-10}
Pentagonal Dodecahedron	2.91×10^{-10}
Truncated Octahedron	2.84×10^{-10}
Rhombic Dodecahedron	2.38×10^{-10}
Packed Spheres	2.53×10^{-10}

CHAPTER 5

CONCLUSIONS AND RECOMMENDATIONS

5.1 Introduction

This chapter presents the major accomplishments and conclusions concerning the initial investigation of the aging in closed-cell phenolic foam. Also included are future recommendations for the continuation of the project.

5.2 Accomplishments and Conclusions

- A cell geometry study of the closed-cell phenolic foam was completed. The average cell wall thickness was determined to be 0.5 microns. The foam is comprised of 97.1% void space by volume. The percentage of solid polymer contained in the cell walls was determined to be 41.4% with 58.6% contained in the struts. (Section 4.1) By comparison, the percentage of solid polymer in the cell walls of polyurethane foam is reported to be 15% to 20%.
- In order to determine a basic cell shape so as to accurately model the foam's structure, the foam's density was predicted analytically using four polyhedron aggregates. It was found that the pentagonal dodecahedron, rhombic dodecahedron and truncated octahedron shapes most closely approximated the cell shape.
- A basic mass distribution analysis confirmed that, by shifting more polymer from the struts to the cell walls and maintaining the same foam density, the aging properties of the foam will be improved (Section 3.5). Therefore, the doubling of the percentage of material in the cell walls would double the aging time, i.e., permeability of the foam.

- A film test apparatus was designed and built which measured volumetric flowrates due to gas permeation through phenolic film. The initial project approach was to determine the permeability of the polymer and analytically predict the foam permeability using models of the geometry. The inability to obtain representative film samples without micro-holes prevented the continuation of this approach. A range of film permeabilities were then calculated by using the experimental foam permeability and the assumed geometries (Section 4.4).
- A test apparatus to determine the foam permeability coefficient was designed and constructed. By totally isolating the foam test cell from all ambient changes in temperature and pressure, the equipment was capable of detecting constant pressure volume changes on the order of 0.1 mm^3 . Initial tests utilizing an accelerated steady-state technique suggested that induced foam cell damage had occurred and created a situation for mass transport other than Fickian diffusion. It was felt that the high temperatures and the exposure to dry test gases had desiccated the hygroscopic phenolic polymer. The 8 psi pressure differential would then stress and fracture the cell walls.
- A subsequent low temperature test (30°C , 86°F) with carbon dioxide was successful which resulted in a permeability coefficient 30-45 times less than that of polyurethane foams. Transient mass flux charts were utilized to predict this permeability coefficient.

The following recommendations are presented for future work concerning the aging in closed-cell phenolic foam:

- 1) Further efforts are needed to produce a representative phenolic polymer film that is adequate for the film permeability tests.

- 2) The foam permeability tests need to be repeated with other test gases, i.e., oxygen and nitrogen, so that the transient aging phenomenon in phenolic foam can be predicted with the computer code.
- 3) The constants for the Arrhenius temperature relationship for permeation need to be determined in order to verify the current accelerated aging tests used in industry.
- 4) Due to the extremely low foam permeation rates expected for other gases, the accelerated steady-state technique is needed. Therefore, the effects of high temperature on the physical properties of the foam need to be investigated. It is suggested that the excessive drying of the foam can be avoided by controlling the humidity in the high and low pressure reservoirs.
- 5) The degree of cell breakage due the pressure differentials used in the foam tests needs to be determined. It is felt that a more effective method may be to use a fluorocarbon gas at atmospheric pressure in the upper chamber, while placing the test gas, also at atmospheric pressure, in the lower chamber. This provides an effective test gas partial pressure difference of 1 atmosphere across the foam, but maintains a zero total pressure difference.
- 6) Since a large portion of the closed-cell phenolic is used in the low-slope roofing industry, the effects of excessive moisture on the foam's performance should be investigated. It is assumed that any condensed moisture inside the cells will increase the thermal conductivity, but little is known about the effects of moisture on polymer permeability and aging.

REFERENCES

1. Ostrogorsky, A.G., "Aging of Polyurethane Foams", PH.D. Thesis, Department of Mechanical Engineering, MIT, 1985.
2. Dvorchak, M.J., Koppers Co., Inc., Pittsburgh, PA., Personal Communication, January, 1985.
3. Manufactured by Koppers Company, Inc., Pittsburgh, PA.
4. Carlson, J.D., et.al., "Phenolic Foam and Composition and Method for Preparing the Same", U.S. Patent #4,444,912, April 24, 1984.
5. Carlson, J.D., et.al., "Method for Preparing Phenolic Foams Using Anhydrous Aeryl Sulfonic Acid Catalysts", U.S. Patent #4,478,958, October 23, 1984.
6. Schuetz, M.A., "Heat Transfer in Foam Insulation", S.M. Thesis, Department of Mechanical Engineering, MIT, 1982.
7. Reitz, D.W., Schuetz, M.A., Glicksman, L.R., "A Basic Study Of Aging of Foam Insulation", Cellular Plastics, 20, 2., pp. 104-113, 1984.
8. Graham, T., Transactions of the Royal Society (London), 156, pp. 399, 1866.
9. Reitz, D.W., "A Basic Study of Gas Diffusion in Foam Insulation", S.M. Thesis, Department of Mechanical Engineering, MIT, 1983.
10. Brown, T.L., LeMay, H.E., Chemistry-The Central Science, Prentice-Hall, Inc., Englewood Cliffs, New Jersey, pp. 355, 1977.
11. Geankoplis, C.J., Mass Transfer Phenomena, Holt, Richard and Winston, Inc., pp. 451-455.
12. Rohsenow, W.M., Choi, H., Heat, Mass, and Momentum Transfer, Prentice-Hall, Inc., Englewood Cliffs, New Jersey, pp. 280, 1961.
13. Ostrogorsky, A., Glicksman, L.R., Reitz, D.W., "Aging of Polyurethane Foams", ASME Winter Annual Meeting, New Orleans, 1984.
14. Kifer, E., Koppers Co., Inc., Pittsburgh, PA, Personal Communication, January, 1986.
15. Bluhm, J., Koppers Co., Inc., Pittsburgh, PA, Personal Communication, May, 1985.

16. Valenzuela, J.A., Glicksman, L.R., "Thermal Resistance and Aging of Rigid Urethane Foam Insulation", Proceedings of DOE-ORNL Workshop on Mathematical Modeling of Roofs, November 3-4, 1981, Atlanta, GA., Conf-811179, pp. 261.
17. Dynatech Corporation, Cambridge, Massachusetts, February, 1986.

APPENDIX A
PHYSICAL PROPERTIES OF PHENOLIC FOAM

TABLE A-1

PHYSICAL PROPERTIES OF CLOSED-CELL PHENOLIC FOAM
(Courtesy, Koppers Co., Inc., Pittsburgh, PA)

Thickness, inches	2.0
k-Factor (ASTM C518)	.104
Comp. Strength, psi 10% Consolidation (ASTM D 1621)	23.7
Elasticity of Comp., psi	729
Core Density, pcf (ASTM d 1622)	2.41
Water Absorption - 24 hr., g/cc (ASTM C272)	.135
Tumbling Friability, % Mass Loss (ASTM C421-77)	27.0
Dimensional Stability, % Change (158 - 4°F & 97 + 3%) (ASTM D2126, Procedure C)	
Weight	+3.48
Length	+1.14
Width	+1.38
Thickness	-1.04
Tensile Strength, psi (ASTM D1623)	
Minimum	14.4
Maximum	24.1
Average (4 Specimens)	20.2
Machine Direction	
Modulus, psi	2623
Strength, psi	64
Strain, %	3.5
Transverse Direction	
Modulus, psi	2751
Strength, psi	71
Strain, %	3.9
Fastener Pull-Through, lbs. Steel Tru-Fast Plates (4 specimens)	
Mean	230
Minimum	164
Maximum	257

APPENDIX B
SAMPLE CALIBRATION CURVE FOR FOAM TEST CELL

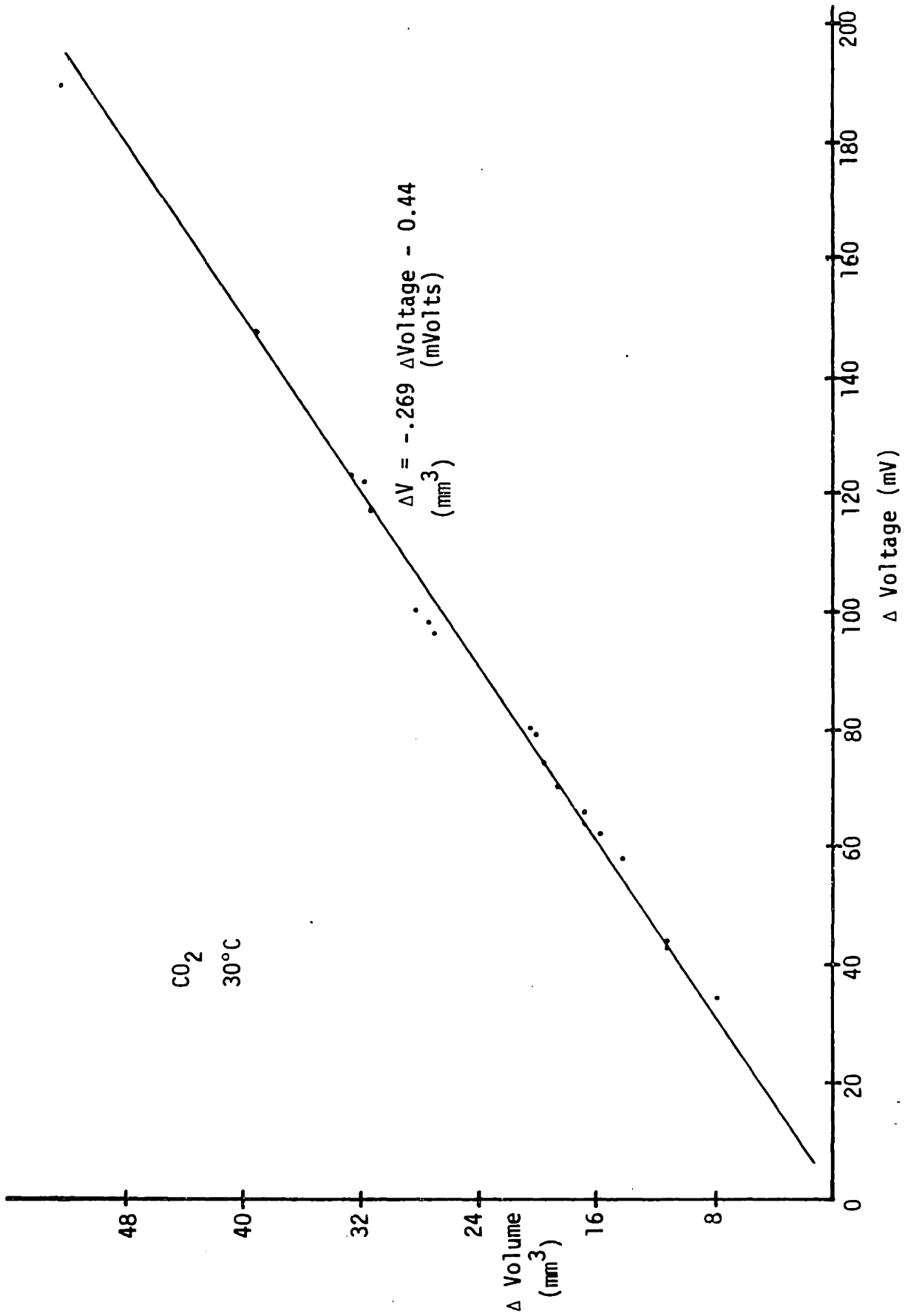
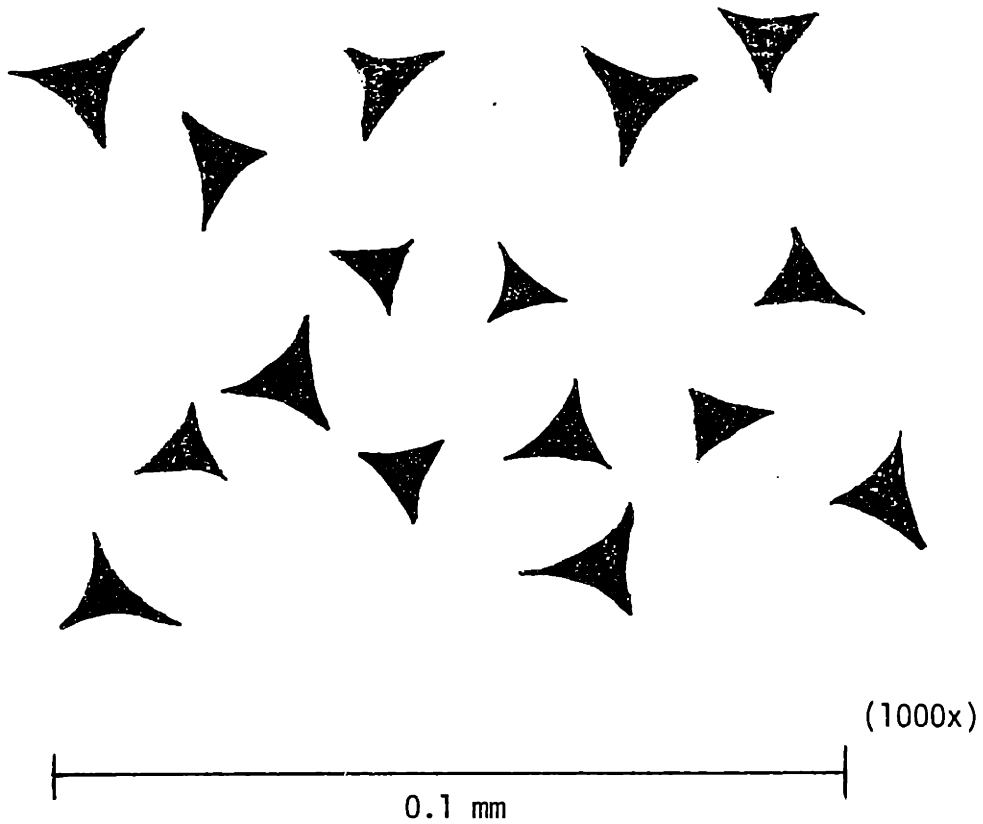


FIGURE B-1: VOLUME/VOLTAGE CALIBRATION CURVE FOR FOAM TEST CELL

· APPENDIX C
STRUT AREA ANALYSIS



*** STATISTICS OF Detected area ***

Number	= 14 features	(mm ²)
Min	= 2.21597E-6	
Max	= 5.27711E-6	
Total value	= 4.32495E-4	
Mean	= 3.09530E-5	
Std deviation	= 9.95239E-6	
Variance	= 9.90451E-11	
Skew	= -2.34546E-13	
Kurtosis	= 1.35426E-20	

Sample identifier : PHENOLICSTRUT

APPENDIX C: SAMPLE OF TRACED STRUT AREAS AND MAGISCAN
IMAGE ANALYZER DETECTED AREA

APPENDIX D

USE OF TRANSIENT CHARTS TO DETERMINE THE FOAM PERMEABILITY COEFFICIENT

Figure D-1 shows a sample of the transient charts developed by Ostrogorsky in [1]. These charts are similar to the Heisler charts in heat transfer.

$$J^* = \frac{J_{\text{measured}}}{J_{\text{reference}}}$$

where, $J_{\text{measured}} = \frac{(P_{e_{\text{measured}}})\Delta P}{L}$

• $J_{\text{reference}} = \frac{S(L)(\Delta P)}{t}$

$P_{e_{\text{measured}}}$ = measured permeability coefficient at time, t

L = foam thickness

S = solubility = $1 \frac{\text{cm}^3 \text{ STP}}{\text{cm}^3 \cdot \text{atm}}$

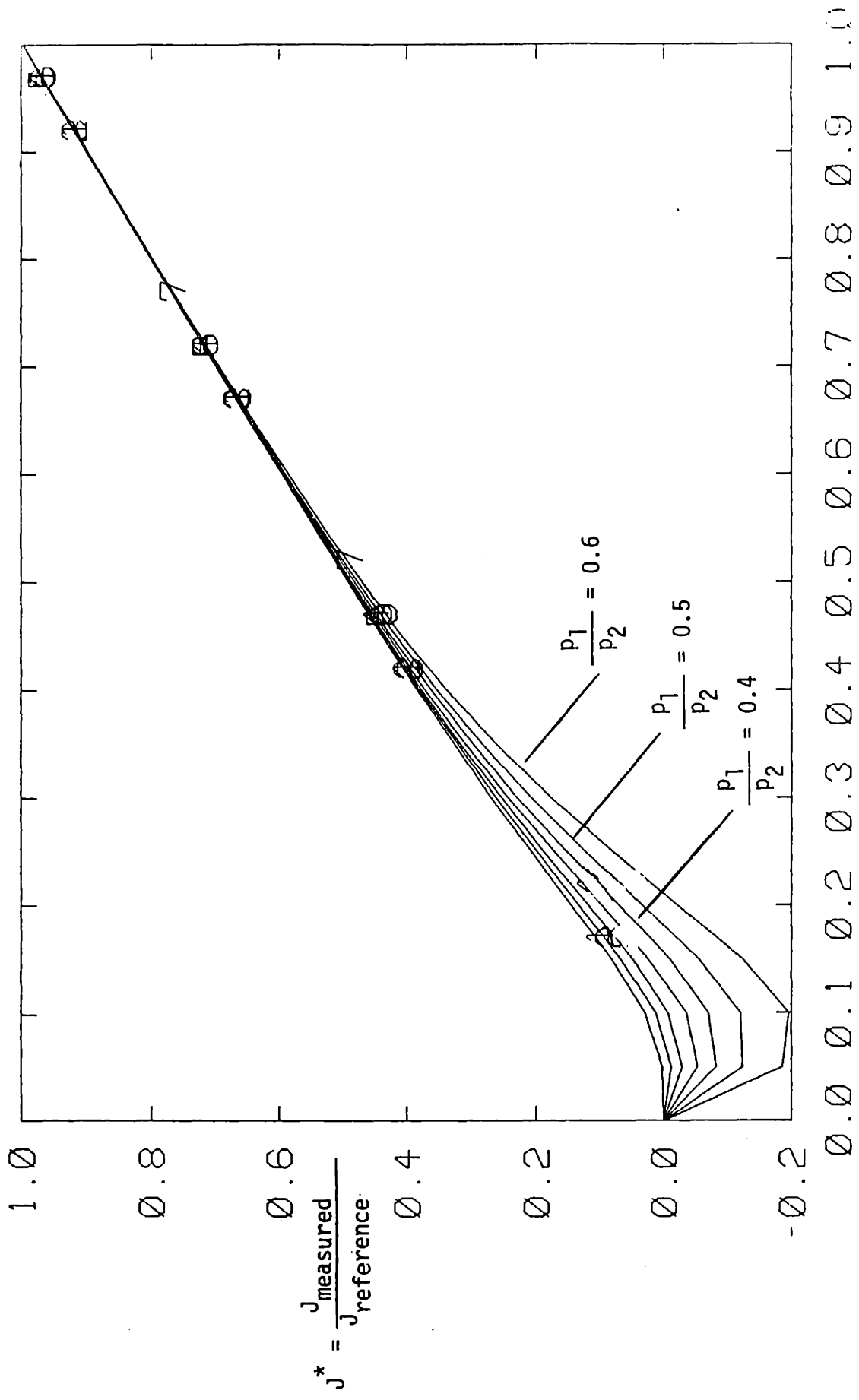
ΔP = $P_2 - P_1$

t = time

Fo = Fourier number = $\frac{Dt}{L^2}$

where D = Diffusion coefficient

The diffusion coefficient was found by calculating J^* from data at different times. The corresponding Fo was found from the charts which permitted D to be determined. The diffusion coefficient should be equal at all times. See Reference [1] for more details.



$$Fo = \frac{Dt}{L^2}$$

FIGURE D.1: TRANSIENT CHARTS FOR MASS FLUX THROUGH FOAMS

TABLE D.1: CALCULATION OF FOAM DIFFUSION COEFFICIENT WITH TRANSIENT CHARTS

Time (sec)	P_e $\left(\frac{\text{cm}^3 \text{ STP}}{\text{cm}^2 \cdot \text{s} \cdot \text{atm}}\right)$	J_{measured} $\left(\frac{\text{cm}^3 \text{ STP}}{\text{cm}^2 \cdot \text{s}}\right)$	J_{ref} $\left(\frac{\text{cm}^3 \text{ STP}}{\text{cm}^2 \cdot \text{s}}\right)$	J^*	F_0	D $\left(\frac{\text{cm}^2}{\text{s}}\right)$
9.23×10^5	2.68×10^{-8}	2.55×10^{-8}	3.37×10^{-7}	0.076	0.264	9.36×10^{-8}
1.05×10^6	3.50×10^{-8}	3.33×10^{-8}	2.96×10^{-7}	0.11	0.280	8.72×10^{-8}
1.13×10^6	3.31×10^{-8}	3.15×10^{-8}	2.75×10^{-7}	0.15	0.301	8.72×10^{-8}
1.20×10^6	3.40×10^{-8}	3.23×10^{-8}	2.59×10^{-7}	0.12	0.284	7.74×10^{-8}
1.29×10^6	3.52×10^{-8}	3.35×10^{-8}	2.41×10^{-7}	0.14	0.294	7.46×10^{-8}
$\text{AVG} = 8.40 \times 10^{-8}$ $\pm 9\%$						

Phenolic Foam Density = 40 kg/m^3 ($2.50 \times 1\text{b/ft}^3$)

CO_2 @ 30°C Sample
 Thickness = 0.572 cm (0.225 in)